

Volume 39 Number 3

SEPTEMBER 2008

ISSN 0046-5828

# GEOTECHNICAL ENGINEERING

*Journal of the*  
SOUTHEAST ASIAN GEOTECHNICAL SOCIETY

*Sponsored by*  
ASIAN INSTITUTE OF TECHNOLOGY



# GEOTECHNICAL ENGINEERING

Vol. 39, No. 3, SEPTEMBER 2008

## CONTENTS

### Main Papers:

Back-propagation Neural Network for Assessment of Highway Slope Failure in Taiwan by T. L. Lee, H. M. Lin, D. S., Jeng and Y. P. Lu .....	121
Analytical Solutions for Passive Earth Pressure Considering Different Failure Mechanisms with Nonlinear Failure Criterion by X.L. Yang and J.H. Yin .....	129
Geotechnical Properties of Soil-fiber Mixture as a Landfill Cover Barrier Material by T. Harianto, Y. J. Du, S. Hayashi, D. Suetsugu and Y. Nanri .....	137
Secondary Compression Behavior in Three Types of Consolidation Tests by B. Sompie, K. Arai and A. Kita .....	145

### Technical Papers

A Short-cut Method for Predicting Strength of Cement Treated Soft Bangladesh Clays and the Alteration of other Engineering Parameters by M. M. Rahman, M.A. Taiyab, A. Siddique and M. K. Uddin .....	159
Frequency Effect on Liquefaction using Shake Table Tests by J. Kumar and P. Samui .....	169

## **GEOTECHNICAL ENGINEERING**

Published by the  
SOUTHEAST ASIAN GEOTECHNICAL SOCIETY

---

### **EDITOR**

NOPPADOL PHIENWEJ

### **CO-EDITOR**

JIAN CHU

---

### **EDITORIAL ADVISERS**

A.S. BALASUBRAMANIAM, *Australia*  
E.W. BRAND, *U.K.*  
R.P. BRENNER, *Switzerland*  
V.F.B. DE MELLO, *Brazil*  
W.H. TING, *Malaysia*

T.W. LAMBE, *U.S.A.*  
S.L. LEE, *Singapore*  
Z.C. MOH, *Taiwan*  
H.G. POULOS, *Australia*  
C.D. OU, *Taiwan*

---

### **SEAGS GENERAL COMMITTEE**

C.T. CHIN ( <i>President</i> )	J. CHU
K.Y. YONG ( <i>Immediate Past President</i> )	J.C. LI
Z.C. MOH	W.H. TING
T.A. OOI	A.S. BALASUBRAMANIAM
C.D. OU	S.K. TANG
S.L. LEE	Y.Y. WENG
M. L. LIN	H.D. LIN
S. SAMBHANDARAKSA	K.S. YEE
W. GASALUCK	D.T. BERGADO ( <i>Secretary-General</i> )
N. PHIENWEJ ( <i>Editor</i> )	

*Geotechnical Engineering* is the official journal of the Southeast Asian Geotechnical Society. It is published four times a year in March, June, September and December and is sent free to members of the Society. The annual subscription rate for non-members is US\$30 to individuals, and US\$50 to libraries and companies. Back issues are available. Cheques or money orders should be made payable to the Asian Institute of Technology. Membership application forms and other details can be obtained from:

*The Secretariat, SEAGS  
Rm 211, AIT Library  
Asian Institute of Technology  
P.O. Box 4, Klong Luang  
Pathumthani 12120, Thailand*

**Cover Photograph:** Construction of piled foundation and pier of the western pylon of the long span cabled stayed bridge of the Outer Bangkok Southern Ring Road across the Chao Phraya River (Courtesy of Ch. Karnchang Public Company & Expressway Authority of Thailand)

# **GEOTECHNICAL ENGINEERING**

## **EDITORIAL PANEL**

Dr. R.P. Brenner  
Weinfelden  
Switzerland

Prof. Cheng-Hsing Chen  
National Taiwan University  
Taipei, Taiwan

Prof. In Mo Lee  
Korea University  
Seoul, Korea

Prof. San-Shyan Lin  
Taiwan Ocean University  
Keelung, Taiwan

Dr. Warakorn Mairiang  
Kasetsart University  
Bangkok, Thailand

Prof. Harianto Rahardjo  
Nanyang Technological University  
Singapore

Dr. Satoru Shibuya  
Kobe University  
Kobe, Japan

Dr. Jiro Takemura  
Tokyo Institute of Technology (TIT)  
Tokyo, Japan

Dr. Tanaka, Hiroyuki  
Port and Airport Research Institute  
Yokosuka, Japan

Prof. Wilson H. Tang  
The Hong Kong University of Science & Technology  
Kowloon, Hong Kong

Dr. T.H. Seah  
MAA Geotechnics, Co., Ltd.  
Bangkok, Thailand

Dr. Jin-Chun Chai  
Saga University  
Saga, Japan

Prof. B. Indraratna  
University of Wollongong  
Wollongong, Australia

Prof. Chun-Fai Leung  
National University of Singapore  
Singapore

Prof. Madhira R. Madhav  
Indian Institute of Technology  
Kanpur, India

Prof. Hiroyasu Ohtsu  
Kyoto University  
Kyoto, Japan

Dr. Mohamad R. Selamat  
University Sains Malaysia  
Pulau Penang, Malaysia

Prof. Mitsutaka Sugimoto  
Nagaoka University of Technology  
Nagaoka, Japan

Prof. Siew Ann Tan  
National University of Singapore  
Singapore 117576

Prof. Jian Zhao  
Nanyang Technological University  
Singapore 639798

Dr. Charles W. W. Ng  
The Hong Kong University of Science and Technology  
Kowloon, Hong Kong

Dr. S.L. Shen  
Shanghai Jiao Tong University  
Shanghai, China

## NOTES FOR GUIDANCE TO AUTHORS

SEAGS encourages the submission of scholarly and practice-oriented articles to its journal. Starting from 2008, the journal will be published quarterly. Before you submit an article, please review the guidelines stated herein for the manuscript preparation and submission procedures.

Geotechnical Engineering Journal accepts submissions via electronic or postal mail(by sending a CD). The manuscript file (text, tables and figures) in pdf format together with the submission letter should be submitted to the Editor, Geotechnical Engineering Journal, c/o School of Engineering and Technology, Asian Institute of Technology, P.O. Box 4, Klong Luang, Pathumthani 12120, Thailand. E-mail [noppadol@ait.ac.th](mailto:noppadol@ait.ac.th) or [seags@ait.ac.th](mailto:seags@ait.ac.th). Papers under review, accepted for publication, or published elsewhere are not accepted. The review and publication procedures will be faster if the basic requirements listed below are followed.

1. The manuscript including abstract and references must be typed double-spaced in Times New Roman 12 on one side of A4 paper with a margin of 25 mm on each side.
2. The length of titles must not exceed 70 characters and spaces.
3. The maximum length of papers in the print format of the Journal is 12 two-column pages in single-spaced in Times New Roman 9 including figures and tables. A Journal page contains approximately 1,040 words. Authors can approximate manuscript length by counting the number of words on a typical manuscript page and multiplying that by the number of total pages (except for tables and figures). Add word-equivalents for figures and tables by estimating the portion of the journal page each will occupy when reduced to fit on a 160 mm x 240 mm journal page. A figure reduced to one-quarter of a page would be 260 word-equivalents. When reduced, the figure must be legible and its type size no smaller than 6 point font (after reduction).
4. Figures: Line art should be submitted in black ink or laser printed; halftones and color should be original glossy art. Figures should be submitted at final width i.e. 90 mm for one column and 185 mm for two columns. The font of the legends should be in Times New Roman and should use capital letters for the first letter of the first word only and use lower case for the rest of the words. Background screening and grids are not acceptable.
5. Each table must be typed on one side of a single sheet of paper.
6. All mathematics must be typewritten and special symbols identified. Letter symbols should be defined when they first appear.
7. The paper must end with a set of conclusions.
8. Practical applications should be included, if appropriate.
9. If experimental data and/or relations fitted to measurements are presented, the uncertainty of the results must be stated. The uncertainty must include both systematic (bias) errors and imprecisions.
10. Authors need not be Society members. Each author's full name, Society membership grade (if applicable), present title and affiliation, and complete mailing address must appear as a footnote at the bottom of the first page of the paper.
11. Each author must use SI (International System) units and units acceptable in SI. Other units may be given in parentheses or in an appendix.
12. Maximum of five keywords should be given.
13. References should appear in the text as the author name(s) followed by the year of publication in parentheses. A list of references must be given at the end of the text in alphabetical order in capitals and double spacing must be used between references. An example of the format to be used in reference list are given below:

HOEK, E. and BROWN, E.T. (1982). *Underground Excavations in Rock (2nd Edition)*. London: The Institution of Mining and Metallurgy, 527p.

PUN, W.K. and AMBRASEYS, N.N. (1992). Earthquake data review and seismic hazard analysis for the Hong Kong region. *Earthquake Engineering and Structural Dynamics*, Vol. 21, No. 1, pp. 433-443.

RAMASAMY, N. (1992). Soft ground tunneling in Bangkok subsoils, M. Eng. Thesis, Asian Institute of Technology, Bangkok, Thailand.

TATSUOKA, F. and KOHATA, Y. (1994). Stiffness of hard soils and soft rocks in engineering applications. *Proceedings of the 1<sup>st</sup> International Conference on Prefailure Behaviour of Geomaterials*, Balkema, Rotterdam, The Netherlands, Vol. 2, pp. 947-1063.

# BACK-PROPAGATION NEURAL NETWORK FOR ASSESSMENT OF HIGHWAY SLOPE FAILURE IN TAIWAN

T. L. Lee<sup>1</sup>, H. M. Lin<sup>2</sup>, D. S. Jeng<sup>3</sup> and Y. P. Lu<sup>4</sup>

**ABSTRACT:** The highway slope failure during typhoons and earthquakes is a major geotechnical engineering problem in Taiwan. Intensive studies have been carried out in recent years. However, conventional investigations for determining slope failure have focused on the linear relationships between the dominant factors, such as slope angle, slope height, material, construction, rainfall, earthquake and etc., although it should be a complicated nonlinear relationship. In this paper, a back-propagation neural network is proposed as an assessment tool for the slope failure. On-site slope failure data at the A-Li-San Highway in southern Taiwan are used to test the performance of the artificial neural network model. The numerical results demonstrate the effectiveness of the artificial neural network in the evaluation of slope failure potential with five major factors, such as slope gradient angle, slope height, cumulative precipitation, surface acceleration and strength of material.

**Keywords:** highway slope failure, back-propagation neural network.

## INTRODUCTION

A slope failure is a phenomenon that a slope collapses abruptly due to weakened self-retainability of the earth during an event of rainfalls or strong earthquakes. For the highway, rocks, soil and other debris can fall onto the roadways causing detours, traffic delays and dangerous driving conditions. Therefore, the problem of the highway slope failure after typhoon or earthquakes has been concerned by geotechnical engineers in recent years.

Taiwan is an island, which is located in a sub-duction zone between Phillipine Sea and Eurasian Plates, it has been often attacked by typhoon and earthquake in East Asia. During 31 July and 1 August, 1996, Taiwan was struck by a strong typhoon "Herb", which carried a highest sustained wind speed up to 60 m/s and a radius of 320 km. According to the reports, there were 1,315 landslides, more than 20 debris flows, 101 road closures and 49.6 km of embankment failure. Moreover, there were 73 deaths, 463 wounded, 1,383 houses destroyed or damaged and over one billion USD in property losses.

A devastating earthquake (Chi-Chi earthquake) with the Richter magnitude of 7.3 struck the central region of Taiwan in the early morning on September 21 in 1999. It was known as Chi-Chi earthquake. As exhibited by the statistics, over 2,350 people were killed, 10,000 were injured, and 35 were missing in the earthquake. Moreover, approximately 10,000 buildings or houses collapsed and 7,500 damaged. During the earthquake, slope failures happened throughout extensive areas, and 9,272 places are larger than 625 m<sup>2</sup> (Liao, 2000).

As mentioned above, slope failure was often resulted by earthquakes and typhoons. For the secondary slope failure after earthquakes occurred, Inoue (2000) introduced two landslides at Tokuyama Shiratani and Neo Shiratani in Japan to demonstrate the occurrence of secondary disasters

for a torrential rainfall even 84 years after the Nobi earthquake ( $M=8.0$ ). On the other hand, many slopes remaining unstable after attack of an earthquake are considered to have the secondary disasters in the coming raining seasons. Numerous researches have been devoted to the connection between landslides and rainfall (Caine, 1980; Cannon, 1985; Keefer, 1987 and Wasowski, 1998). However, they have been only concerned with the critical conditions of debris flow occurrence caused by rainfall.

In fact, there are many factors that often are uncertainty, but significantly affected the slope failure of highway. For example, variability of geologic materials cannot be taken into account by conventional deterministic methods of slope stability analysis. Slope stability analysis in the past relied heavily on the use limiting equilibrium method. This method has proved effective assessment the slope failure for most engineering applications. In recent years, risk analysis and assessment has become an important tool in addressing uncertainty inherent in slope failures (Fell and Hartford, 1997). However, not all uncertainties are random or objective quantity. Some uncertainties, especially those based on incomplete information are due to cognitive sources. These uncertainties cannot be handled satisfactorily in the classic theory and these data-based in most cases is quite limited. Therefore, this situation makes the application of classical estimation procedure extremely difficult.

Artificial neural network (ANN) is being widely applied to various areas to overcome the problem of exclusive and the nonlinear relationships. The back-propagation neural network (BPN) developed by Rumelhart et al. (1986) is the most representative learning model for the artificial neural network. The procedure of the BPN repeatedly adjusts the weights of the connections in the network so as to minimize the measure of the difference between the actual output vector of the net and the desired output vector. The BPN is widely applied in a variety of scientific areas especially in applications involving diagnosis and forecasting.

Recently, ANN has been widely applied to overcome the problem of exclusive and the nonlinear relationships (French et al., 1992; Mase, 1995; Campolo et al., 1997; Tsai and Lee, 1999; Lee et al., 2002; Coppola et al., 2003; Jeng et al., 2004; Lee 2004; Makarynskyy 2005; Lee 2006; Bateni et al., 2007; Lee 2008).

<sup>1</sup>Professor, Department of Construction and Facility Management, Leader University, Taiwan, ROC. (Corresponding author: Fax: +886-6-2553225, Email: tlee@mail.leader.edu.tw)

<sup>2</sup>Assistant Professor, Department of Construction and Facility Management, Leader University, Taiwan, ROC.

<sup>3</sup>Professor, Division of Civil Engineering, School of Engineering, University of Dundee, DD1 4HN Scotland, UK.

<sup>4</sup>Master, Department of Resource and Environment, Leader University, Taiwan, ROC.

This paper is aimed to propose the application of BPN for the investigations slope failures of typhoon triggered and earthquake provoked highway. The precipitation records of slope failure data from 1984 to 2001 at the A-Li-San Highway are collected to test the proposed model. The dominant factors, including slope gradient angle, slope height, cumulative precipitation, daily rainfall, surface acceleration, strength of material, slope direction and earthquake magnitude, will be selected to assess the effect of highway slope failures.

## NEURAL NETWORK

The ANN is an information-processing system mimicking the biological neural network of the brain by interconnecting many artificial neurons. The neuron accepts inputs from a single or multiple sources and produces outputs by simple calculating processing with a predetermined non-linear function. Since the principle of ANN has been well documented in the literature, only a brief is given in this section.

A typical three-layered network with an input layer (*I*), a hidden layer (*H*) and an output layer (*O*) (see Fig. 1) is adopted in this study. Each layer consists of several neurons and the layers are interconnected by sets of correlation weights. The neurons receive inputs from the initial inputs or the interconnections and produce outputs by transformation using an adequate nonlinear transfer function. A common transfer function is the sigmoid function expressed by  $f(x) = (1 + e^{-x})^{-1}$ , it has a characteristics of  $df/dx = f(x)[1 - f(x)]$ . The training processing of neural network is essentially executed through a series of patterns. In the learning process, the interconnection weights are adjusted within input and output value.

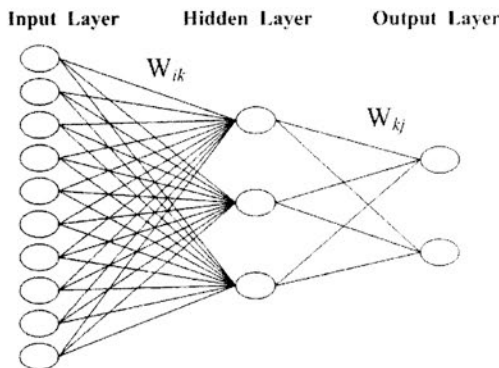


**Fig. 1 Structure of an artificial neural network.**

The Back-Propagation Neural Network (BPN) is the most representative learning model for the artificial neural network. The procedure of the BPN is the error at the output layer propagates backward to the input layer through the hidden layer in the network to obtain the final desired outputs. The gradient descent method is utilized to calculate the weight of the network and adjust the weight of interconnections to minimize the output error. The error function at the output neuron is defined as:

$$E = \frac{1}{2} \sum_k (T_k - O_k)^2 \quad (1)$$

where  $T_k$  and  $O_k$  are separately the value of target and output.

The gradient decent algorithm adapts the weights according to the gradient error, which is given by

$$\Delta W_{ij} = -\eta * \frac{\partial E}{\partial W_{ij}} \quad (2)$$

where  $\eta$  is the learning rate, and the general form of the  $\frac{\partial E}{\partial W_{ij}}$  term is expressed by

$$\frac{\partial E}{\partial W_{ij}} = -\delta_j^n \cdot A_i^{n-1} \quad (3)$$

Substituting (3) into (2), the gradient error becomes

$$\Delta W_{ij} = \eta \cdot \delta_j^n \cdot A_i^{n-1} \quad (4)$$

in which  $A_i^{n-1}$  is the output value of the sub-layer related to the connecting weight ( $W_{ij}$ ),  $\delta_j^n$  is the error signal, which is computed considering whether or not the *j*-th neuron is in the output layer. If the neuron *j* is one of the output neurons, then

$$\delta_j = (T_j - Y_j) \cdot Y_j \cdot (1 - Y_j) \quad (5)$$

If neuron *j* is the neuron of the hidden layer, then

$$\delta_j = \left[ \sum_h \delta_h \cdot (W_{jh})_{hj} \right] \cdot H_h \cdot (1 - H_h) \quad (6)$$

where  $H_h$  is the value of the *h*-th unit in hidden layer.

Finally, the values of the weights can be expressed as:

$$W_{ij}^m = W_{ij}^{m-1} + \Delta W_{ij}^m = W_{ij}^{m-1} + \eta \cdot \delta_j^n \cdot A_i^{n-1} \quad (7)$$

To accelerate the convergence of the error in the learning procedure, Jacobs (1988) proposed to include the momentum term with the momentum gain  $\alpha$  into the equation (7):

$$W_{ij}^m = W_{ij}^{m-1} + \eta \delta_j^n \cdot A_i^{n-1} + \alpha \Delta W_{ij}^{m-1} \quad (8)$$

where  $\alpha$  ranges from 0 to 1.

The value of the learning rate  $\eta$  significantly affects the convergence of the learning algorithm, while the momentum factor  $\alpha$  is used to avoid stopping the learning process at a local minimum instead of the global one (Jacobs, 1998). Either low  $\eta$  or high  $\alpha$  are expected to accelerate the convergence of the training process.

## CASE STUDY

To illustrate the capability of the proposed model, the highway slopes of the A-Li-San Highway in southern Taiwan are the investigating targets in this study. The locations of the highway are shown in Fig. 2. The A-Li-San highway passes through the south portion of the investigating area, and its length is 56 km. The

investigating area is located at the Western Foothills thrust belt of Taiwan. The Chukou Fault divides this area into two zones. In the east part, the mountains are at the height of 1000~1800 m. However, the configurations in west part are hills and terraces. All of the strikes are flexed into NE-SW trending. (Keng, 1986).

The formations of the investigated area are formed during the Tertiary and Quaternary periods. The outcrop formations are Nanchuang Formation, Kueichulin Formation, Chinshui Shale, Chaolan Formation and Toukoshan Formation (Liu, 1989). Lee et al. (2001) point the slopes have highest possibility to fail in Chinshui Formation. And, many failures occurred at the slopes with gradient angles larger than 40°. According to the analysis, most of the failures occurred at the slope with 10~30 m height. Most of the slope failures have the slope directions toward south east, south and south west. As for the landslides with scale less than 500 m<sup>3</sup> have highest percentage under the effects of a typhoon or an earthquake.

Two photographs of highway slope failure after Chi-Chi earthquake and at Toraji typhoon the A-Li-San Highway are shown in Figs. 3 and 4.

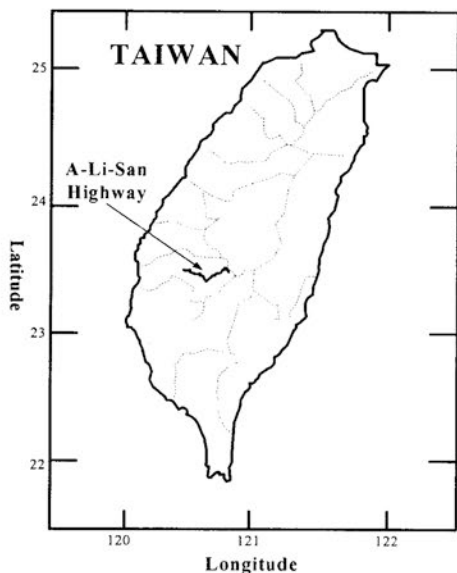


Fig. 2 Locations of the A-Li-San Highway, Taiwan.

The normalized root mean squared error (RMS) and correlation coefficient (CC) were used for the agreement index to present the accuracy of the present model, given as

$$RMS = \sqrt{\sum_{k=1}^n (y_k - \hat{y}_k)^2 / \sum_{k=1}^n \hat{y}_k^2} \quad (9)$$

$$CC = \frac{\sum_{k=1}^n (y_k - \bar{y}_k)(\hat{y}_k - \bar{\hat{y}}_k)}{\sqrt{\sum_{k=1}^n (y_k - \bar{y}_k)^2 \sum_{k=1}^n (\hat{y}_k - \bar{\hat{y}}_k)^2}} \quad (10)$$

in which  $\hat{y}_k$  is the value of observation and  $y_k$  denotes the value of prediction.  $\bar{y}_k$  is the mean of observation ( $\bar{y}_k = 1/n \sum_{k=1}^n y_k$ ) and  $\bar{\hat{y}}_k$  is the mean value of prediction ( $\bar{\hat{y}}_k = 1/n \sum_{k=1}^n \hat{y}_k$ ).



Fig. 3 A photograph of highway slope failure after Toraji at the A-Li-San Highway.

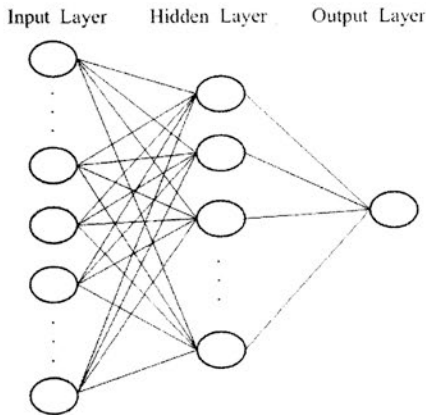


Fig. 4 A photograph of highway slope failure after Chi-Chi earthquake at the A-Li-San Highway.

#### The ANN Model for Highway Slope Failure

Conventional deterministic methods of slope stability analysis, involving with some uncertainties and unsatisfied treatments, i.e., many uncertain factors affect the slope failure of highway directly, thus, the determination the optimal variable is a challenge task.

In this study, we try to employ the BPN to assess the highway slope failure in this study. Firstly, we chose the parameters determining form the field measurement as the eight input neurons, such as slope gradient angle, slope height, cumulative precipitation, daily rainfall, and surface acceleration, strength of material, slope direction and earthquake magnitude. Then, the highway slope failure site is expressed as the "output" column, in which "1" denotes the observation of failure, while "0" represents no failure. The structure of highway slope failure forecasting for BPN model is shown in Fig. 5.



**Fig. 5 Structure of the highway slope failure forecasting for BPN.**

In this paper, ten cases will demonstrate the application of the proposed BPN model at the A-Li-San Highway. According to the reported data, there are 350 sets of data, which are categorized into three situations based on in-situ survey, including for earthquake induced in slope failure (64 sets of data), slope failure affected without earthquake (58 sets of data) and no slope failure (228 sets of data). To ensure the proposed BPN model can effectively assess the occurrence of slope failure, ten sets of case are considered (Cases E1-E10) with different training sets to forecast the occurrence of slope failure, shown in the Table 1.

#### Effects of neural network structure

An optimized neural network structure is used to illustrate the performance for assessing the highway slope failure. Since the neural network is a non-linear procedure and the network parameters will affect each other, the adjustment of each parameter to optimize the whole network is not an easy task. This section discusses how the neural network structures affect the performance of the forecasting model, which includes the number of hidden layers, the learning rate,  $\eta$ , the momentum factor,  $\alpha$ , the number of training iterations (Epochs) and the number of neurons in each layer. To assess the performance of the neural network with these parameters, the agreement indices of the success ratio are used. The success ratio is defined by Derin and Hasan (1998) as the following:

$$\text{success ratio} = \frac{\text{the number of success samples}}{\text{the number of total samples}} \quad (11)$$

In this paper, an error value greater than  $|0.2|$  denotes an error; whereas if the results are less than  $|0.2|$ . In general, the effect of hidden layer has been widely used with one hidden layer. This is because that the interaction of input neuron can not be mapped without hidden layer. However, more hidden layers will lead to the complexity of neural networks and result in a significant error. Therefore, most investigators choose one hidden layer as its best performance.

The performance of the neural network structures with

different training data sets (i.e., 100, 150, 200 and 250) and forecasting data sets (i.e., 50, 100 and 150) is presented in Table 2 for the one hidden layer, the 8 number of neurons in input layer, the 6 number of neurons in hidden layer, the learning rate  $\eta = 0.01$ , the momentum factor  $\alpha = 0.9$  and after 18000 training iterations.

**Table 1 Training and forecasting data set.**

Case	Training data sets			Forecasting data sets		
	Failure	No failure	Numbers	Failure	No failure	Numbers
E1	32	68	100	23	27	50
E2	46	104	150	23	27	50
E3	64	136	200	23	27	50
E4	32	68	100	35	65	100
E5	46	104	150	35	65	100
E6	64	136	200	35	65	100
E7	87	163	250	35	65	100
E8	32	68	100	58	92	150
E9	46	104	150	58	92	150
E10	64	136	200	58	92	150

Table 2 shows the success ratio is improved when the number of training data sets increases. However, a large number of forecasting data sets in the output layer will decrease the accuracy with the same training data sets. Figs. 6 and 7 present the training and forecasting results of Cases E3 and E10. In these figures, dashed lines denote the results of BPN, solid lines are measured data. As seen in the Figs. 6 and 7, the Case E3 of training and forecasting result agrees with the observation. Thus the neural network structures for 200 training data sets and 50 forecasting data sets (Case E3) are recommended in this study because of the satisfactory prediction performance.

**Table 2 Performance of the neural network structures with different training data sets and forecasting data sets.**

Case	Training data sets	Forecasting data sets	Number of Neurons	$\eta$	$\alpha$	Epoch	Success ratio
E1	100	50	6	0.01	0.9	18000	80(%)
E2	150	50	6	0.01	0.9	18000	86(%)
E3	200	50	6	0.01	0.9	18000	92(%)
E4	100	100	6	0.01	0.9	18000	70(%)
E5	150	100	6	0.01	0.9	18000	80(%)
E6	200	100	6	0.01	0.9	18000	82(%)
E7	250	100	6	0.01	0.9	18000	87(%)
E8	100	150	6	0.01	0.9	18000	66(%)
E9	150	150	6	0.01	0.9	18000	71(%)
E10	200	150	6	0.01	0.9	18000	78(%)

The number of neurons in the hidden layer also affects the performance of the BPN. Figure 8 shows the success ratio for various neurons structures. It shows that the forecasting performance of the BPN is improved when the number of neurons increases. However, a large number of neurons in the hidden layer decrease the accuracy owing to over-learning. Thus, the number of neurons in the hidden layer is recommended to be six because of the satisfactory prediction performance.

The value of the learning rate ( $\eta$ ) significantly affects the convergence of neural network learning algorithm and the momentum factor ( $\alpha$ ) is used to avoid stopping the learning process at a local minimum instead of global

minimum (Jacobs, 1988). To have a better performance, either low  $\eta$  or high  $\alpha$  is expected to accelerate the convergence of the training process. Based on some preliminary tests, there is the highest success ratio (86%) at the learning rate of 0.01 and a momentum factor of 0.9, which are shown Figs. 9 and 10.

As for the number of training iterations affects the performance of the ANN, it can be found that the number of training iterations is equal to 18000 has the good performance from 10000 to 25000 (Fig. 11). Thus the neural network parameters listed in Table 2 is recommended in this study for assessment the highway slope failure.

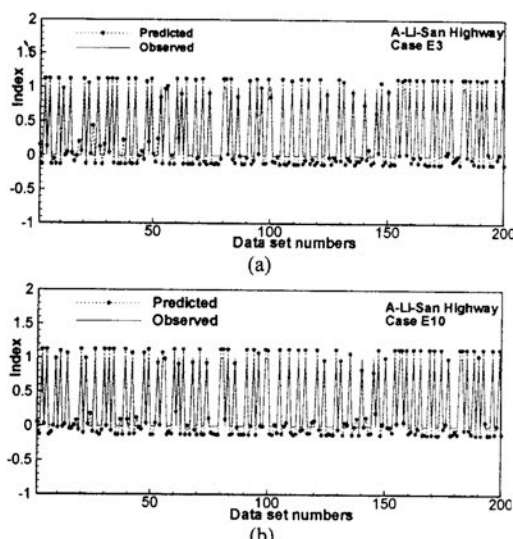


**Fig. 6 The training results of Cases E3 and E10 versus the observation.**

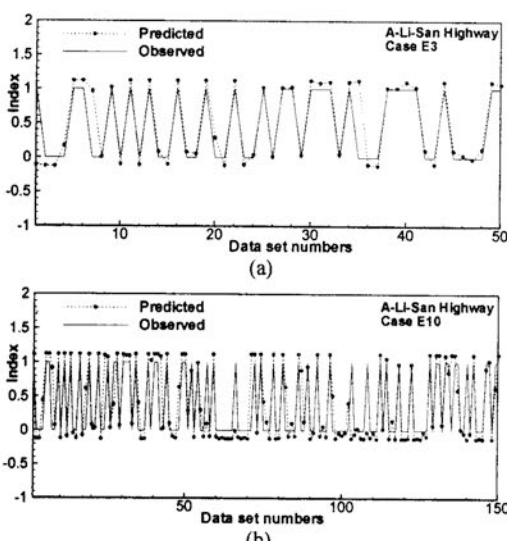


**Fig. 7 The forecasting results of Cases E3 and E10 versus the observation.**

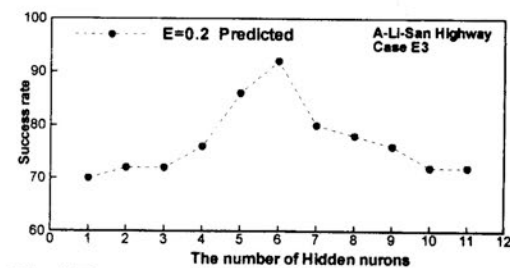


**Fig. 8 The success ratio for various neurons structures in the hidden layer.**

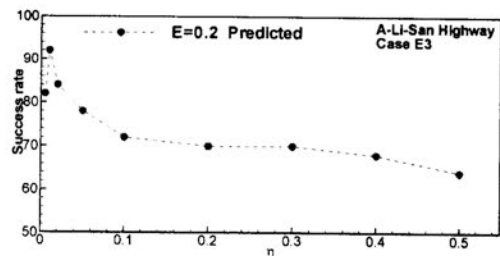


**Fig. 9 The success ratio for different learning factors.**

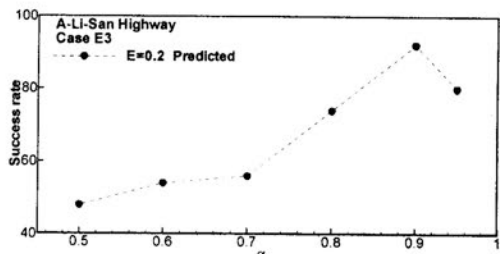


**Fig. 10 The success ratio for different momentum factors.**

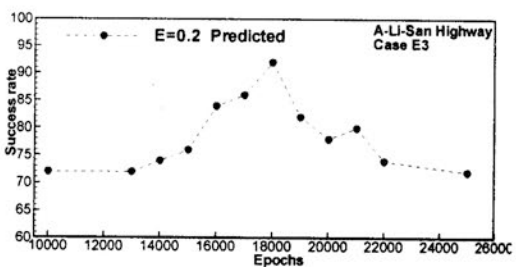


**Fig. 11 The success ratio for different training iterations.**

#### Determination the Influence Factors of Highway Slopes

In general, the influence factors of highway slopes include the slope gradient angle, slope height, cumulative precipitation, daily rainfall, surface acceleration, strength of material, slope direction and earthquake magnitude. Using more the influence factors, the accuracy of the prediction of highway slopes failure will certainly be enhanced. However, there are many factors cannot easily obtained in site after passing complex analysis. Therefore, appropriate influence

factors must be determined in this paper. First, we depend on the influence degree of highway slopes failure using artificial neural network to determine the main factors. Secondly, everyone influence factors will be considered the contribution ratio after deleting itself.

In order to conduct an influence factors analysis from Table 3, eight factors, including slope gradient angle, slope height, cumulative precipitation, daily rainfall, surface acceleration, strength of material, slope direction and earthquake magnitude, are selected. For example, in the F1 Case study, only seven the influence factors, slope height, cumulative precipitation, daily rainfall, surface acceleration, strength of material, slope direction and earthquake magnitude, were used while the factor of slope gradient angle typhoon was not considered in the BPN model.

From the Table 3, we can found that Case F1 is to delete the factor of slope gradient angle and its contribution ratio is 18%, and the success ratio of prediction is only 74%. In other word, this factor of slope gradient angle plays an important key for the evaluation of slope failure potential.

As for the other cases, the success ratio and its contribution ratio of prediction for every factor are illustrated in Table 3. From the table, we also found that Case F8 is to delete the factor of slope direction and its contribution ratio is only 6%. Therefore, we will delete this factor in next step.

Table 4 presents the analysis results of seven influence factors. We can find that the earthquake magnitude only has a minor effect on efficiency of the network (e.g. its contribution ratio is only 2%).

As for using six influence factors (e.g. slope gradient angle, slope height, cumulative precipitation, daily rainfall, surface acceleration and strength of material) to analysis, it can be found that the contribution ratio of deleting daily rainfall (Case H4 from Table 5) is 4%. Obviously, the importance of daily rainfall is smaller than rainfall cumulative precipitation to the landslide. This result is same with Crosta and Frattini (2003). Moreover, its success ratio still can be more than 80%, and its training and prediction result are shown in Fig. 12.

**Table 3 Testing result of using eight influence factors.**

Case	Delete the factor	Success ratio	Contribution ratio for deleted factor
F1	Slope gradient angle	74%	18%
F2	Slope height	76%	16%
F3	Cumulative precipitation	72%	20%
F4	Daily rainfall	78%	14%
F5	Surface acceleration	72%	20%
F6	Strength of material	78%	14%
F7	Earthquake magnitude	82%	10%
F8	Slope direction	86%	6%

**Table 4 Testing result of using seven influence factors.**

Case	Delete the factor	Success ratio	Contribution ratio for deleted factor
G1	Slope gradient angle	74%	12%
G2	Slope height	74%	12%
G3	Cumulative precipitation	72%	14%
G4	Daily rainfall	76%	10%
G5	Surface acceleration	72%	14%
G6	Strength of material	74%	12%
G7	Earthquake magnitude	84%	2%

**Table 5 Testing result of using six influence factors.**

Case	Delete the factor	Success ratio	Contribution ratio for deleted factor
H1	Slope gradient angle	70%	14%
H2	Slope height	72%	12%
H3	Cumulative precipitation	68%	16%
H4	Daily rainfall	80%	4%
H5	Surface acceleration	74%	10%
H6	Strength of material	78%	6%

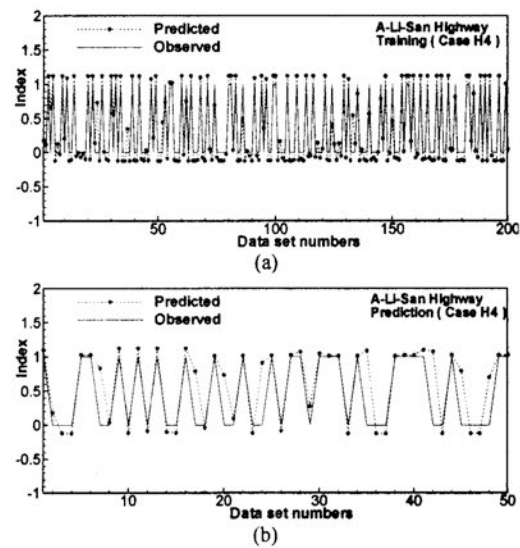


**Fig. 12 The training and prediction result of Case H4.**

Additionally, comparing the prediction results of Case E3 (eight influence factors) and Case H4 (five influence factors) are shown on Table 6. From the table, we can find that the success ration of these two cases is quite high, such as Case E3 is 92%, while Case H4 is 80%.

**Table 6 Comparisons between Case E3 and Case H4 predicted the success ratio of slope failure.**

Case	Case E3	Case H4
The factor of input parameters	Slope gradient angle, Slope height, Cumulative Precipitation, Daily rainfall, Surface acceleration, Strength of material, Slope direction, Earthquake magnitude	Slope gradient angle, Slope height, Cumulative Precipitation, Surface acceleration, Strength of material
The number of input parameters	8	5
Success ratio	92%	80%

## CONCLUSIONS

In this study, the back-propagation neural network for assessing the slope failure of highway is established. In addition, in site slope failure data at the A-Li-San Highway in southern Taiwan were used to test the performance of the present model. From the results for case study, there are two conclusions can be obtained as follows:

- (1) The traditional method on the research of slope failure at the highway often requires tedious test or experience formula to be conducted. In this investigation, the artificial back-propagation neural network with the gradient descent algorithm is adopted to predict the slope failure by learning and recalling processes using the five major factors.
- (2) On the premise of not influencing result of assessing, there are investigated by simplifying the influence factor in this paper. From the results for everyone factor, it can found that the good prediction of slope failure at the A-Li-San Highway and its success rate has 80% using slope gradient angle, slope height, cumulative precipitation, surface acceleration and strength of material.

## REFERENCES

- BATENI, S.M., JENG, D.S. and MELVILLE, B. W. (2007). Bayesian neural networks for prediction of equilibrium and time-dependent scour depth around bridge piers, *Advances in Engineering Software*, Vol. 38, No. 2, pp. 102-111.
- CAINE, N. (1980). The rainfall intensity-duration control of shallow landslides and debris flow. *Geografiska Annaler*, Vol.62, pp. 23-27.
- CAMPOLI, M., ANDREUSSI, P. and SOLDATI, A. (1997). River flood forecasting with a neural network model. *Water Resources Research*, Vol. 35, No. 4, pp. 1191-1197.
- CANNON, S.H. and ELLEN., S.D. (1985). Rainfall conditions for abundant debris avalanches in San Francisco bay region California. *California Geology*, Vol. 38, No. 12, pp. 267-272.
- COPPOLA JR. E., SZIDAROVSKY, F., POULTON, M., and CHARLES, E. (2003). Artificial neural network approach for predicting transient water levels in a multilayered groundwater system under variable state, pumping, and climate conditions, *Journal of Hydrologic Engineering*, Vol. 8, No. 6, pp. 348-360.
- DERIN N.U. and HASAN, S. (1998). Liquefaction Assessment by Artificial Neural Networks. *The Electronic Journal of Geotechnical Engineering*, No. 3.
- FELL, R. and HARTFORD, D. (1997). *Landslide risk management*. Balkema, Rotterdam, pp. 51-109.
- FRENCH, M.N., KRAJEWSKI, W.F. and CUYKENDALL, R.R. (1992). Rainfall forecasting in space and time using a neural network. *J. of Hydrology*, pp. 137, 1-31.
- INOUE, K. (2000). The prediction of soil movement for earthquake. *Earthquake Preventing Sand Erosion*, kokon in Japan, pp. 102-120.
- JACOBS, R.A. (1988). Increased rates of convergence through learning rate adaptation, *Neural Network*, Vol. 1, pp. 295-307.
- JENG, D.S., CHA, D.H. and BLUMENSTEIN, M. (2004). Neural Network model for the prediction of the wave-induced liquefaction potential in a porous seabed", *Ocean Engineering*, Vol. 31, No. 17-18, pp. 2073-2086.
- KEEFER (1987). Real-Time Landslide Warning during Heavy Rainfall. *Science*, Vol. 238, pp. 921-925.
- KENG, W.P. (1986). Geology of the area between Chushan and Chiayi, *Central Taiwan Bulletin of the Central Geological Survey*, Issue 4, pp. 1-26.
- LEE, T.L. (2006). Neural Network Prediction of a Storm Surge, *Ocean Engineering*, Vol. 33, No. 3-4, pp. 483-494.
- LEE, T.L. (2008). Back-propagation neural network for the prediction of the short term storm surge in Taichung harbor, Taiwan, *Engineering Applications of Artificial Intelligence*, Vol. 21, pp.63-72.
- LEE, T.L. and JENG, D.S. (2002). Application of artificial neural networks in tide forecasting. *Ocean Engineering*, Vol. 29, No. 9, pp. 1003-1022.
- LEE, T.L. (2004). Back-propagation neural network for long-term tidal predictions. *Ocean Engineering*, Vol. 31, No. 9, pp. 225-238.
- LEE, T.L., JENG, D.S., LIN C. and SHIEH, S.J. (2002). Assessment of earthquake-induced liquefaction by artificial neural networks, *The 9<sup>th</sup> International Conference for Computing in Civil and Building Engineering*, Taipei, Taiwan, R.O.C, pp. 55-60.
- LEE, S., RYU, J., MIN, K. and WON, J. (2001). Development of two artificial neural network methods for landslide susceptibility analysis. *Geoscience and Remote Sensing Symposium*, Vol. 5, pp.2364-2366.

- LEE, D.H., LIN, H.M. FANG, S.C. and WU, P.H. (2001). Investigations on highway slope failure induced by typhoon Toraji in the Ali-San area, *Conference of the Debris Flow Preventions*, Tainan, Taiwan, pp. 41-56. (In Chinese)
- LIN, C.W. (1998). The geologic structures and fault at Rueili, *Conference of the geologic structures and fault at 1998*, Taiwan, pp. 3-19. (In Chinese)
- LIAO, H.W. (2000). Landslides triggered by Chi-Chi earthquake. Master's thesis, Institute of Geophysics, National Central University.
- MAKARYNSKYY, O. (2005). Artificial neural networks for wave tracking, retrieval and prediction, *Pacific Oceanography*, Vol. 3, No. 1, pp. 1-30.
- MASE, H. (1995). Evaluation of artificial armour layer stability by neural network method, *Proceedings of the 26<sup>th</sup> IAHR Congress*, London, pp. 341-343.
- RUMELHART, D.E., HINTON, G.E. and WILLIAMS, R.J. (1986). Learning representations by back-propagating errors. *Nature*, No. 323, pp. 533-536.
- TSAI, C.P. and LEE, T.L. (1999). Back-propagation neural network in tidal-level forecasting, *ASCE Journal of Waterway, Port, Coastal and Ocean Engineering*, Vol. 12, No. 4, pp. 195-202.
- WASOWSKI, J. (1998). Understanding rainfall-landslide relationships in man-modified environments: a case-history from Caramanico Terme, Italy. *Environmental Geology* Vol. 35, No. 3, pp. 197-209.

# ANALYTICAL SOLUTIONS FOR PASSIVE EARTH PRESSURE CONSIDERING DIFFERENT FAILURE MECHANISMS WITH NONLINEAR FAILURE CRITERION

X.L. Yang<sup>1</sup> and J. H. Yin<sup>2</sup>

**ABSTRACT:** The analytical solutions to passive earth pressure, using Rankine's theory and upper bound theorem, are often based on a linear Mohr-Coulomb failure criterion. However, numerous experimental evidences show that the strength envelopes of almost all geomaterials have the nature of nonlinearity. In this paper, the backfill failure follows a nonlinear failure condition. Analytical solutions for passive earth pressure are derived with the nonlinear failure criterion using two different methods. One is based on kinematical approach of limit analysis. An improved method using a generalized tangential technique to approximate the nonlinear failure criterion is employed to estimate the passive earth pressure. One-rigid-body translation and one-rigid-body log-spiral rotation failure mechanisms are considered and the formulation of the passive earth pressure is a classical nonlinear programming problem. A nonlinear sequential quadratic programming algorithm is used to search for the lowest solutions. The other is based on Mohr's circle analysis. Extended Rankine's solution for passive earth pressure is derived with the nonlinear failure criterion. The upper bound solutions using the rigid translation failure mechanism are equal to extended Rankine's theoretical solutions, but are slightly more than those using the rigid rotation failure mechanism. A study is carried out to illustrate the effects of the nonlinear coefficient and material parameters on the passive earth pressure with the nonlinear failure criterion.

**Keywords:** analytical solutions, passive earth pressure, nonlinear failure criterion, optimization

## INTRODUCTION

The problem associated with passive earth pressure acting on retaining wall is one of the topics in civil engineering field, and a segment of soil mechanics that has been widely studied in the previous literature. Although much research had been performed and appreciable advancement made in the past regarding the distribution of earth pressures and on the analysis of a wide range of earth-retaining structures, some theories, such as Coulomb earth pressure in 1776 and Rankine earth pressure in 1857, still remain as the fundamental approaches to the analysis of most earth-supporting structures. For a vertical and smooth retaining wall with a horizontal backfill, the well-known Rankine's passive earth pressure  $P_p$ , which depends on the internal friction angle  $\phi$  and the cohesion  $c$  of the backfill soil, can be expressed as:

$$P_p = \frac{1}{2} \gamma H^2 \tan^2(45^\circ + \frac{\phi}{2}) + 2cH \tan(45^\circ + \frac{\phi}{2}) \quad (1)$$

where  $H$  is the height of retaining wall, and  $\gamma$  is the unit weight of backfill. The analytical solution of Eq. (1) is derived using a linear Mohr-Coulomb (MC) failure criterion, which is known as Rankine solution. Zhu and Qian derived the passive earth pressure coefficients using limit equilibrium method and a linear MC failure criterion (Zhu and Qian, 2000). However, the analytical solution of Eq. (1) and solution of Zhu and Qian(2000) is significantly less dependable for the soils obeying a nonlinear failure criterion.

Analytical solutions for any practical engineering problem are very valuable and important in the field of mechanics research. From the mechanics point of view, analytical solutions have the following advantages: (1) any numerical method has to be validated before it is put into applications, and analytical solution can provide a powerfully credible tool to validate the result using numerical method; (2) analytical solution can provide a better understanding of physical meaning for practical engineering problems. Using nonlinear failure criterion, Yang and Yin (2004) developed the analytical solution for static stability of soil slopes. Yang et al.(2004) also developed the analytical solution for seismic stability of rock slopes. Recently, Soon and Drescher (2007) explored the effect of nonlinearity of the failure criterion on the passive thrust, and they focused on smooth and rough walls. However, to the best knowledge of the author, analytical solutions for passive earth pressure with nonlinear failure criterion are not available in the previous literature. Therefore, in this paper, using One-rigid-body translation and one-rigid-body log-spiral rotation failure mechanisms, analytical solutions for passive earth pressure are derived with a nonlinear failure criterion in the framework of limit analysis of plasticity, and extended Rankine's solutions are used to validate the upper bound solutions. From the comparison of the results between them, it is found that the upper bound solutions using the translation failure mechanism are equal to extended Rankine theoretical solutions, and are slightly more than those using the log-spiral rotation failure mechanism by less than 3%, which indicates the analytical solutions are effective. This paper extends the calculations of the passive earth pressure in previous literature using a linear failure criterion to that using a nonlinear failure criterion.

## NONLINEAR FAILURE CRITERION

The previous literature associated with earth pressure analysis is focused on the linear MC failure criterion or the

<sup>1</sup>Department of Civil and Architectural Engineering, Changsha Railway College, The Central South University, Hunan 410075, China (Corresponding author: yangxl@mail.csu.edu.cn)

<sup>2</sup>Department of Civil and Structural Engineering, The Hong Kong Polytechnic University, Hung Hom, Kowloon, Hong Kong, China

von Mises failure criterion. However, experiments have shown that the strength envelopes of soils have the nature of nonlinearity. The friction angle decreases in most soils, and particularly granular soils, with increasing confining pressures, and Mohr's envelope is curved. In the past, various strength envelopes have been proposed to represent nonlinear strength envelopes for soils. Therefore, the effects of nonlinearity on passive earth pressure should be considered when the soil behind the wall follows a nonlinear failure criterion. For example, Lefebvre used a bilinear envelope to approximate the nonlinear failure criterion (Lefebvre, 1981). Mello approximated the nonlinear failure criterion using a tri-linear envelope (Mello, 1997). A simple power-law relation of the form  $\tau = A\sigma_n^{1/m}$  was given in the literature where the parameters A and m were constants (Mello De, 1997; Maksimovic, 1989; Perry, 1994 and Baker, 2004). Nonlinear failure criteria for geomaterials are widely used in engineering (Hoek, 1983; Hoek And Brown, 1997 and Zhang and Chen, 1987). In general, a nonlinear failure criterion can be expressed as (Zhang and Chen, 2001)

$$\tau = c_0(1 + \sigma_n/\sigma_i)^{1/m} \quad (2)$$

where  $\sigma_n$  and  $\tau$  are the normal and shear stresses on the failure surface respectively, and the parameter values of  $c_0$ ,  $\sigma_i$  and  $m$  are determined by triaxial tests. When  $m=1$ , Eq. (2) reduces to the well-known linear MC failure criterion. If a stress state represented by a vector from the origin is increased from zero, yielding will happen when the vector reaches the curve in the  $(\sigma_n, \tau)$  space. By introducing a mobilized internal friction angle  $\phi_i$  as an intermediate variable, since  $\tan \phi_i = d\tau/d\sigma_n$ , the normal stress  $\sigma_n$  and shear stress  $\tau$  of the nonlinear failure criterion can be expressed as (Yang and Yin, 2004)

$$\left. \begin{aligned} \sigma_n &= \sigma_i \left( \frac{m\sigma_i \tan \phi_i}{c_0} \right)^{\frac{1}{m}} - \sigma_i \\ \tau &= c_0 \left( \frac{m\sigma_i \tan \phi_i}{c_0} \right)^{\frac{1}{m}} \end{aligned} \right\} \quad (3)$$

The tangential line to the curve at the location of tangency point M as shown in Fig. 1 is expressed as

$$\tau = c_i + \sigma_n \tan \phi_i \quad (4)$$

where  $c_i$  is the intercept of the straight line on the  $\tau$ -axis. The  $c_i$  is determined by the following form:

$$c_i = \frac{m-1}{m} c_0 \left( \frac{m\sigma_i \tan \phi_i}{c_0} \right)^{\frac{1}{m}} + \sigma_i \tan \phi_i \quad (5)$$

#### PASSIVE EARTH ANALYSIS

Recently, the upper and lower bound theorems of limit analysis are widely used to determine the stability problems. The unknown quantity of the stability problems may be the bearing capacity of foundations, the earth pressures on retaining walls or the stability factors of slopes. By using

the two theorems, the range, in which true solution falls, can be found. This range can be narrowed finding the highest possible lower bound solution and the lowest possible upper bound solution (Hoek, 1983; Hoek and Brown, 1997; Zhang and Chen, 1987 and Wang et al., 2001). The upper bound theorem, which assumes a perfectly plastic soil model, states that the internal energy dissipated by any kinematically admissible velocity field can be equated to the work done by external loads, and so enables a strict upper bound on the actual solution to be deduced. The lowest possible upper bound solution is sought with an optimization scheme by trying various possible kinematically admissible failure mechanisms. A kinematically admissible velocity field is one that satisfies compatibility, the flow rule and the velocity boundary conditions. The lower bound theorem, which also assumes a perfectly plastic soil model, considers stress fields which are in equilibrium with surface tractions and body forces, and do not violate the failure criterion anywhere in the soil mass, as shown in Yang et al. The application of the lower bound theorem will provide a lower bound estimation of the true solution (Yang et al., 2004). The highest possible lower bound solution can be sought by trying various possible statically admissible stress fields. In this paper, the kinematical approach is used, and the following assumptions have been made:

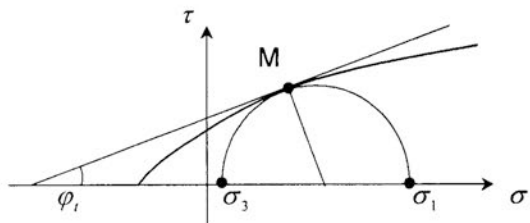


Fig. 1 Nonlinear failure criterion

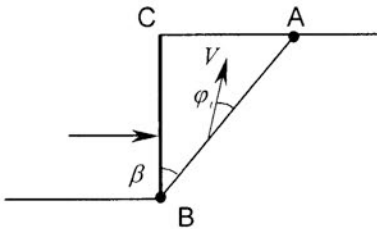


Fig. 2 Translation failure mechanism for passive earth pressure

- (a). The backfill is homogeneous and isotropic material, and frictional forces between the retaining wall and the backfill are assumed negligible.
- (b). The rigid wall is vertical, and the surface of the backfill is horizontal.
- (c). The backfill failure is obeyed by a nonlinear failure criterion. The sliding surface is assumed to be a plane for translation failure mechanism, a log-spiral surface for rotation failure mechanism.

In above assumptions, (a) and (b) agree with the assumptions of Rankine in 1857. The only difference is that a nonlinear failure criterion is used in the present analysis rather than a linear MC failure criterion

### Generalized Tangential Technique

A limit load computed from a convex failure surface, which always circumscribes the actual failure surface, will be an upper bound on the actual limit load (Chen, 1975). This is due to the fact that the strength of the convex failure surface is equal to or larger than that of the actual failure surface. A tangential line to the nonlinear failure criterion at Point  $M$  is used and shown in Fig. 1. From Fig. 1, it can be seen that the strength of the tangential line equals or exceeds that of the nonlinear failure criterion at the same normal stress. Thus, the linear failure criterion represented by the tangential line will give an upper bound on the actual load for the material, whose failure is governed by the nonlinear failure criterion. In order to ensure that the tangential line always lies outside of the curve, and that the strength corresponding to the tangential line is more than or equal to the strength corresponding to the nonlinear curve, the requirement  $m > 1$  is to be satisfied. In the present study, the linear failure criterion, which is always tangential to the curve of the nonlinear failure criterion shown in Fig. 1, is adopted for upper bound analysis.

Based on upper bound theorem, the kinematical admissibility condition requires that the failure surface for a rigid collapse must be a log-spiral surface or plane surface, and that the velocity inclines the velocity discontinuity line at a constant angle for the linear MC failure criterion. Similar to the linear MC failure criterion, the velocity at velocity discontinuity for a soil following a nonlinear failure criterion inclines at an angle, tangential angle  $\varphi_t$ , with respect to the velocity discontinuity line. The tangential angle  $\varphi_t$  varies at different normal stresses, which implies that the normal strain rate relates to the shearing strain rate at the velocity discontinuity by the form  $\dot{\epsilon}/\dot{r} = -\tan \varphi_t$  is also varying. Thus, the rate of energy dissipation per unit volume  $\dot{D}$  along the velocity discontinuity takes the form by

$$\dot{D} = \tau V \cos \varphi_t - \sigma_n V \sin \varphi_t \quad (6)$$

The velocity  $V$  involved in Eq. (6) inclines the velocity discontinuity line at the tangential angle  $\varphi_t$ . From Eq. (6), it can be seen that the expression of the rate of energy dissipation involves three variables of the shear stress  $\tau$ , normal stress  $\sigma_n$  and tangential angle  $\varphi_t$ . If the value of  $\varphi_t$  is given, then the values of  $\tau$  and  $\sigma_n$  can be determined by Eq. (3) using its shear failure envelop. Thus, the internal energy dissipation rate in Eq. (6) only involves one variable  $\varphi_t$ . To avoid the difficulty of calculation of energy dissipation rate, the tangential line (a linear MC failure criterion) is employed to evaluate energy dissipation rate, such, the inclined angle  $\varphi_t$  along the entire slip surface (velocity discontinuity) is unchangeable, but its value is unknown. Therefore, the rate of energy dissipation in Eq. (6) becomes similar to that for a soil obeying the linear MC failure criterion as proposed by Chen (Chen, 1975). The difference is that the value of  $\varphi_t$  is unknown in Eq. (6) for the nonlinear failure criterion rather than the known value of internal friction angle for the linear MC failure criterion.

### Earth Pressure Formulation (Translation)

Based on upper bound theorem, a translation failure mechanism is used to obtain the passive earth pressure for a smooth vertical wall with a horizontal backfill, as shown in Fig. 2. The passive earth pressure corresponds to an inward motion of the wall. Therefore, the soil weight is assumed to be act as a wedge moving up and inward along the sliding surface  $AB$ . This mechanism is a compatible velocity field for an upper bound solution, since the velocity  $V$  of the soil mass  $ABC$  is at an angle  $\varphi_t$  to the discontinuity line  $AB$ . The rate of external work is composed of two parts, the rate of work done by the soil weight moving up and inward and the rate of work done by the passive earth pressure  $P_p$  moving horizontally:

$$-0.5\gamma H^2 \tan \beta \cdot V \cos(\beta - \varphi_t) + P_p V \sin(\beta - \varphi_t) \quad (7)$$

Assuming that a smooth wall which implies that no energy dissipated along the surface between wall and backfill, the rate of internal energy is only dissipated along the discontinuity line  $AB$ , which is:

$$c_t V \cos \varphi_t \cdot H / \cos \beta \quad (8)$$

Equating the rate of internal energy dissipation to the rate of the external work, we can obtain:

$$P_p = \frac{0.5\gamma H^2 \sin \beta \cos(\beta - \varphi_t) + c_t H \cos \varphi_t}{\cos \beta \sin(\beta - \varphi_t)} \quad (9)$$

where  $c_t$  is determined by Eq. (5). By the upper bound theorem of limit analysis, Eq. (9) gives an upper bound for the critical value of the passive earth pressure. The function  $P_p(\beta, \varphi_t)$  has two variables  $\beta$  and  $\varphi_t$ . Herein, we employ the sequential quadratic programming to optimize the objective function of Eq. (9) with respects to  $\beta$  and  $\varphi_t$  to get the minimum value of passive earth pressure.

### Earth Pressure Formulation (Rotation)

The rotational log-spiral discontinuity mechanism for the present analysis is shown in Fig. 3. The region  $DEF$  rotates as a rigid body about the center of rotation  $O$  with the material below the logarithmic spiral surface remaining at rest. Due to the usage of the tangential line (a linear MC failure criterion), the angle  $\varphi_t$  along the entire slip surface is unchangeable (its value being unknown), such, the  $c_t$  is also unchangeable along the entire slip surface according to Eq. (5). By equating the energy dissipation rate along the velocity discontinuity line to the work rate of the external forces in any kinematically admissible velocity will lead to a limit load that is not less than or at most equal to the actual limit load. The best upper bound solutions are obtained by optimization. The homogeneous soil masses being rigid, the internal energy is only dissipated along the sliding surface, while the external rate of work is done by passive earth pressure and the soil mass weight bounded by the boundary line  $DEF$  and the log-spiral sliding surface. The rate of work due to the soil mass weight can be expressed as

$$\dot{W}_{\text{soil}} = -\gamma r_0^3 \dot{\omega} [f_1 - f_2 - f_3] \quad (10)$$

where the  $\dot{\omega}$  = angular velocity. The  $f_1 - f_3$  are non-dimensional functions, which depend on geometry parameters  $\theta_h$ ,  $\theta_o$  and tangential line angle  $\varphi_t$ . The definitions of those geometrical parameters  $\theta_h$ ,  $\theta_o$  and  $\varphi_t$  can be found in Fig. 1 and Fig. 3. The expressions for  $f_1 - f_3$  are reported in the Appendix of this paper. The rate of work due to the passive earth pressure can be expressed as

$$\dot{Q}_p = P_p r_0 \dot{\omega} f_4 \quad (11)$$

where the  $f_4$  is a non-dimensional function, which is reported in the Appendix of this paper. For the rigid material considered, the internal energy is only dissipated along the log-spiral sliding surface. The rate of energy dissipation  $\dot{W}_{\text{int}}$  can be expressed as

$$\dot{W}_{\text{int}} = c_i r_0^2 \dot{\omega} f_5 \quad (12)$$

where the  $f_5$  is a non-dimensional function, which is reported in the Appendix of this paper. Equating the work rate of external forces to the internal energy dissipation rate, we can obtain:  $\dot{W}_{\text{soil}} + \dot{Q}_p = \dot{W}_{\text{int}}$ . Substituting the expressions for  $\dot{W}_{\text{soil}}$ ,  $\dot{Q}_p$  and  $\dot{W}_{\text{int}}$  into it, we can obtain:

$$P_p = [c_i r_0 f_5 + \gamma r_0^2 (f_1 - f_2 - f_3)] / f_4 \quad (13)$$

In the preceding discussion, Eq. (13) is obtained using the assumption that failure surface follows the shape of a log-spiral. The location of the log-spiral is controlled by two parameters,  $\theta_h$  and  $\theta_o$ , that are regarded as two variables. The location of tangency point  $M$  is controlled by one parameter,  $\varphi_t$ , that is also regarded as a variable. We employ the sequential quadratic programming to optimize the objective function (13) with respect to  $\theta_h$ ,  $\theta_o$  and  $\varphi_t$ , to get the lowest solution of the passive earth pressure.

#### EXTENDED RANKINE THEORETICAL SOLUTION

Some research data and experience indicate that assumptions related to pressure distributions on the retaining walls, or on the failure surface of backfill, are not quite those depicted by these early investigators, but substantial evidences show that the analysis and design efforts based on their theories give acceptable results for ( $\phi$ - $\phi$ ) backfill. The basic concept behind Rankine's theory can be depicted via Mohr's circle. Herein, the Mohr circle may be used to estimate the passive earth pressure on the retaining wall with the backfill soil whose shear strength may be governed by Eq. (2). We consider a vertical and smooth retaining wall with a horizontal backfill soil surface. At a given depth  $z$  on the element shown in Fig. 4, the vertical stress (minor principal stress)  $\sigma_3$  is equal to  $\gamma z$ . The horizontal stress (major principal stress)  $\sigma_1$  is unknown. The corresponding Mohr circle for this case is shown in Fig. 1. From Fig. 1, we can obtain the magnitude

of the shear and normal stresses at the tangency point  $M$ :

$$\left. \begin{aligned} \sigma_n &= \frac{\sigma_1 + \gamma z}{2} - \frac{\sigma_1 - \gamma z}{2} \sin \varphi_t \\ \tau &= \frac{\sigma_1 - \gamma z}{2} \cos \varphi_t \end{aligned} \right\} \quad (14)$$

Combining Eqs. (14) and (3), we can obtain the following expression:

$$\left. \begin{aligned} \frac{\sigma_1 - \gamma z}{2} \cos \varphi_t &= c_0 \left( \frac{m \sigma_1 \tan \varphi_t}{c_0} \right)^{\frac{1}{m}} \\ \frac{\sigma_1 + \gamma z}{2} - \frac{\sigma_1 - \gamma z}{2} \sin \varphi_t &= \sigma_1 \left( \frac{m \sigma_1 \tan \varphi_t}{c_0} \right)^{\frac{m}{m+1}} - \sigma_1 \end{aligned} \right\} \quad (15)$$

In Eq. (15), if the material parameter values of  $m$ ,  $c_0$ ,  $\sigma_1$  and  $\gamma$  are given, there are three variables,  $\sigma_1$ ,  $z$  and  $\varphi_t$ , and two equations. Solving the two equations, we can get the expression of  $\sigma_1(z)$ . The corresponding resultant  $P_p$  is

$$P_p = \int_0^H \sigma_1(z) dz \quad (16)$$

Passive earth pressure is obtained from Eq. (16) with the nonlinear failure criterion.

#### NUMERICAL RESULTS

Numerical results are obtained for the smooth and vertical retaining walls with the sliding surface being a plane and a log-spiral surface respectively. These results are summarized in Tables 1 and Table 2. Example problems are selected to include the following: (a) comparisons are made between the solutions obtained from the upper bound approach (translation and rotation) and the solutions obtained from the extended Rankine's theory, and (b) effects of nonlinear coefficient  $m$ , initial cohesion  $c_0$  and tensile stress  $\sigma_t$  on the passive earth pressure are studied.

#### Comparison

The smooth and vertical retaining wall with a horizontal backfill is analyzed using both the present upper bound method and the extended Rankine's theory. For the translation failure mechanism shown in Fig. 2, upper bound solutions are obtained by minimizing Eq. (9) with respects to  $\beta$  and  $\varphi_t$ . For the rotation failure mechanism shown in Fig. 3, upper bound solutions are obtained by minimizing Eq. (13) with respects to  $\theta_h$ ,  $\theta_o$  and  $\varphi_t$ . Extended Rankine theoretical solutions are obtained by using Eq. (16). Table 1 presents the values of passive earth pressures for  $\gamma=18.0 \text{ kN/m}^3$ ,  $H=4.0 \text{ m}$ ,  $c_0=90 \text{ kPa}$  and  $\sigma_t=247.3 \text{ kPa}$ , with the nonlinear coefficient,  $m$  varying from 1.2 to 2.0 (Example One). Table 2 presents the values of passive earth pressures for  $\gamma=18.0 \text{ kN/m}^3$ ,  $H=4.0 \text{ m}$ ,  $c_0=50 \text{ kPa}$  and  $\sigma_t=200 \text{ kPa}$ , with the nonlinear coefficient  $m$  varying from 1.2 to 2.0 (Example Two).

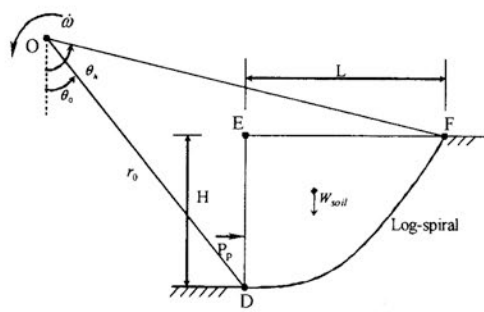


Fig. 3 Log-spiral rotational failure mechanism for passive earth pressure

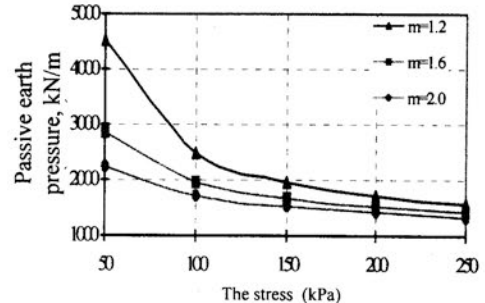


Fig.6 Influences of tensile stress on passive earth pressures ( $\gamma = 17.0 \text{ kN/m}^3$ ,  $H = 5.0 \text{ m}$ ,  $c_o = 90 \text{ kPa}$ )

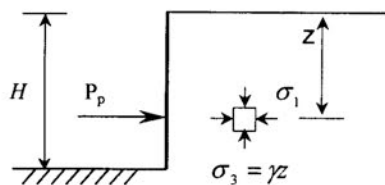


Fig. 4 Stress field for a vertical retaining wall

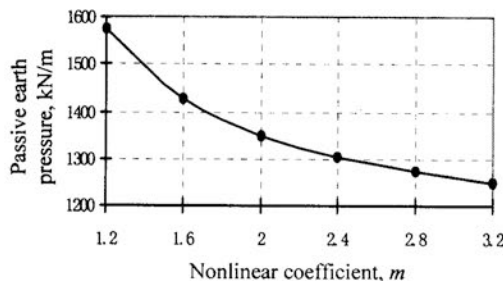


Fig. 5 Influences of nonlinear coefficient on passive earth pressures ( $\gamma = 17.0 \text{ kN/m}^3$ ,  $H = 5.0 \text{ m}$ ,  $c_o = 90 \text{ kPa}$ ,  $\sigma_t = 247.3 \text{ kPa}$ )

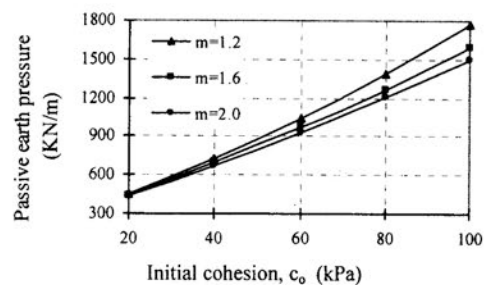


Fig.7 Influences of initial cohesion on passive earth pressures ( $\gamma = 17.0 \text{ kN/m}^3$ ,  $H = 5.0 \text{ m}$ ,  $\sigma_t = 247.3 \text{ kPa}$ )

Table 1. Comparison between upper bound solutions and Extended Rankine solutions (Example One)

	Coefficient $m$					
	1.2	1.4	1.6	1.8	2.0	
Upper bound solutions (kN/m)	Translation	1216.3	1149.7	1104.0	1070.8	1045.6
	Rotation	1186.9	1119.9	1074.1	1040.8	1015.6
Difference		29.4	29.8	29.9	30.0	30.0
Extended Rankine solutions (kN/m)		1216.3	1149.7	1104.0	1070.8	1045.6

( $\gamma = 18.0 \text{ kN/m}^3$ ,  $H = 4.0 \text{ m}$ ,  $c_o = 90 \text{ kPa}$  and  $\sigma_t = 247.3 \text{ kPa}$ )

Table 2. Comparison between upper bound solutions and Extended Rankine solutions (Example Two)

	Coefficient $m$					
	1.2	1.4	1.6	1.8	2.0	
Upper bound solutions (kN/m)	Translation	703.5	674.6	654.5	639.8	628.5
	Rotation	687.8	658.7	638.4	623.6	612.2
Difference		15.7	15.9	16.1	16.2	16.3
Extended Rankine solutions (kN/m)		703.5	674.6	654.5	639.8	628.5

( $\gamma = 18.0 \text{ kN/m}^3$ ,  $H = 4.0 \text{ m}$ ,  $c_o = 50 \text{ kPa}$  and  $\sigma_t = 200 \text{ kPa}$ )

It is found from Table 1 and Table 2 that the upper bound solutions using a translation failure mechanism are equal to extended Rankine theoretical solutions for the vertical retaining wall. The upper bound solutions using the translation failure mechanism are slightly more than those using the log-spiral rotation failure mechanism, with the maximum difference being less than 3%. Therefore, the generalized tangential technique is an effective technique for evaluating passive earth pressures with the nonlinear failure criterion. However, the approximation of the upper bound solutions using the rotation failure mechanism in Fig. 3, and the upper bound solutions using the translation failure mechanism in Fig. 2, does not mean both the velocity fields are the actual ones. It is surprising to find that the absolute difference between the solutions using the translation failure mechanism and the solutions using the log-spiral rotation failure mechanism is almost unchangeable when the nonlinear coefficient  $m$  varying from 1.2 to 2.0. For example, the absolute difference approximates or equals 30.0 kN/m for  $\gamma = 18.0 \text{ kN/m}^3$ ,  $H = 4.0 \text{ m}$ ,  $c_0 = 90 \text{ kPa}$  and  $\sigma_t = 247.3 \text{ kPa}$ , with the nonlinear coefficient  $m$  varying from 1.2 to 2.0.

#### Effects of Nonlinear Coefficient $m$

The values of the passive earth pressures corresponding to  $\gamma = 17.0 \text{ kN/m}^3$ ,  $H = 5.0 \text{ m}$ ,  $c_0 = 90 \text{ kPa}$ ,  $\sigma_t = 247.3 \text{ kPa}$  with the nonlinear coefficient  $m$  varying from 1.2 to 3.2 are illustrated in Fig. 5 using the translation failure mechanism. From Fig. 5, it can be seen that the nonlinear coefficient  $m$  has a significant influence on passive earth pressures. If the nonlinear failure criterion is reduced to a linear MC failure criterion  $m = 1.0$ , the present upper bound solutions agree well with Rankine theoretical results.

#### Effects of tensile stress $\sigma_t$

With the translation failure mechanism of kinematical approach, the numerical results of passive earth pressures are represented in Fig. 6 for  $\gamma = 17.0 \text{ kN/m}^3$ ,  $H = 5.0 \text{ m}$ ,  $c_0 = 90 \text{ kPa}$  and with  $\sigma_t$  varying from 50 kPa to 200 kPa, while the nonlinear coefficient  $m$  is equal to 1.2, 1.6 and 2.0. It is seen from Fig. 6 that passive earth pressures decrease significantly with increasing stress  $\sigma_t$ .

#### Effects of Initial Cohesion $c_0$

The values of passive earth pressures obtained from the translation failure mechanism of kinematical approach are shown in Fig. 7 for  $\gamma = 17.0 \text{ kN/m}^3$ ,  $H = 5.0 \text{ m}$ ,  $\sigma_t = 247.3 \text{ kPa}$  with  $c_0$  varying from 20 kPa to 100 kPa, while the nonlinear coefficient  $m$  is equal to 1.2, 1.6 and 2.0. It is seen from Fig. 7 that passive earth pressures increase with increasing initial cohesion,  $c_0$ .

In the preceding analysis of passive earth pressures, a smooth and vertical retaining wall with a flat backfill is assumed. The case where the inclined backfill or/and inclined wall is not considered in this paper. However, there is no difficulty in principle in extending this present method to deal with passive earth pressure problems with an inclined backfill or/and inclined wall.

## CONCLUSIONS

Considering the fact that almost all geomaterials have the nature of nonlinearity over wide range of normal stresses, the paper has focused the efforts on the derivation of analytical solution with a nonlinear failure criterion. An improved method using the tangential line (a linear failure criterion) to formulate the objective function is developed on the basis of the upper bound theorem of plasticity. For the one-rigid-body translation failure mechanism, applying a nonlinear sequential quadratic programming algorithm, upper bound solutions are obtained by minimizing the objective function (9) with respects to  $\beta$  and  $\varphi_t$ . For the one-rigid-body rotation failure mechanism, also applying the algorithm, upper bound solutions have been obtained by minimizing Eq. (13) with respects to  $\theta_h$ ,  $\theta_0$  and  $\varphi_t$ . Based on extended Rankine's theory, the solutions of passive earth pressure are presented using Eq. (16) with the nonlinear failure criterion. The upper bound solutions using the one-rigid-body translation failure mechanism are equal to extended Rankine theoretical solutions, and are slightly more than those using the one-rigid-body log-spiral rotation failure mechanism by less than 3%. Based on the analysis above, the following conclusions are drawn:

- (a).Based on the one-rigid-body translation and one-rigid-body log-spiral rotation failure mechanisms, it is found that the generalized tangential technique is an effective technique for evaluating passive earth pressure with the nonlinear failure criterion.
- (b).Analytical solutions for passive earth pressure are derived with the nonlinear failure criterion using two different methods for practical use in practical engineering.
- (c).Using the one-rigid-body failure mechanism with the nonlinear failure criterion, the effects of the nonlinear coefficient  $m$ , the tensile stress  $\sigma_t$  and the initial cohesion  $c_0$  have been investigated and discussed. It is found that the parameters  $m$ ,  $\sigma_t$  and  $c_0$  have large influences on the passive earth pressures.

## ACKNOWLEDGEMENTS

The preparation of the paper has received financial supports from the Foundation for the Author of National Excellent Doctoral Dissertation of China (No.200550) and the National Natural Science Foundation of China (No.50408020). The financial supports are greatly appreciated.

## Appendix

$$f_1 = \frac{(3 \tan \varphi_t \sin \theta_h - \cos \theta_h) \exp[3(\theta_h - \theta_0) \tan \varphi_t] - (3 \tan \varphi_t \sin \theta_0 - \cos \theta_0)}{3(1 + 9 \tan^2 \varphi_t)} \quad (A1)$$

$$f_2 = \frac{L}{r_0} \cos \theta_h \frac{\exp[(\theta_h - \theta_0) \tan \varphi_t]}{6} \left( 2 \sin \theta_h \exp[(\theta_h - \theta_0) \tan \varphi_t] - \frac{L}{r_0} \right) \quad (A2)$$

$$f_3 = \frac{1}{3} \frac{H}{r_0} \sin^2 \theta_0 \quad (A3)$$

$$f_4 = \cos \theta_0 - \frac{1}{3} \frac{H}{r_0} \quad (A4)$$

$$f_s = \frac{\exp[2(\theta_h - \theta_0) \tan \phi_i] - 1}{2 \tan \phi_i} \quad (A5)$$

$$\frac{H}{r_0} = \cos \theta_0 - \cos \theta_h \exp[(\theta_h - \theta_0) \tan \phi_i] \quad (A6)$$

$$\frac{L}{r_0} = \sin \theta_h \exp[(\theta_h - \theta_0) \tan \phi_i] - \sin \theta_0 \quad (A7)$$

## References

- AGAR J.G., MORGENSTERN N. and SCOTT J. (1985). Shear strength and stress-strain behavior of Athabasca oil sand at elevated temperatures and pressure. *Canadian Geotechnical Journal*, Vol. 24, No.1: pp. 1-10.
- BAKER R. (2004). Nonlinear Mohr envelopes based on triaxial data. *ASCE Journal of Geotechnical and Geoenvironmental Engineering*, Vol. 130, No. 5: pp. 498-506.
- CHEN W.F. (1975). *Limit Analysis and Soil Plasticity*. Amsterdam: Elsevier Science.
- HOEK E. (1983). Strength of jointed rock masses. *Geotechnique*, Vol. 33: 187-223.
- HOEK E. and BROWN E.T. (1997). Practical estimate the rock mass strength. *International Journal of Rock Mechanics and Mining Sciences*, Vol. 34: pp.1165-1186.
- LEFEBVRE G. (1981). Strength and slope stability in Canadian soft clay deposits. *Canadian Geotechnical Journal*, Vol. 18, No. 3: pp. 420-442.
- MAKSIMOVIC M. (1989). Nonlinear failure envelope for soils. *ASCE Journal of Geotechnical Engineering*, Vol. 115, No.4: pp. 581-586.
- MELLO De VBF (1997). Reflections on design decisions of practical significance to embankment dams—17th Rankine Lecture. *Geotechnique*, Vol. 27, No. 3: pp. 281-354.
- PERRY J. (1994). A technique for defining nonlinear shear strength envelopes and their incorporation in a slope stability method of analysis. *Quarterly Journal of Engineering Geology*, Vol. 27, No. 3:pp. 231-241.
- SOON S.C. and DRESCHER A. (2007). Nonlinear failure criterion and passive thrust on retaining walls. *International Journal of Geomechanics*, Vol. 7, No. 4: pp. 318-322.
- WANG Y.J., YIN J.H. and LEE C.F. (2001). The influence of a non-associated flow rule on the calculation of the factor of safety of the soil slopes. *International Journal for Numerical and Analytical Methods in Geomechanics*, Vol. 25: pp.1351-1359.
- YANG X.L. and YIN J.H. (2004). Slope stability analysis with nonlinear failure criterion. *ASCE Journal of Engineering Mechanics*, Vol. 130, No. 3, pp. 267-273.
- YANG X.L., LI L. and YIN J.H. (2004). Seismic and static stability analysis for rock slopes by a kinematical approach. *Geotechnique*, Vol. 54, No. 8: pp. 543-549.
- YU H.S., SALGADO R. and SLOAN S.W.(1998). Limit analysis versus limit equilibrium for slope stability. *ASCE Journal of Geotechnical and Geoenvironmental Engineering*, Vol. 124, No. 3: pp. 265-276.
- ZHANG X.J. and CHEN W.F. (1987). Stability analysis of slopes with general nonlinear failure criterion. *International Journal for Numerical and Analytical Methods in Geomechanics*, Vol. 11, No. 1: pp. 33-50.
- ZHU D.Y. and QIAN Q.H. (2000). Determination of passive earth pressure coefficients by the method of triangular slices. *Canadian Geotechnical Journal*, Vol. 37, no. 2, pp. 485-491.

# GEOTECHNICAL PROPERTIES OF SOIL-FIBER MIXTURE AS A LANDFILL COVER BARRIER MATERIAL

T. Harianto<sup>1</sup>, Y. J. Du<sup>2</sup>, S. Hayashi<sup>3</sup>, D. Suetsugu<sup>4</sup> and Y. Nanri<sup>5</sup>

**ABSTRACT:** In order to study the potential future uses of the landfill site for other applications (i.e. residential, park, etc.), some of the geotechnical properties need to be investigated when the landfill cover is used as a bearing layer during the post-closure period. The problem that could be encountered in the post-closure landfill is cracking due to the desiccation and differential settlement. An alternative solution to overcome this problem is the inclusion of polypropylene fibers ( $C_3H_6$ ) additives in the soil specimens. In this study, the investigation of the geotechnical properties such as compaction characteristics, unconfined compressive strength, tensile strength, and hydraulic conductivity were performed. It was found that the inclusion of fiber additive could improve the geotechnical properties of the soil specimens. The maximum dry density ( $\gamma_{dmax}$ ) of the soil-fiber mixtures increased. The compressive strength and ductility also significantly increased with the increase in the fiber content. Moreover, with the increase in the fiber content, the ductility in the post-peak region increased. The tensile strength of the soil-fiber mixture increased with the increase in the fiber content. The hydraulic conductivity tests showed that with the inclusion of fiber, the hydraulic conductivity of the soil-fiber mixtures change within acceptable levels. From the above tests, it has been concluded that fiber inclusion could significantly improve the geotechnical properties of landfill cover barrier material. The soil-fiber mixtures could be used as a landfill cover barrier material.

**Keywords:** Akaboku soil, fiber additive, compaction, strength, hydraulic conductivity, cover barrier, landfill

## INTRODUCTION

Landfill cover barrier systems have designed over the years using natural material or a combination of natural and synthetic materials. Since the compacted clay liner (CCL) soil have been widely used as a barrier system material to cover waste disposal sites for many years, their performance on the engineering properties have long been questioned such as the CCL must be as ductile as possible to accommodate differential settlement and must be resistant to cracking from moisture variation (i.e. desiccation). Therefore, to satisfy the functional requirement, analysis and design methods have been developed by researcher to evaluate the performance of the material used alone or in combination of soil mixtures.

The interest in using fibers has arisen to improve soil performance on the geotechnical properties of soil mixtures. The inclusion of fibers in soil specimens is expected to increase the soil strength and improve the stability if it is used as a bearing layer. Some researchers were conducted research by use randomly oriented discrete geosynthetic fiber to reinforced sand, such as Gray and Ohashi (1983), Park and Tan (2005) and Latha and Murthy (2007). Nataraj and McManis (1997) studied the strength and deformation characteristics of soil reinforced with randomly distributed fibers compared to natural soil. Tang et al. (2007) concluded that using fiber as reinforcement is advantageous attributed to increase in the strength, decrease in the stiffness and decrease in brittleness of soil-cement. Ziegler et al. (1998) found that with an inclusion of discrete

polypropylene fibers, the tensile strength of clays tend to increase and induce more ductile failures. The compaction path also significantly effected to the tensile strength (Ibarra et al., 2005). The polypropylene fibers have been found to increase the hydraulic conductivity of soil which is used as material for waste containment soil liners (Miller and Rifai, 2004). The study by Cai et al. (2006) reported that there is a significant improvement on the engineering properties of the fiber-lime treated soil. However, very few studies on the use of soil-fiber mixture as a material for landfill cover barrier have been reported. Harianto et al. (2007) found that with the fiber inclusion, soil could well resist desiccation crack problems, which are commonly encountered in the landfill cover system.

The purpose of this study is to evaluate geotechnical properties of the compacted soil-fiber mixture as an alternative material in landfill cover barrier system. Knowledge of geotechnical properties of the compacted soil-fiber mixtures is required to asses the design of landfill cover barrier system. The parameters for the design of cover barrier layer such as compaction characteristic, unconfined compressive strength, tensile strength and hydraulic conductivity were investigated to evaluate the suitability of the soil-fiber mixture being used as a material for landfill cover barrier system. The effect of the fiber content on the compaction properties, shear strength, tensile strength, and hydraulic conductivity of the compacted soils were discussed.

## MATERIALS AND METHOD

### Materials

The soil used in this study was locally obtained from Kumamoto Prefecture, Kyushu region of Japan. The basic properties of soil such as grain size analysis, specific gravity of soil solids and Atterberg limits (liquid limit, plastic limit and shrinkage limit) were determined according to standard practice the American Society of Testing Materials (ASTM) D422-63, D854-58, D4318-00,

<sup>1</sup>PhD Student, Institute of Lowland Technology, Saga University  
1 Honjo Saga 840-8502, Japan (Corresponding author. email : triharianto72@yahoo.com)

<sup>2</sup>Professor, Institute of Geotechnical Engineering, Southeast University Nanjing 210096, P.R. China

<sup>3</sup>Professor, Institute of Lowland Technology, Saga University 1 Honjo Saga 840-8502, Japan

<sup>4</sup>Lecturer, Institute of Lowland Technology, Saga University 1 Honjo Saga 840-8502, Japan

<sup>5</sup>Undergraduate student, Institute of Lowland Technology, Saga University 1 Honjo Saga 840-8502, Japan

and D427-61. Table 1 summarizes the basic properties of the soil which is used in this study.

Polypropylene fiber is the most common synthetic material used to reinforce soil and concrete (Maher and Ho 1994; Al Wahab and El-Kedrah 1995). The primary attraction is that of low cost (Moncrieff 1979). It is easy to mix with soil and has relatively high melting point which makes it possible to place the soil-fiber mixture in the oven and conduct the moisture tests. Also, polypropylene is a hydrophobic and chemically inert material which does not absorb or react with the soil moisture or leachate. The polypropylene fiber used in this study is RCP17T with 10mm in length and 50  $\mu\text{m}$  in diameter. The summary of the properties of polypropylene fiber are presented in Table 2.

**Table 1 Basic properties of Akaboku soil**

Properties	Values
<b>Specific gravity, Gs</b>	2.59
<b>Consistency limit :</b>	
Liquid limit, $w_L$ (%)	162.0
Plastic limit, $w_P$ (%)	81.7
Shrinkage limit, $w_S$ (%)	48.9
Plasticity index, PI (%)	80.3
<b>Grain size analysis :</b>	
Sand (%)	35
Silt (%)	52
Clay (%)	13

**Table 2 Properties of polypropylene fiber**

Properties	Value
Specific gravity	0.91
Fineness (dtex) <sup>1</sup>	15-19
Tensile strength (MPa)	2.0 - 6.0
Elongation at break (%)	70 - 150
Melt point (°C)	160

<sup>1</sup>dtex = 10 $\mu\text{g}/\text{cm}$

## Methods

The sampled soil was slight air dried to bring water content below the measured optimum moisture content (OMC). The soil retrieved in its in-situ state was above its OMC, therefore it was necessary to air dried the soil first. The air dried soils were grinded passed through a No. 10 sieves. The weight of specific content of fibers was calculated based on the weight of the soil (oven-dried basis). Certain amount of distilled water was added to the soil-fiber mixture until the water content reach OMC. The soil-fiber mixture was mixed for 5 minutes at low speed (1430 rpm) and additional 2.5 minutes at high speed (1720 rpm). The specimens were prepared by mixing the soil with various percentages of fiber content (FC) and the percentages of mixtures (by weight) are shown in Table 3.

The compaction tests were performed based on the ASTM D698-70 standard test, with compaction energy of

593 kJ/m<sup>3</sup>. The result is shown in Fig. 1. Summary of the compaction test results are presented in Table 4.

**Table 3 Composition of mixtures**

Serial No.	By weight (%)
1	Natural soil (0.0% Fiber)
2	0.2% Fiber
3	0.4% Fiber
4	0.6% Fiber
5	0.8% Fiber
6	1.0% Fiber
7	1.2% Fiber

**Table 4 Compaction test result for various fiber contents**

Fiber Content (%)	Optimum Moisture Content (%)	Max. Dry Density (kN/m <sup>3</sup> )
0.0	78.0	8.13
0.2	74.0	8.19
0.4	73.0	8.27
0.6	69.3	8.58
0.8	68.2	8.73
1.0	65.0	9.03
1.2	70.8	8.42

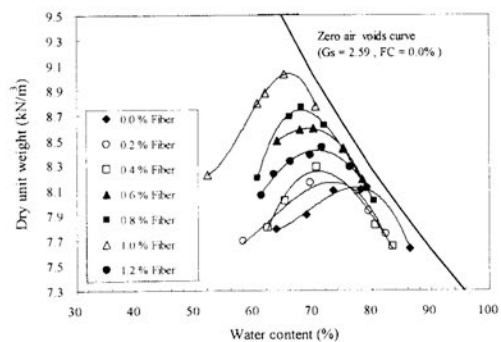


**Fig. 1 Compaction curves for the Akaboku soil with various fiber contents**

The unconfined compression test was used for obtaining the compressive strength of the soil samples and according to ASTM D2166-66. The soil samples were compacted at OMC and maximum dry density ( $\gamma_d$  max) using a Harvard miniature compacter. Figure 2 showed the relation between the compressive stress and axial strain ( $\epsilon$ ) of soil-fiber mixtures. Using the stress-strain curves obtained in this test, the stiffness properties (i.e. the secant modulus) of the soil-fiber mixtures can be evaluated. The secant modulus can be used to characterize the stiffness of soil and also can be used for the calculation of settlement in the practical application. The  $E_{50}$  (secant modulus at 50% of the unconfined compressive strength ( $q_u$ ) was used as a parameter in determining the stiffness of the soil-fiber mixtures. The  $E_{50}$  is determined as the slope of a tangent line at the origin point to the point of 50% maximum compressive stress in the stress-strain curve. The  $E_{50}$  is calculated by the following equation:

$$E_{50} = \frac{q_u / 2}{\epsilon_{50}} \quad (1)$$

where  $q_u$  is the unconfined compressive strength and  $\epsilon_{50}$  is the strain which corresponds to the 50% of  $q_u$ . The energy absorption capacity (toughness index) was also determined in this study. The toughness index (TI) can be expressed as the area under the normalized stress-strain curve from an initial state to a post-peak state in a specific stress level as shown in Fig. 3. The TI value greater than unity (i.e. FC=1.0% and 1.2%) indicates a significant increase in energy absorbing capacity, resulting in a higher ductility in the post-peak region. The TI can be determined by the following equation:

$$TI = \int_0^{\epsilon'} f(\epsilon') d\epsilon' \quad (1)$$

where  $\epsilon'$  is the normalized strain ( $\epsilon/\epsilon_f$ ),  $\epsilon_f$  is the strain at failure,  $f(\epsilon')$  is the function of the normalized stress ( $\sigma/q_u$ ), and  $\epsilon'_r$  is defined as the  $\epsilon'$  at  $\sigma/q_u = r$  ( $r < 1$ ). In this study,  $r = 0.8$  was taken and  $\epsilon'_r$  may be alternatively taken simply that is larger than  $\epsilon_f$ , i.e.  $\epsilon'_r = 2 \epsilon_f$  or  $3 \epsilon_f$ .

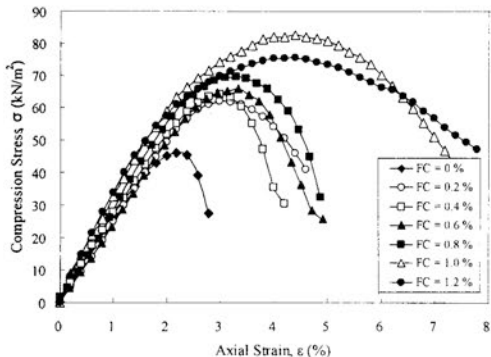


Fig. 2 Stress-strain curves of Akaboku soil with various fiber contents

In order to observe the behavior of soil-fiber mixtures on the tensile force due to differential settlement, the tensile test was performed. The specimens were prepared cylindrical with 12.74 cm in height and 10 cm in diameter. The soil samples were compacted at OMC and  $\gamma_{dmax}$  using a standard Proctor compacter. Also, the FC is the same as the tests mentioned in the previous section. Figure 4 showed the schematic diagram of the modified indirect tensile apparatus which is used in this study. The design of the apparatus for measuring soil tensile strength ( $\sigma_T$ ) followed a principle similar to the device used for Brazilian test. The compression loading with a rate of 1 mm min<sup>-1</sup> was applied to the specimens until specimens failed. The tensile test was conducted by applying load along the soil thickness in between two flat parallel plates according to the indirect Brazilian test described by Dexter and Kroesbergen (1985). The  $\sigma_T$  value was determined based on the following equation proposed by Frydman (1964).

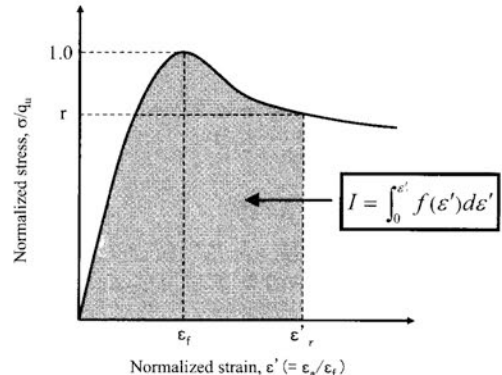


Fig. 3 Schematic normalized stress-strain curve for evaluation of TI

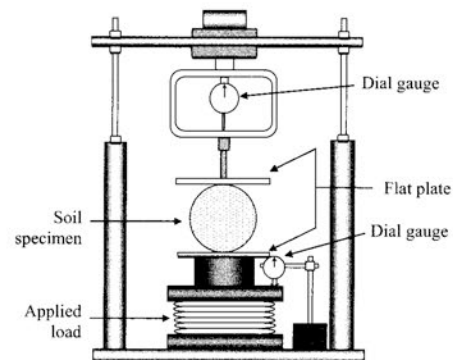


Fig. 4 Schematic diagram of the modified indirect tensile apparatus

$$\sigma_T = \frac{2Fg(x)}{\pi dl} \quad (3)$$

where  $F$  is the applied force,  $d$  and  $l$  represent specimen diameter and thickness. Frydman (1964) suggested a flattening coefficient  $g(x)$  by the following relation:

$$g(x) = \left( -\frac{d}{2a} \right) \left\{ 2x - \sin 2y - \left( \frac{2y}{d} \right) \ln \left( \frac{\pi}{4} + \frac{x}{2} \right) \right\} \quad (4)$$

where  $x$  is the flattening ratio such that  $x = a/y$ ,  $a$  is the width of flattened portion, and  $y$  is the vertical distance between the flattened portions at failure. The equation (3) may be applied if the value of  $g(x)$  greater than 0.9. Otherwise, the  $\sigma_T$  is calculated based on the following equation:

$$\sigma_T = \frac{2F}{\pi dl} \quad (5)$$

The hydraulic conductivity test was also conducted in this study. Similar to the tensile test, soil samples were also prepared at OMC and  $\gamma_{dmax}$  using a standard Proctor compacter. The compacted soil specimen was placed in a flexible-wall permeameter for hydraulic conductivity test in accordance with ASTM D2434-68. The specimens were prepared cylindrical in 12.74 cm in height and 10 cm in

diameter. The FC is the same as in the test that previously mentioned above. For all specimens, the hydraulic gradient ( $i$ ) was set to 24 and confining stress of 60 kPa was applied. The hydraulic conductivity test that was performed at low confining stress for barrier materials provides the most practical approach to simulate the worst condition (Mooyoung and Zimmie, 1996a; Inazumi, 2003).

## RESULTS AND DISCUSSION

From Fig. 5, it can be seen that the addition of fibers affected both the  $\gamma_{d\max}$  and OMC. The  $\gamma_{d\max}$  of soil-fiber mixtures increased with the increase in FC, and reached a peak at FC = 1.0 %. At FC = 1.0%, the  $\gamma_{d\max}$  increased about 11% higher than that of the soil without fiber additives as shown in Fig. 5. Moreover, the value of OMC varied within approximately 13% lower than that of the soil without fiber additives. The change is mainly due to the displacement and rearrangement of soil particles induced by inclusion of fiber. With higher FC, more fibers filled the soil voids and therefore the soil specimen density became higher. Except for FC = 1.2%, with the increase of FC,  $\gamma_{d\max}$  increased while OMC decreased. In the case of FC = 1.2 %,  $\gamma_{d\max}$  decreased while OMC increased as compared with the case of FC = 1.0%. This observation implies that there is an optimum value of FC in this study. It can be explained that this behavior might be due to the rearrangement of soil particles and fibers. Fiber may not effectively fill in the pore spaces of the soil-fiber mixture. As a result,  $\gamma_{d\max}$  decreased.

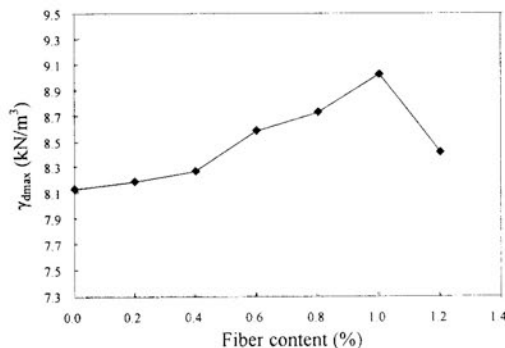


Fig. 5 Change in  $\gamma_{d\max}$  with various fiber contents

The unconfined compression test showed that the fiber additives have a significant effect on the stress-strain behavior of the soil-fiber mixture. The variation of  $q_u$  and  $\epsilon_f$  with various fiber contents are showed in Fig. 6. The addition of fibers increased the peak stress and ductility of the soil specimen. The values of  $q_u$  and  $\epsilon_f$  of the soil specimens are given in Table 5. For any FC studied, the  $q_u$  increased and reach a peak value at FC = 1.0%, and then decreased at FC = 1.2 %. The maximum value of  $q_u$  (FC = 1.0%) increased about 80% as compared with FC = 0%. The mechanism that fiber inclusion increased the shear strength of soil-fiber mixture could be explained by the development of interfacial force and interlock between soil particles and fibers. The total contact area between soil particles and fibers increased with the increase in the FC, which contributed to the increase in the resistance to externally applied forces, and consequently the strength of the soil-fiber mixtures increases. Furthermore, in the Fig. 6, the soil-fiber mixtures exhibited a highly ductile behavior

which is indicated by less loss of peak strength and larger  $\epsilon_f$  value. The similar trend with the  $q_u$  is shown for the  $\epsilon_f$  at various FC. With increase in FC, the  $\epsilon_f$  increased up to FC = 1.0%, and slightly decreased with FC = 1.2%. This can be attributed to the increased in the bonding resistance with the increase in FC. However, at FC = 1.2%, the interface contact between the soil particle and the fiber would be less. The above observation indicates that the soil-fiber mixtures are able to hold more deformation and higher strain at rupture.

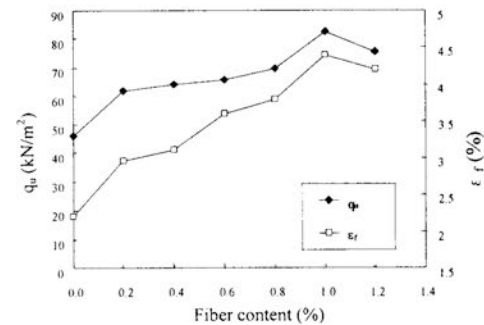


Fig. 6 Variation of strength and strain with various fiber contents

Table 5 Value of  $q_u$ ,  $\epsilon_f$  and  $\sigma_T$  for various fiber contents

Fiber content (%)	Compression test		$\sigma_T$ ( $\text{kN}/\text{m}^2$ )
	$q_u$ ( $\text{kN}/\text{m}^2$ )	$\epsilon_f$ (%)	
0.0	46.02	2.2	9.53
0.2	61.82	3.0	13.55
0.4	63.98	3.2	16.73
0.6	65.61	3.6	22.23
0.8	69.48	3.8	26.68
1.0	82.54	4.4	27.53
1.2	75.52	4.2	26.47

Table 6 The equation of  $f(\epsilon')$  for various fiber contents

Fiber content (%)	$f(\epsilon')$
0.0	$-2.98x^6 + 9.65x^5 - 12.79x^4 + 8.29x^3 - 2.91x^2 + 1.74x + 0.0012$
0.2	$-1.15x^5 + 1.22x^4 + 0.89x + 0.0056$
0.4	$-1.20x^3 + 1.16x^2 + 1.01x + 0.0293$
0.6	$-1.37x^3 + 1.60x^2 + 0.78x - 0.0227$
0.8	$-0.99x^3 + 0.75x^2 + 1.31x - 0.0511$
1.0	$-0.03x^3 - 0.95x^2 + 1.98x + 0.0027$
1.2	$0.26x^3 - 1.52x^2 + 2.25x - 0.0005$

The elasticity modulus ( $E$ ) is often used to characterize the stiffness of the soil. The relationship between the  $E_{50}$  and FC were plotted in Fig. 7. At the  $FC \leq 0.6\%$ , the lower stiffness value was found compared to the soil with  $FC = 0\%$ . On the other hand, when the  $FC = 0.8\%$  or above, the higher  $q_u$  tends to be associated with higher secant modulus, and the stiffness became higher and the stress-strain curves changes became more ductile behavior. It can be concluded that in terms of the stiffness and ductile

behavior with different FC, the effectiveness of the fiber additive was found for the  $FC \geq 0.8\%$ .

Figure 8 showed the normalized stress-strain curve of the soils at different FC. From the normalized stress-strain curves, the values of TI were determined for soils at various FC. The  $f(\epsilon_f)$  equations of each FC curve were tabulated in Table 6. Figure 9 showed the TI of the Akaboku soil with various FC. It can be seen that the TI increased as the FC increases. Initially, a slightly increase of the TI occurred up to  $FC = 0.8\%$  and significantly increased for the  $FC > 0.8\%$ . This result indicated that the soil-fiber mixtures can absorb much energy against induced strain, and subsequently the stress-strain curves change to a ductile behavior.

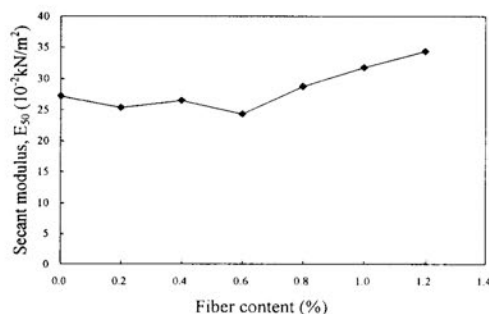


Fig. 7 Variation of modulus elasticity ( $E_{50}$ ) for various fiber content

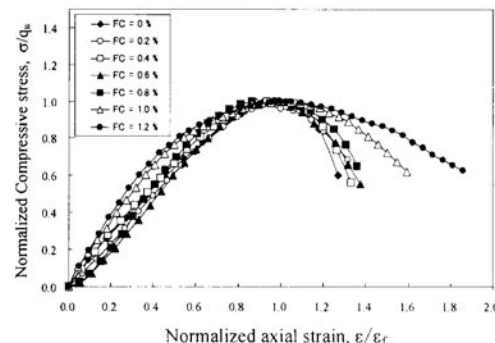


Fig. 8 Normalized stress-strain curve

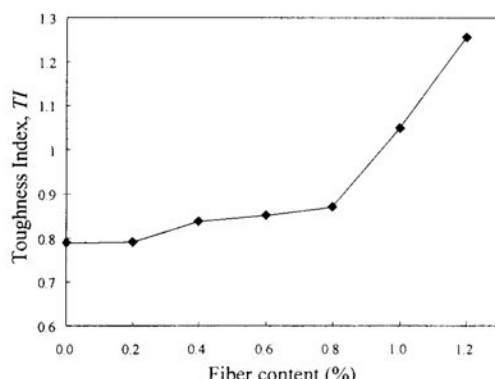


Fig. 9 Toughness index with various fiber contents

Figure 10 showed the  $\sigma_T$  behavior at different FC and indicated that the inclusion of fibers increased the  $\sigma_T$  of the

soil. The results of the tensile test with various FC are summarized in Table 5. Initially  $\sigma_T$  increased up to  $FC = 1.0\%$  (increased by approximately 190% from soil without fiber additive) and decreased for  $FC = 1.2\%$ . This trend is similar to the unconfined compression test result. The effectiveness of fiber additives depends on the interaction between fibers and soil. The mechanism of the fibers interacts to the Akaboku soil mainly controlled by the adhesion force. When the tensile force needs to be mobilized in the fibers, such as that which occurs in a desiccation cracks and differential settlement, only adhesion restrain the fibers from pullout and allows for its tensile resistance to develop. The amount of the adhesion force developed related to the surface contact area of the fibers in the soil (Ziegler et al., 1998). It can be explained that the adhesion force increased by increasing the surface contact area between the soil and fibers as can be achieved by increase the FC in the soil specimens. In the case of  $FC = 1.2\%$ , the decreased in  $\sigma_T$  might be due to the fibers not effectively fill in the pore spaces of the soil-fiber mixture and therefore the tensile resistance could not fully mobilized. Moreover, the fiber additives provide the linkage effect in the soil-fiber mixtures to suppress the development of tension cracks as shown in Fig. 11.

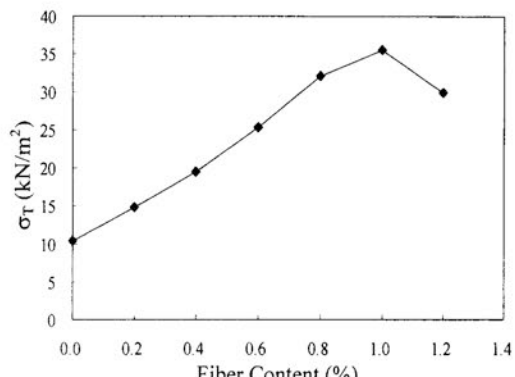


Fig. 10 Tensile strength with various fiber contents

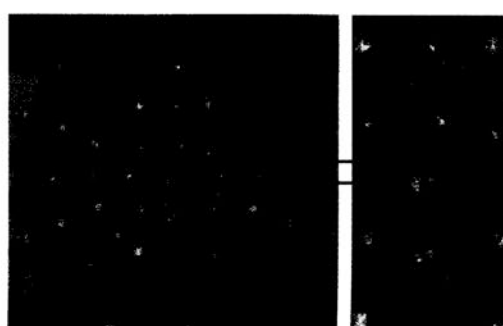


Fig. 11 The linkage behavior of fiber admixtures in suppressing cracks in tensile test

With the increase in FC, the hydraulic conductivity of the soils firstly decreased ( $FC = 0.2\%$ ) and then increased as shown in Fig. 12. The increase in hydraulic conductivity was most significant for  $FC > 0.8\%$ , which is consistent with the previous study by Miller and Rifai (2004). According to USEPA (1989) regulation for non-hazardous

waste facility, the barrier layer should have the hydraulic conductivity ( $k$ )  $\leq 1 \times 10^{-5}$  cm/s. In this study, fiber contents up to 1.0% maintained the hydraulic conductivity ( $8.6 \times 10^{-7}$  cm/s) within acceptable limit. The aforementioned test results indicate that this soil-fiber mixture can be potentially used as a material for landfill cover barrier layer.

In geotechnical engineering practice, it is useful to use simple physical properties such as dry density to predict the strength. In this study, the relationship between the soil parameters such as  $\gamma_{d\max}$ ,  $q_u$  and  $\sigma_T$  with various of FC were investigated. From Fig. 13(a), it can be seen that the  $q_u$  increased with increasing in  $\gamma_{d\max}$ . The relationship between  $\gamma_{d\max}$  and  $q_u$  is obtained as:

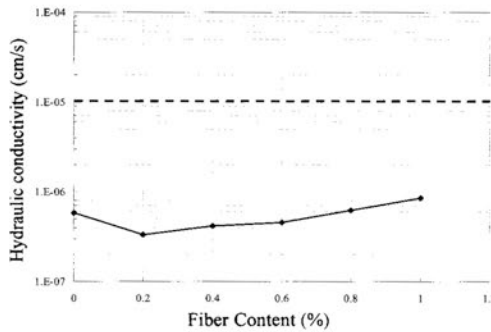
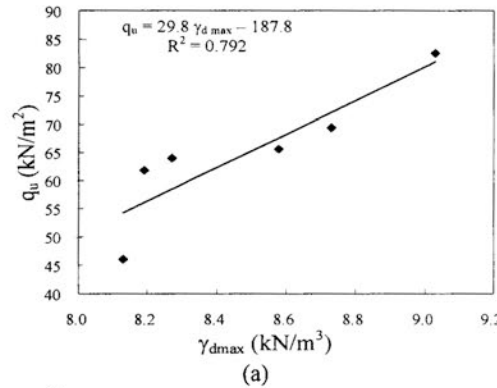
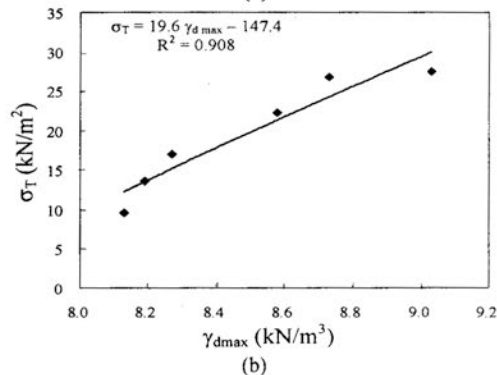


Fig. 12 Hydraulic conductivity for various fiber contents



(a)



(b)

Fig. 13 Relation between  $\gamma_{d\max}$  and UCS-ITS with various fiber contents (a)  $\gamma_{d\max}$  versus  $q_u$ , (b)  $\gamma_{d\max}$  versus  $\sigma_T$

$$q_u = 29.8 \gamma_{d\max} - 187.8 \quad (6)$$

The relationship between  $\gamma_{d\max}$  and  $\sigma_T$  is presented in Fig. 13(b), and relationship is obtained as:

$$\sigma_T = 19.6 \gamma_{d\max} - 147.4 \quad (7)$$

The  $\sigma_T$  generally increased with increasing  $\gamma_{d\max}$ . The relationship between  $q_u$  and  $\sigma_T$  was also observed in this study, as shown in Fig. 14. The relationship between  $\sigma_T$  and  $q_u$  is obtained as:

$$\sigma_T = 0.6 q_u - 17.2 \quad (8)$$

The equation obtained from this interrelationship can be used interchangeably to predict the values of  $\sigma_T$  and  $q_u$ .

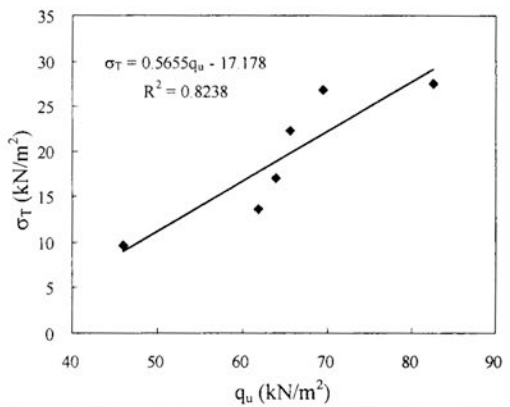


Fig. 14 Relation between UCS and ITS with various fiber contents

## CONCLUSIONS

Based on the above results, following conclusions can be drawn:

1. The contribution of fiber to the compaction characteristics (i.e. maximum dry density) increases with increasing fiber contents. A slight decrease of the maximum dry density was found for fiber content of 1.2%, which indicate that there is an optimum value of fiber content.
2. The fiber inclusion increased the compressive strength, ductility, and decreased the loss of the post-peak strength. Furthermore, with the inclusion of fibers, the toughness index of the soil-fiber mixtures increases which indicates that the energy absorbing capacity increases, resulting in higher ductility in the post-peak region.
3. The inclusion of fibers increased the tensile strength of the soil-fiber mixtures. This is mainly due to the increase in the adhesion force as the surface contact area between the soil and fibers increase by increasing the fiber content.

4. The highest compressive and tensile strength of soil-fiber mixtures occurred at the highest dry density of the soil specimen due to the rearrangement and dense packing of the particles by inclusion of fibers.
5. The hydraulic conductivity of soil-fiber mixtures increased with increasing fiber content. However, the hydraulic conductivity of various fiber contents is within the acceptable limit.
6. Significant improvements in the mechanical behavior of the soil-fiber mixtures indicate that there is some potential for the use of fiber additives in engineering practice (i.e. landfill cover barrier material).

## REFERENCES

- AL WAHAB, R.M. and EL-KEDRAH, M.A. (1995). Using fibers to reduce tension cracks and shrink/swell in compacted clay. *Geoenviroment 2000, Geotechnical Special Publication No. 46*, ASCE, New York, 791-805.
- CAI, Y., SHI, B., NG, C.W.W., and TANG, C. (2006). Effect of polypropylene fibre and lime admixture on engineering properties of clayey soil. *Engineering Geology* 87, pp. 230-240.
- DEXTER, A.R. and KROESBERGEN, B. (1985). Methodology for determination of the tensile strength of soil aggregates. *Journal of Agricultural Engineering Research*, Vol. 31, pp. 139-147.
- FRYDMAN, S. (1964). The applicability of the Brazilian (indirect tension) test to soils. *Journal of Applied Science*, Vol. 15, pp.335-343.
- GRAY, D.H. and OHASHI, H. (1983). Mechanics of fiber reinforcement in sand. *Journal of Geotechnical Engineering*, Vol. 109, No. 3, pp. 335-353.
- HARIANTO, T., HAYASHI, S., D.U, Y.J. and SUETSUGU, D. (2007). An evaluation of fiber admixtures on the desiccation crack behavior of the compacted Akaboku soil potentially used as a landfill cover barrier material. *Proceedings of the 60<sup>th</sup> Canadian Geotechnical Conference and 8<sup>th</sup> Joint CGS/IAH-CNC Groundwater Conference*, Vol. 1, pp. 1377-1382.
- IBARRA, S.Y., McKEYE, E. and BROUGHTON, R.S. (2005). Measurement of tensile strength of unsaturated sandy loam soil. *Soil and Tillage Research* 81, pp.15-23.
- INAZUMI, S. (2003). Waste Sludge Barrier for Landfill Cover System. Doctoral Thesis, Kyoto University.
- LATHA, G.M. and MURTHY, V.S. (2007). Effects of reinforcement form on the behavior of geosynthetic reinforced sand, *Geotextile and Geomembrane*, Vol. 25, pp. 23-32.
- MAHER, M.H. and HO, Y.C. (1994). Mechanical properties of kaolinite fiber soil composite. *Journal of Geotechnical Engineering*, Vol. 120, No. 8, pp.1381-1393.
- MILLER, C.J. and RIFAI, S. (2004). Fiber reinforcement for waste containment soil liners. *ASCE Journal of Environmental Engineering*, Vol. 8, pp.891-895.
- MOO-YOUNG, H.K. and ZIMMIE, T.F. (1996a). Geotechnical properties of paper mill sludges for use in landfill covers. *ASCE Journal of Geotechnical Engineering*, Vol. 122, No. 9, pp.768-774.
- MONCRIEFF, R.W. (1979). *Man Made Fibers*, Newnes-Butterworths, U.K.
- NATARAJ, M.S. and McMANIS, K.L. (1997). Strength and deformation properties of soil reinforced with fibrillated fibers. *Geosynthetics International*, Vol. 4, No. 1, pp.65-79.
- PARK, T. and TAN, S.A. (2005). Enhanced performance of reinforced soil walls by the inclusion of short fiber. *Geotextiles and Geomembrane*, Vol. 23, No. 4, pp.348-361.
- TANG, C., SHI, B., GAO, W., CHEN, F. and CAI, Y. (2007). Strength and mechanical behaviour of short polypropylene fiber reinforced and cement stabilized clayey soil. *Geotextiles and Geomembrane*, Vol. 25, pp. 194-202.
- USEPA (1989). Technical guidance document, final cap on hazardous waste landfills and surface impoundment, EPA/530-SW-89-047, Washington, D.C.
- ZIEGLER, S., LESHCHINSKY, D., LING, H.I. and PERRY, E.D. (1998). Effect of short polymeric fibers on crack development in clays. *Soils and Foundations* Vol. 38, No. 1, pp. 247-253.

## SECONDARY COMPRESSION BEHAVIOR IN THREE TYPES OF CONSOLIDATION TESTS

B. Sompie<sup>1</sup>, K. Arai<sup>2</sup> and A. Kita<sup>3</sup>

**ABSTRACT:** The Constant Strain Rate Consolidation (CSRC) and Constant Loading Rate Consolidation (CLRC) tests which appear to be promising types of rapid consolidation tests, may not provide sufficient information about the time dependency in stress-strain response such as the secondary compression. Subjected to remolded young clay, this paper shows that the time dependent behavior in the Standard Consolidation (SC), CSRC and CLRC tests is represented systematically by a simple assumption concerning the time dependency of volume change due to shear. In SC test, at the first stage of each loading step little volumetric strain due to shear takes place and the strain begins to occur several minutes after each step loading. At the latter stage of each loading step, the volumetric strain occurs proportionally with the logarithm of elapsed time, which is observed as the secondary compression. In CSRC and CLRC tests, some time period after the stress state has entered the normally consolidated region, the volumetric strain due to shear tends to occur rapidly with the increase in stress ratio. Since most of the volumetric strain due to shear has taken place at the earlier stage of consolidation, little volumetric strain or secondary compression occurs at the later stage of CSRC or CLRC process. This tendency makes the specimen stiffer with the passage of time, and makes the vertical pressure and pore water pressure increase substantially at the last stage of CSRC or CLRC process. Consideration to such behavior may be effective to correctly interpret the result of CSRC and CLRC tests. Based on these results, this paper proposes an approximate method for estimating the secondary compression coefficient from CSRC or CLRC test and discusses about the effect of loading rate to the consolidation yield stress.

**Keywords:** clay, consolidation test, volumetric strain due to shear, secondary compression, time effect.

### INTRODUCTION

The Constant Strain Rate Consolidation (CSRC) and the Constant Loading Rate Consolidation (CLRC) tests appear to be promising types of rapid consolidation tests, because of its simple manipulation and reliability. However the time dependency in stress-strain response such as the secondary compression has not been sufficiently clarified yet in CSRC and CLRC tests. For instance, Leroueil et al (1985) and Yin and Graham (1988) practiced various types of oedometer tests including CSRC and CLRC tests, and proposed a unique stress-strain-time relationship, while the rheological characteristics for CSRC and CLRC processes are not clarified in detail. Arai (1994) has shown that both many time effects observed in triaxial compression test and the secondary compression in the Standard Consolidation (SC) test are realistically simulated by a numerical procedure based on a simple postulate concerning the time dependency of volume change due to shear. The numerical analysis solves the following two equations as a simultaneous equation. One equation specifies the volumetric strains due to consolidation and shear. The other equation constrains the lateral displacement of specimen to be zero. Note that the analysis does not use any plastic flow rule. This paper applies the numerical analysis to SC, CSRC and CLRC tests, and aims to clarify the time dependent behavior of soft clay in the three types of consolidation tests. As the initial step of research study, our concern was restricted to only the behavior observed in remolded young clay, and the infinitesimal strain theory is used.

### PRELIMINARY DEFINITIONS

#### Fundamental Parameters

For the  $K_0$  consolidation process, a stress state is described by mean effective stress  $p^n$  and stress difference  $q^n$

$$p^n = (\sigma_v^n + 2\sigma_h^n)/3, q^n = \sigma_v^n - \sigma_h^n \quad (1)$$

and the corresponding strains are

$$v^n = \epsilon_v^n, \epsilon^n = 2\epsilon_v^n / 3 \quad (2)$$

where  $\sigma_v^n$  and  $\sigma_h^n$ : vertical and horizontal stresses,  $v^n$  and  $\epsilon^n$ : volumetric and shear strains,  $\epsilon_v^n$ : vertical strain, and  $n$ : a discretized time step number. Hereafter regard the normal stresses as effective stress unless otherwise defined. The term  $p^n/q^n$  is referred to 'stress ratio'.

#### Time Dependency of dilatancy

Subjected to remolded and saturated clays, Shibata (1963) performed a lot of drained triaxial compression tests keeping the mean effective stress constant, and found that the volumetric strain due to shear increased with the ratio of stress difference to mean effective stress. Ohta (1970) presented the experimental results as Eq. (3) which was a more general expression of volumetric strain due to shear  $v_d^n$  when neglecting the time dependency.

$$v_d^n = D \cdot \frac{q^n}{p^n}, D = (\lambda - \kappa)/(1 + e_o) M \quad (3)$$

<sup>1, 2</sup>Department of Architecture and Civil Engineering, Fukui University, 3-9-1, Bunkyo, Fukui, 910-8507 Japan.  
(Corresponding author: e-mail: katuhiko@anc.anc-d.fukui-u.ac.jp)

<sup>3</sup>Soil and Rock Engineering Co. Ltd., 2-21-1, Shonai-Sakae, Toyonaka, Osaka, 561-0834, Japan.

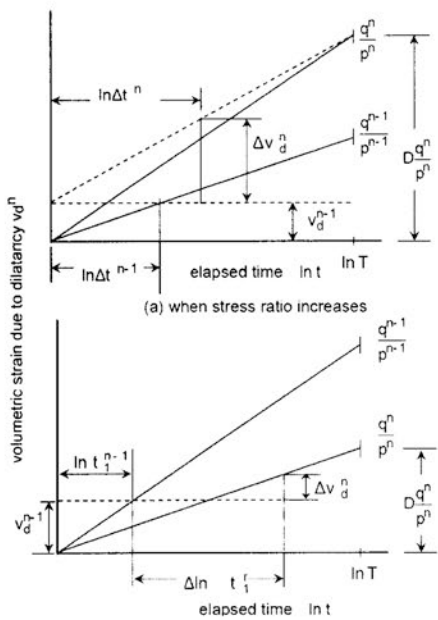


Fig. 1. Meaning of Eqs. (4), (5a) and (5b)

in which D: dilatancy coefficient,  $\lambda = 0.434C_c$  ( $C_c$ : compression index),  $\kappa = 0.434C_s$  ( $C_s$ : swelling index),  $e_0$ : initial void ratio, and M: slope of critical state line. Based on the expression, Otha (1970) and Sekiguchi and Otha (1970) developed a constitutive model which was equivalent to the Cam Clay model. It shows the reliability of Eq. (3) that the Otha model and Cam Clay model provide the same result for triaxial compression tests. When the stress state within clay specimen changes with the passage of time, Arai (1993) assumed that the volumetric strain due to shear  $v_d^n$  took place as

$$\Delta v_d^n = \left( D \cdot q^n / p^n - v_d^{n-1} \right) L^n \quad (4)$$

in which,

$$L^n = \ln \Delta t^n / \ln T : \quad (5a)$$

when the stress ratio increases

$$L^n = \Delta \ln t_i^n / \ln T \quad (5b)$$

for other cases

where  $\Delta t^n$ : length of discretized time step,  $t_i^n$ : elapsed time after stopping the increase in the stress ratio, T: time length required to make dilatancy take place completely, and  $\Delta$ : increment of succeeding physical quantity. Figure 1 illustrates the physical meaning of Eqs. (4), (5a) and (5b) as follows. Firstly the volumetric strain due to dilatancy is represented by Eq. (3) when neglecting the time dependency. Secondly we assume that the dilatancy takes place in proportion to the logarithm of elapsed time under the constant stress ratio. The total time required for complete occurrence of dilatancy is T. When the stress ratio changes with the passage of time, the difference between

Eq. (3) and the volumetric strain having occurred until the preceding time step may take place in proportion to the logarithm of elapsed time as shown in Fig. 1. The value of T in Eq. (5) affects very little the value of  $\Delta v_d^n$ , because the term T is evaluated by the logarithm. Equation (4) is not sufficient to duplicate the behaviour of volumetric strain

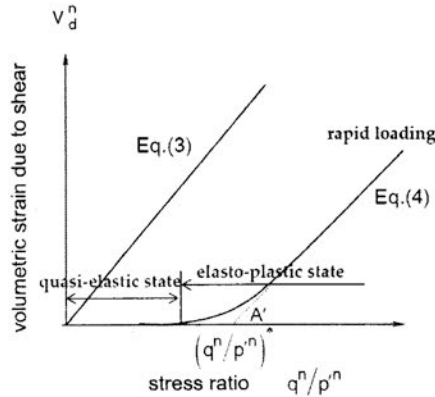


Fig. 2. Characteristics of volume change due to shear

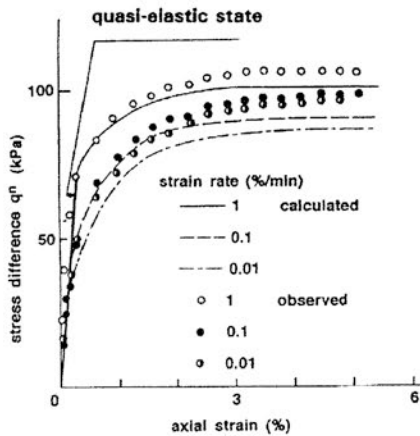


Fig. 3. Stress-strain relationship in triaxial compression test  
(after Arai, 1994)

due to shear for a sudden increase in stress ratio. As illustrated schematically in Fig. 2, when a shearing process originates at an almost static state where the stresses and strains are approximately constant with the passage of time, for instance, the final stage of consolidation, it is assumed that little volumetric strain is generated at the early stage of shear until the value of  $v_d^n$  calculated by Eq. (4) exceeds a certain prescribed value  $v_d^*$ . Since we observed usually this phenomenon at the early stage of conventional triaxial test, we can determine the value of  $v_d^*$  by using the effective stress path in the test. When the undrained triaxial compression test is carried out subsequently after the completion of isotropic and normal consolidation, the typical stress path of constant strain rate shear is illustrated in Fig. 3. The rapid increase in pore water pressure beyond the point A in Fig. 4 is explain by the mechanism that the volumetric strain due to shear induces the accumulation of

pore water pressure after the stress path is beyond the point A' in Fig. 2. That is, the point A in Fig. 4 is thought to

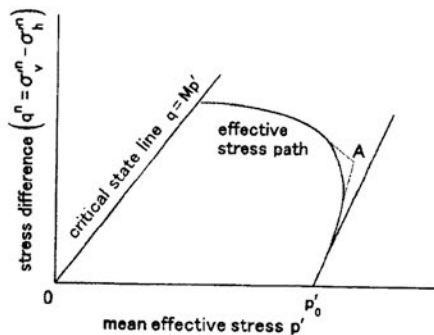


Fig. 4. Typical stress path in undrained shear of isotropically consolidated clay

correspond to the point A in Fig. 2. The value of  $\Delta v_d^n$  obtained by substituting the conditions at the point A in Fig. 4 into Eq. 4 and 5a corresponds to the  $v_d^*$  defined above. Arai (1985) applied this procedure to a lot of triaxial test results and found that the value of  $v_d^*$  became nearly constant for each kind of clay. Arai (1994) showed that the time dependent behavior in triaxial compression test can be simulated realistically by using these assumptions concerning the time dependency as shown in

Fig. 2. In the  $K_0$  consolidation test, our assumption is that the secondary compression arises from the time dependency of volumetric strain due to shear. In this paper, we try to simulate the secondary compression behavior by using Eq. 18 and the expression of  $v_d^*$ . It is shown later that the secondary compression starts when  $v_d^n$  exceeds  $v_d^*$ , while the secondary compression has been considered to start at the end of primary consolidation conventionally. Our target is to represent systematically the time dependent behavior in shearing process by a unified assumption concerning the time dependency of volumetric strain due to shear.

#### Elastic and Plastic Strains:

The elastic and plastic components of strains are considered as follows. The volumetric strain due to shearing which is represented by Eqs. (4) and (5), is regarded as being perfectly plastic. Incremental volumetric strain due to consolidation  $\Delta v_c^n$  is supposed to be the sum of elastic component  $\Delta v_{ce}^n$  and plastic component  $\Delta v_{cp}^n$ , which are assumed to be time independent, since little time dependency was observed in isotropic consolidation tests.

$$\Delta v_c^n = \Delta v_{ce}^n + \Delta v_{cp}^n \quad (6)$$

$$\Delta v_{ce}^n = \frac{K}{1+e_o} \cdot \frac{\Delta p^n}{p^n} \quad (7)$$

$$\Delta v_{cp}^n = \frac{(\lambda - \kappa)}{1+e_o} \cdot \frac{\Delta p^n}{p^n} \quad (8)$$

Although incremental shear strain  $\Delta e^n$  consists of elastic and plastic components,  $\Delta e^n$  is specified by Eq. (10) for the  $K_0$ -consolidation process, without defining these components.

#### TEST PROCEDURE

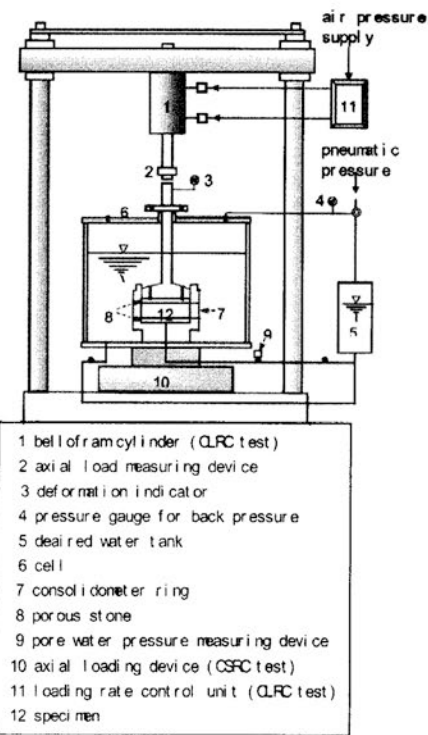


Fig. 5. Equipment of CSRC and CLRC tests

The soil used for consolidation tests is the remolded Ota clay from Fukui Prefecture, which has the following index properties: specific gravity, 2.67; liquid limit, 53.2%; plastic limit, 25.4%; clay fraction, 60%; silt fraction, 36.7%; and fine sand fraction, 3.3%. The clay was mixed with water into slurry (moisture content = 72 %) and consolidated under the preconsolidation pressure of 98 kPa in a consolidometer. After being stored for more than 2 weeks, a test specimen 20 mm in height and 60 mm in diameter was carefully trimmed from the preconsolidated cake which was fully saturated. Subsequently SC, CSRC and CLRC tests were performed separately. In SC test, the loading pressures were applied step by step as 9.8-19.6-39.2-78.4-156.8-313.6-627.2-1254.4 kPa, each of which was maintained constant for 24 hours. CSRC test was carried out under the specified strain rates of 0.1, 0.05 and 0.01 %/min. During CSRC process we did not control the strain rate itself but deformation rate. CLRC test was performed under the loading rates of 9.8, 1.96 and 0.49 kPa/min. CSRC and CLRC tests were performed by the equipment shown in Fig. 5. The upper and lower surfaces of specimen are permeable and impermeable boundaries respectively. Pore water pressure was monitored at the bottom of specimen. In CSRC test, loading pressure was monitored at the upper surface, while in CLRC test the settlement was measured at the upper surface. After setting

a test specimen into the oedometer and after introducing the back pressure of 98 kPa, the specimen was consolidated by the vertical constant pressure of 9.8 kPa for 24 hours under the anisotropic  $K_0$ -condition. This preconsolidation process seems essential for bringing the test specimen into complete contact with the loading plate.

## NUMERICAL ANALYSIS

### Discretization Techniques

Despite treating  $K_0$ -consolidation here, we employ a finite element technique for two-dimensional consolidation analysis developed by Akai and Tamura (1978), because the technique seems to have attained to a sufficiently reliable and popular stage. A consolidation test specimen subjected to analysis is subdivided into rectangular finite elements as shown in Fig. 6. The rectangular element is considered to be composed of four triangular elements, and the stresses, strains and pore water pressure are assumed to be constant throughout each rectangular element.

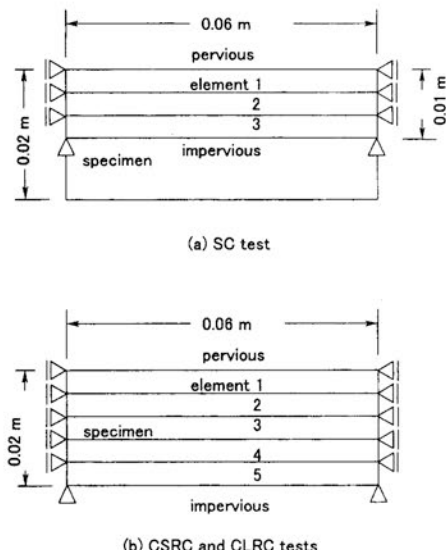


Fig. 6. FE meshing of test specimen

### Nonlinear Stress-Strain Analysis

Our concern is to solve the following two equations as a simultaneous equation, without using the plastic flow rule. One equation specifies the volumetric strain due to consolidation and shearing (Eq. 9). The other equation specifies the shear strain (Eq. 10). Assuming that  $\Delta p^n$  and  $\Delta q^n$  are given at a time step, the volumetric strain is calculated as the sum of the components due to consolidation and shearing, according to Ohta (1971).

$$\left. \begin{aligned} \Delta v^n &= \Delta v_{ce}^n : \\ &\text{over-consolidated state} \\ \Delta v^n &= \Delta v_{ce}^n + \Delta v_{cp}^n + \Delta v_d^n : \\ &\text{normally consolidated state} \end{aligned} \right\} \quad (9)$$

For the  $K_0$ -consolidation process, the shear strain is given as

$$\Delta \varepsilon^n = 2\varepsilon_c^n / 3 = 2\Delta v^n / 3 \quad (10)$$

Using  $\Delta v^n$  and  $\Delta \varepsilon^n$ , hypothetical bulk modulus  $K^n$  and shear rigidity  $G^n$  are calculated from

$$\Delta p^n = K^n \Delta v^n, \Delta q^n = 3G^n \Delta \varepsilon^n \quad (11)$$

Based on  $K^n$  and  $K^n$ , hypothetical Young's modulus  $E^n$  and Poisson's ratio  $v^n$  are given as

$$E^n = 9K^n G^n / (3K^n + G^n), v^n = (3K^n - 2) / (2G^n) \quad (12)$$

These hypothetical elastic constants enable to relate all the stress components to strain components respectively without using the plastic flow rule. The numerical procedure is as follows.

- Assume the trial values of hypothetical Young's modulus  $E^n$  and Poisson's ratio  $v^n$ .
- Using the assumed  $E^n$  and  $v^n$  and known permeability  $k^n$ , perform the elastic consolidation analysis at a discretized time step. In the consolidation analysis, a displacement is specified for CSRC test, and a loading pressure is given for SC and CLRC tests at the upper surface of specimen.
- Employing the incremental stresses obtained by the consolidation analysis, the incremental volumetric and shear strains are calculated respectively from Eqs. (9) and (10).
- Based on these strains, find the hypothetical elastic constants by using Eqs. (11) and (12).
- Replacing the trial values of  $E^n$  and  $v^n$  with those found at step 4), repeat the consolidation analysis until the convergence of elastic constants is obtained.

This iteration procedure is practiced for each discretized time step.

## EXPERIMENTAL AND NUMERICAL RESULTS

### Material Parameters

In CSRC and CLRC tests, void ratio  $e^n$ , effective and vertical consolidation pressure  $\sigma_v^n$  are calculated as (JSSMFE, 1993)

$$e^n = H^n / H_s, -1, \sigma_v^n = P^n / A - 2u^n / 3 \quad (13)$$

Where  $H^n$ : height of the specimen,  $H_s$ : height of solids,  $P^n$ : axial loading force,  $A$ : cross-sectional area of the specimen,  $u^n$ : excess pore water pressure developed at the impervious end of the specimen, and  $n$  denotes a discretized time step number. Coefficient of volume compressibility  $m_v^n$ , and coefficient of consolidation  $c_v^n$  are obtained as

$$\Delta m_v^n = \frac{\Delta H^n / H}{\Delta \sigma_v^n} \quad (14)$$

$$c_v^n = 1440 \Delta t^n H^2 / 2u \Delta t^n$$

$$H = \frac{(H^n + H^{n-1})}{2}, u = \frac{(u^n + u^{n-1})}{2}$$

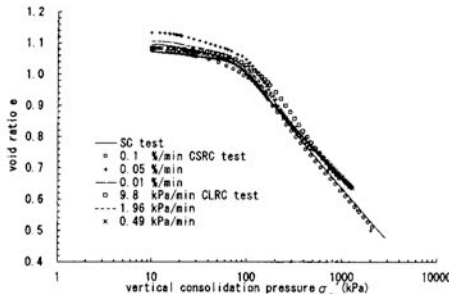


Fig. 7. e-log relationship observed

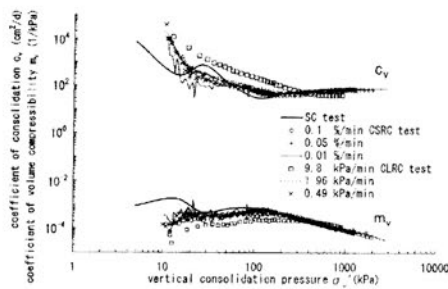


Fig. 8.  $c_v$  and  $m_v$  observed

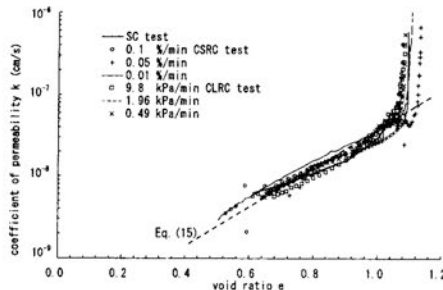


Fig. 9. e-log k relationship observed

Figure 7 shows  $e-\log\sigma_v$  relationship obtained by the three types of consolidation test. The consolidation yield stress is slightly affected by the strain and loading rates. Figure 8 shows  $c_v$  and  $m_v$  obtained by the three types of consolidation tests, which show almost similar tendencies. Figure 9 illustrates the relationship between void ratio  $e$  and permeability  $k$  which is calculated from  $c_v$  and  $m_v$ . As shown in Fig. 8, the three types of consolidation tests seem to give a similar  $e-\log k$  relationship. Except for exceedingly loose state, the relationship is approximated by

$$e - 0.67 = 0.445 \{ \log_{10} k - \log_{10}(8 \times 10^{-9}) \} \quad (15)$$

Though it is not easy to find the correct value of permeability for cohesive soils because of many factors affecting the permeability (e.g. Nagaraj et al., 1994), we employ the above relationship as the first approximation.

Since the slurry sample was preconsolidated in a consolidometer, the consolidation yield stress is given as  $p_c = (98 + 2K_o)98/3 = 63 \text{ kPa}$ .

The value of  $K_o$  is taken as 0.464, which has been monitored by some  $K_o$ -consolidation tests using triaxial equipment at the normally consolidated region (Arai, 1994). Based on these results, the material parameters required for our numerical analysis are determined as  $\lambda = 0.16$ ,  $\kappa = 0.033$ ,  $M = 1.13$ ,  $D = 0.056$ ,  $T = 14$  days,  $v_d^* = 0.004$ ,  $e_o = 1.04$ , and the permeability given by Eq. (15). The values of  $\kappa$ ,  $M$ , and  $v_d^*$  are the same as those used by Arai (1994) which were determined by triaxial compression tests performed separately.

### Initial State

It is difficult to estimate the residual effective stresses or negative pore water pressure which remains within a test specimen, since it is not easy to specify completely the stress history of the specimen until the specimen is placed into the oedometer. Some preliminary calculations have shown that the residual stresses have a negligible effect on the numerical results, when the residual stresses are represented only by the mean effective stress, and when the mean effective stress is taken as the value between 20 and 60 % of mean pre-consolidation pressure. We assume that 40 % of mean effective stress in the consolidometer remains isotropically within the specimen before starting the consolidation test, together with the same value of negative pore water pressure. It is also difficult to estimate the history of volume change with shear prior to placing a test specimen into the oedometer, because it is not easy to evaluate the amount of volume change with shear of the slurry sample in the consolidometer, and because the consolidated sample expands both vertically and laterally when taken out from the consolidometer. As the first approximation, on analogous to the residual effective stresses described above we assume that the volume change with shear estimated by Eq. (3) has taken place almost entirely in the consolidometer, and that 40 % amount of volume change with shear remains within the test specimen in oedometer. This rough approximation provides fairly good numerical results compared to experimental results. The numerical results were not very sensitive to the amount of volume change with shear before placing the specimen into the oedometer.

### Standard Consolidation (SC) Test

Figure 10 shows the time-settlement relationship for the experimental and numerical results of SC test. The numerical results appear to agree fairly well with the experimental ones for most of loading pressures. The discrepancy of settlement at loading pressure 78.4 kPa is attributed to the assumption that we consider no plastic component of volumetric strain at over-consolidated region (see Eq. 9). Figure 11 shows the settlement consolidation of soil sample is plotted against the logarithm of time calculated by numerical analysis and for that observed directly in SC test. In the numerical analysis calculations, the coefficient of volume change with shear,  $D$ , was set at zero for the case with no secondary compression and at 0.056 for when secondary compression does occur. Use of the value  $D$  is 0.056, because of most cases to stand in judgment a fairly good estimate. This is further discussed in estimation of secondary compression coefficient. The

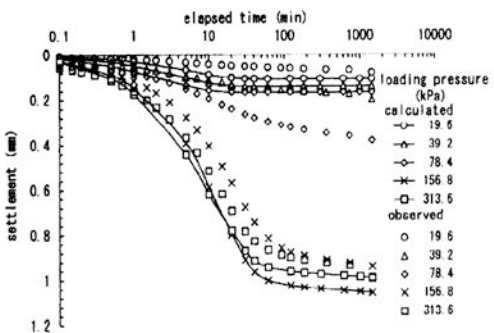


Fig. 10. Settlement curve (SC test)

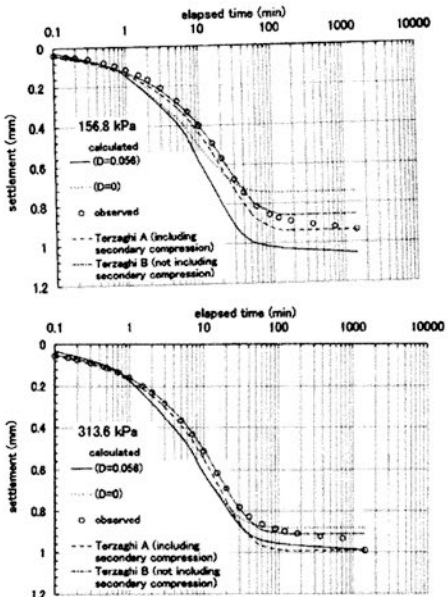


Fig. 11. Comparison with Terzaghi theory

calculated settlement results show when volume change with shear strain occurs in each layer; e.g., for consolidation pressure of 156.8 kPa, volume change with shear strain occurs in the first layer at 1 min, the second and third layers at 5 min. For a consolidation pressure of 313.6 kPa, volume change with shear strain occurs in the first layer at 10 min and at 20 min in layers 2 and 3. The appearance of volumetric strain due to shearing in layers 1 and 3 for consolidation pressure of 156.8 and 313.6 kPa may help to clarify the volumetric strain analyzed in these layers, as shown in figure 13. Occurrence of volumetric strain due to shearing in the primary stages of consolidation took place some of delayed consolidation in the later stages of consolidation. For the case  $D = 0.056$ , the volumetric strain due to shearing that occurred in the primary consolidation region produced a certain amount of secondary consolidation settlement in the numerical analysis. Thus, taking into account both volumetric strain due to shearing and secondary compression the amount of settlement that occurs during the later stages of consolidation increases. Figures 12 through 14 illustrate the change of stress ratio, volumetric strain and hypothetical elastic constant  $E^n$  and Poisson's ratio  $\nu^n$  during

consolidation. The results shown in Figs. 12 through 14 seem to be reliable, because the results give the calculated settlement shown in Fig. 10, which agrees fairly well with the monitored settlement. In Figs. 12 through 14,  $B_i$  designates the point at which the stress state moves to normally consolidated region, and  $C_i$  is the point at which volume change due to shearing begins to occur. As seen in Fig. 13, at the first stage of each loading step, the state of specimen enters the quasi-elastic state as defined in Fig. 2, where little volume change with shear takes place. A little time after each step loading, volume change with shear begins to occur. Although the stress ratio becomes almost constant at the latter stage of each loading step as shown in Fig. 12, the stress ratio continues to increase very slightly with the passage of time. If we apply Eq. (5a) to such a state, the amount of volume change with shear may be overestimated. Thus we employ Eq. (5b) when increasing rate of stress ratio  $\Delta(p^n/q^n)/\Delta t^n$  does not exceed  $10^{-3}/\text{min}$ . Referring to Figs. 12 through 14, the secondary compression observed at the latter stages of SC test is represented by the volumetric strain due to shearing occurrence according to nearly constant stress ratio, which takes place proportionally with the logarithm of elapsed time. Figure 14 indicates the following tendency for hypothetical Young's modulus  $E^n$ . After the stress state moves to the normally consolidated region,  $E^n$  decreases suddenly due to the occurrence of  $v_{cp}^n$ . Subsequently,  $E^n$  increases gradually with the progress of consolidation.

The occurrence of volumetric strain due to shearing reduces  $E^n$  substantially, because the volumetric strain due to shearing increases whereas the effective vertical stress little increases at the latter stage of each loading step. Whether volumetric strain due to shearing occurs or not,  $E^n$  approaches 0 at the final stage of each loading step, because the effective stresses reach constant values in spite of the slight increase in volumetric strain. Hypothetical Poisson's ratio  $\nu^n$  is held constant throughout the consolidation process as shown in Fig. 14.

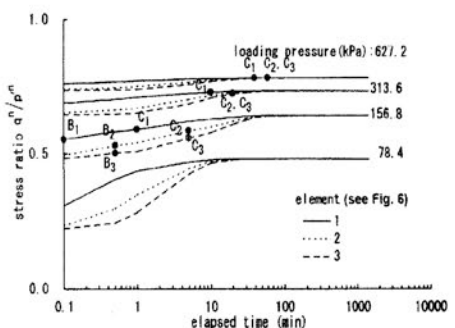


Fig. 12. Stress ratio (SC test)

#### Constant Strain Rate Consolidation (CSRC) and Constant Loading Rate Consolidation (CLRC) Tests

After setting a test specimen into the oedometer, the specimen is consolidated by total vertical pressure of 9.8 kPa for 24 hours under  $K_0$ -condition as stated before. Following this preconsolidation process, CSRC or CLRC test is carried out according to the prescribed strain rate or loading rate. For CSRC test, the numerical analysis is

performed by two separate stages, i.e. the preconsolidation and CSRC processes.

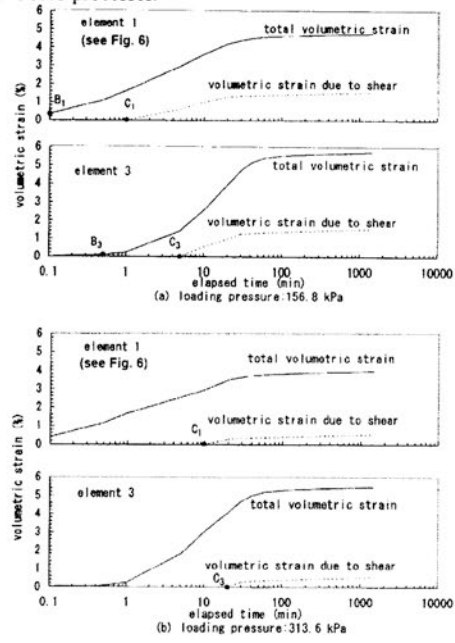


Fig. 13. Components of volumetric strain (SC test)

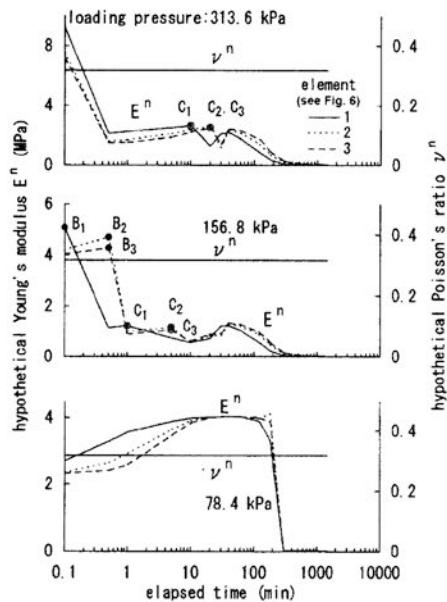
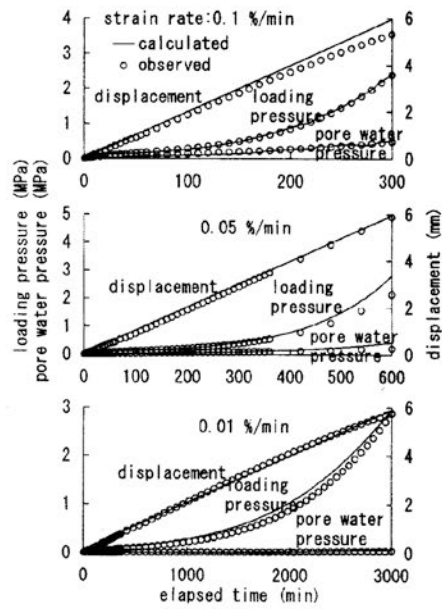


Fig. 14. Hypothetical elastic constants (SC test)

For the preconsolidation process, vertical pressure of 9.8 kPa is specified, while for CSRC process a displacement is prescribed at the upper surface of specimen at each discretized time step. The initial state for the preconsolidation process is the same as the initial state for SC test described previously. The final state for the preconsolidation process corresponds to the initial state for CSRC process.



(a) CSRC test

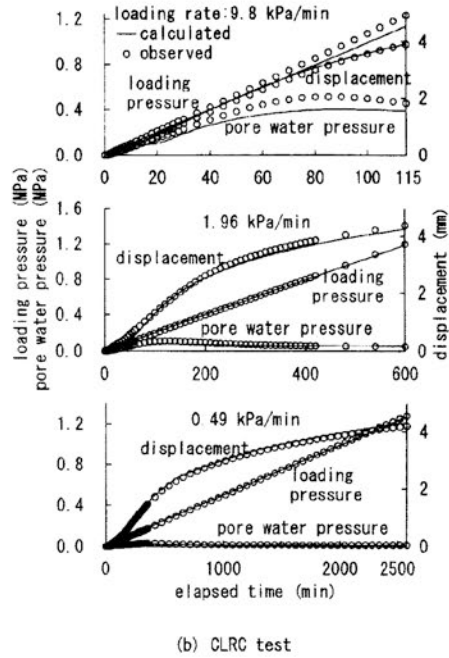
Fig. 15. Comparison between calculated and monitored results

Note that at the final state of the preconsolidation process, vertical stress  $\sigma_v$  (= 9.8 kPa) is less than lateral stress  $\sigma_h$  (= 18.03 kPa), due to the isotropic initial stresses of 24 kPa for the preconsolidation process. For CLRC test, the numerical procedures are the same as those for CSRC test except that a loading pressure is specified at the upper surface of specimen. Figure 15 shows the calculated and monitored quantities in CSRC and CLRC processes respectively as the function of strain rate and loading rate. For convenience of comparison, the results of CSRC and CLRC tests are shown in parallel hereafter. In Fig. 15 (a), the prescribed and monitored displacements at the upper surface of a specimen are slightly different from each other due to the limitations of displacement control system employed. In our numerical analysis, the actual displacement monitored is used for each discretized time step. Thus in the numerical analysis, the fluctuations arising from using the monitored displacements cause the fluctuations in the physical quantities calculated by the proposed procedure (for instance, see Fig. 16). Also in Fig. 15 (b), the monitored loading pressure is slightly different from the prescribed pressure due to the same reason. Conclusively the calculated quantities appear to agree fairly well with the monitored ones both in Figs. 15 (a) and 15 (b). Figures 16 through 20 illustrate some of the detailed numerical results upon which the calculated results shown in Fig. 15 are based. Though it is not possible to directly compare these detailed numerical results with monitored ones, the numerical results seem reliable because the results provide the calculated quantities shown in Figs. 15 (a) and 15 (b) which agree well with the monitored ones. It is emphasized that the detailed numerical results enable to interpret clearly the soft clay behavior during CSRC or CLRC process as follows. In Figs. 16 through 20, vertical stress  $\sigma_v$  is less than lateral stress  $\sigma_h$  until point A<sub>p</sub>, where

suffix  $i$  denotes a finite element number. The definitions of  $B_i$  and  $C_i$  are the same as those given in the discussion about SC test. Note that  $\Delta p^n / \Delta q^n$  is held constant throughout CSRC or CLRC process as illustrated in Fig. 20, although stress ratio  $p^n / q^n$  varies and approaches the following value, as shown in Fig. 17.

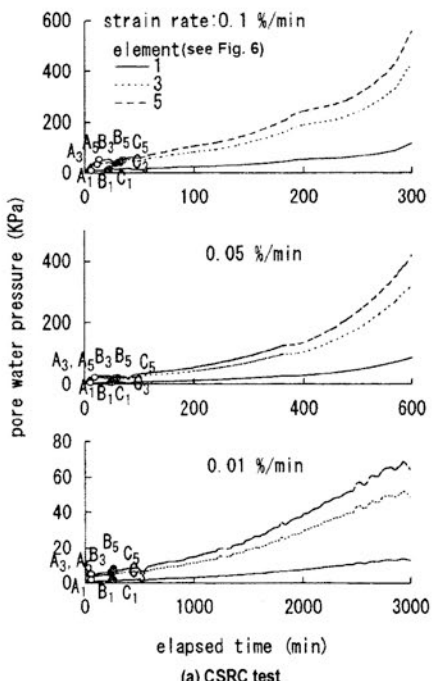
$$\left( p^n / q^n \right)^{\infty} = \frac{\sigma_v - \sigma_v K_o}{(\sigma_v + 2\sigma_v K_o)/3} = 0.834 \quad (16)$$

The constant value of  $\Delta p^n / \Delta q^n$  provides a constant Poisson's ratio of 0.317 throughout CSRC or CLRC process as shown in Fig. 19 as well as in SC test. From the initial state to point  $B_i$ ,  $q^n$  increases from negative value with increasing  $\sigma_v$ , resulting in increase in  $E^n$  as shown in Fig. 19 due to the progress of consolidation. At this state the volumetric strain consists only of  $v_{ce}^n$ . In Figs. 16 through 20, at point  $B_i$ , the stress state of element  $i$  moves to the normally consolidated region. Immediately after passing through  $B_i$ , the specimen enters the quasi-elastic state at which  $v_{ce}^n$  and  $v_{cp}^n$  take place. This transition causes a reduction of  $E^n$  as shown in Fig. 17 due to the considerable increase in volumetric strain, which restrains  $q^n$  or stress ratio  $q^n / p^n$  from increasing further as shown in Fig. 18. The duration of quasi-elastic state is short for this case, because the stress ratio tends to increase rapidly for CSRC or CLRC process. Thus the quasi-elastic state may not have a substantial effect on the overall behaviour during CSRC or CLRC process. Immediately after the specimen has moved through the quasi-elastic state (point  $C_i$  in Figs. 16 through 20), volumetric strain due to shearing  $v_d^n$  takes place and it reduces  $E^n$  as shown in Fig. 19. Subsequently  $E^n$  tends to increase gradually, because the occurrence of volumetric strain due to shearing becomes smaller and smaller with the passage of time as shown in Fig. 18. Note that we assume that the total amount of volumetric strain due to shearing is limited by Eq. (3) as illustrated in Fig. 18. Since most of volumetric strain due to shearing has taken place at the earlier stages of consolidation, little volumetric strain due to shearing occurs at the latter stages of CSRC or CLRC process as in Fig. 18. This means that larger effective stresses are required to produce the constant volumetric strain, which consists of almost only  $v_{ce}^n$  and  $v_{cp}^n$  at the latter stages of CSRC process. This tendency makes the specimen stiffer with the passage of time (see Fig. 19) and makes the total vertical pressure and pore water pressure increase substantially as illustrated in Fig. 15 (a). For CLRC process,  $E^n$  increases proportionally with the elapsed time at the latter stage (Fig. 19b), and the increase in displacement becomes smaller (Fig. 15b), since a loading pressure is specified. Similar to SC test, when the increasing rate of stress ratio is less than  $10^{-3}/\text{min}$ , Eq. (5b) is employed instead of equation (5a). This treatment is applied only to the initial and last stages where volume change with shear takes place for strain rate 0.01 %/min, since the loading pressure for stress ratio continues to increase steadily throughout most stages of the CSRC or CLRC process. In Figs. 16 through 20, the difference of the physical quantities in each finite element is remarkable for the strain rate of 0.1 %/min due to a less uniform distribution of pore water pressure within a specimen, while



(b) CLRC test

Fig. 15. Comparison between calculated and monitored results



(a) CSRC test

Fig. 16. Pore water pressure

this difference seems almost negligible for the strain rate of 0.01 %/min. For instance, Fig. 21 shows the distribution of pore water pressure according to the strain rate in CSRC test. When the strain rate is too fast, the overall material parameters obtained from CSRC test tend to fluctuate

largely, because of the large difference of physical quantities within a specimen. As an example, the difference of Young's modulus in each finite element as shown in Fig. 19, appears to generate the unstable variation in the overall  $c_v$  and  $m_v$  values as shown in Fig. 8.

As seen in Fig. 20,  $\Delta p^n / \Delta q^n$  is held constant throughout CSRC or CLRC process. This is observed also in SC test. This means that  $\Delta \sigma_h / \Delta \sigma_v$  ( $=K_o$ ) is kept constant at the  $K_o$ -consolidation process, while  $\sigma_h / \sigma_v$  varies. This behaviour suggests the possibility that we can estimate the  $K_o$ -value at over-consolidated region from the  $K_o$ -value at normally consolidated region. The constant value of  $K_o$  gives the constant value of Poisson's ratio throughout CSRC, CLRC or SC process as shown in Figs. 14 and 19. The proposed procedure assumes both hypothetical Young's modulus  $E^n$  and Poisson's ratio  $v^n$  to be independent variable, and tries to find these two variables so as to satisfy Eqs. (9) and (10). However for the iteration process to find  $E^n$  and  $v^n$ ,  $v^n$  is maintained as an almost constant value which is the initially assumed trial value. That is, the initially assumed value of  $v^n$  controls the final results of  $E^n$  and  $v^n$ . This may be due to the property of  $K_o$ -consolidation problem in which the lateral deformation is restrained.

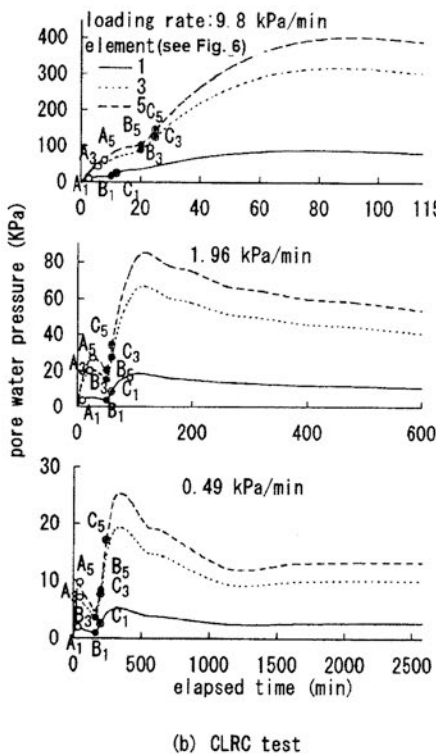


Fig. 16. Pore water pressure

#### Estimation of Secondary Compression Coefficient

Referring to Fig. 12, at the late stage of each loading step in SC test, the stress ratio becomes nearly constant, and the volumetric strain due to shearing occurs in proportion to the logarithm of the elapsed time as seen in Fig. 13. This phenomenon is observed as the secondary compression of remolded young clay as shown in Fig. 10.

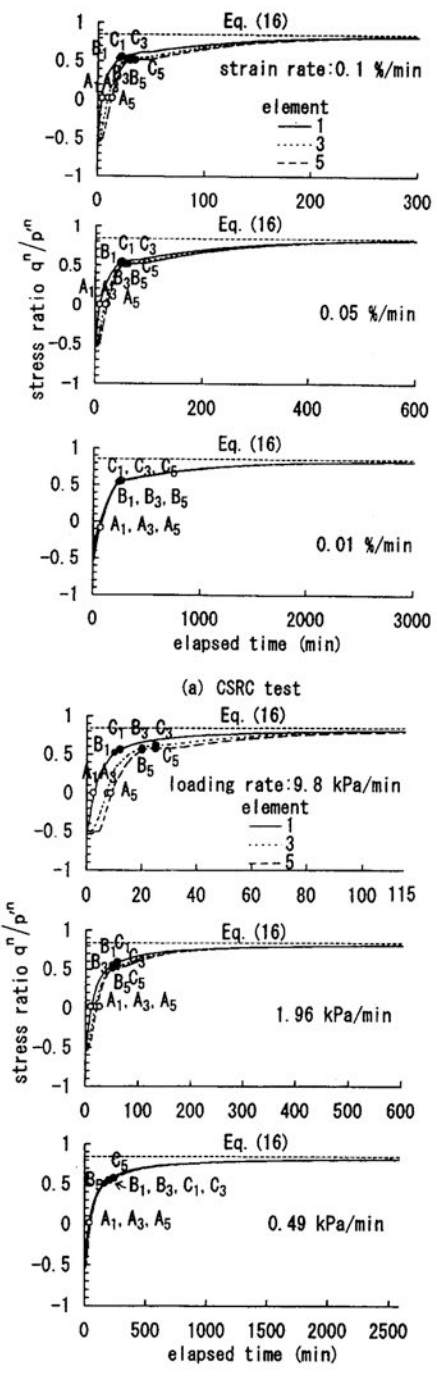


Fig. 17. Stress ratio

In CSRC and CLRC tests, as shown in Fig. 17, the stress ratio continues to increase throughout CSRC or CLRC process. As seen in Fig. 18, most of volumetric strain due to shearing has taken place at the earlier stage of CSRC or CLRC process at any loading rate. This volumetric strain behavior due to shearing at CSRC or CLRC process, makes it difficult to observe the secondary compression for nearly

constant stress ratio, and to find the material parameter representing the time effect. Here we try to estimate an approximate value of the secondary compression coefficient from the result of CSRC or CLRC test. In SC test, the secondary compression coefficient is defined as

$$C_a = \Delta e_v^n / \Delta \log_{10} t^n \quad (17)$$

Considering the stress ratio becomes nearly constant at the latter stage in SC test of normally consolidated state (see Fig. 12), Eq. (18) may give a rough approximation of secondary compression coefficient.

$$C_a = (Dq^n / q^n) / \ln T \quad (18)$$

where the stress ratio is taken as the value given by Eq. (16) which is expected finally in the  $K_0$ -consolidation test. Since  $\ln T$  little changes as stated before, we can calculate  $C_a$  if we can find the value of volume change with shear coefficient  $D$ . Usually  $D$  is estimated by Eq. (3) which requires the result of triaxial compression test. We try to determine the value of  $D$  from the result of CSRC or CLRC test by the following procedure.

- Assume a trial value of  $D$ .
- Perform the numerical calculation by the proposed procedure in which we use the material parameters obtained from CSRC or CLRC test except  $D$  (see Eqs. 13 and 14).
- Calculate the difference between the calculated and monitored pressure at each time step in CSRC test.

The difference is calculated also for pore water pressure both in CSRC and CLRC tests, and for displacement in CLRC test. These differences are evaluated by the sum of the least squares. Figure 22 shows the calculated differences according to  $D$ , where  $J(\sigma_v)$ ,  $J(u)$  and  $J(d)$  are the sum of squares of differences concerning the pressure, pore water pressure and displacement. Since the correct value of  $D$  is 0.056, most of cases appear to give a fairly good estimate. In CLRC test,  $J(u)$  may not provide a good estimate. Figure 23 summarizes the coefficient of secondary compression estimated by each procedure and that monitored in SC test. The procedure based on CSRC or CLRC test overestimates the value, because it uses Eq. (16) whereas the stress ratio in CSRC or CLRC test is smaller than Eq. (16) in SC test. When we make the correction concerning the stress ratio, we can get better estimate of  $C_a$ . Note that we do not assume constant value of secondary compression coefficient, which varies according to the stress ratio and the residual amount of volumetric strain due to shearing as seen in Fig. 23 (Arai, 1994).

#### Consolidation Yield Stress and Loading Rate

In SC test, according to the assumption employed in the present study,  $e - \log \sigma_v$  relationship is constructed as schematically illustrated in Fig. 24. At the normally consolidated state,  $e - \log \sigma_v$  curve moves according to the amount of volume change with shear deformation or the duration of loading.

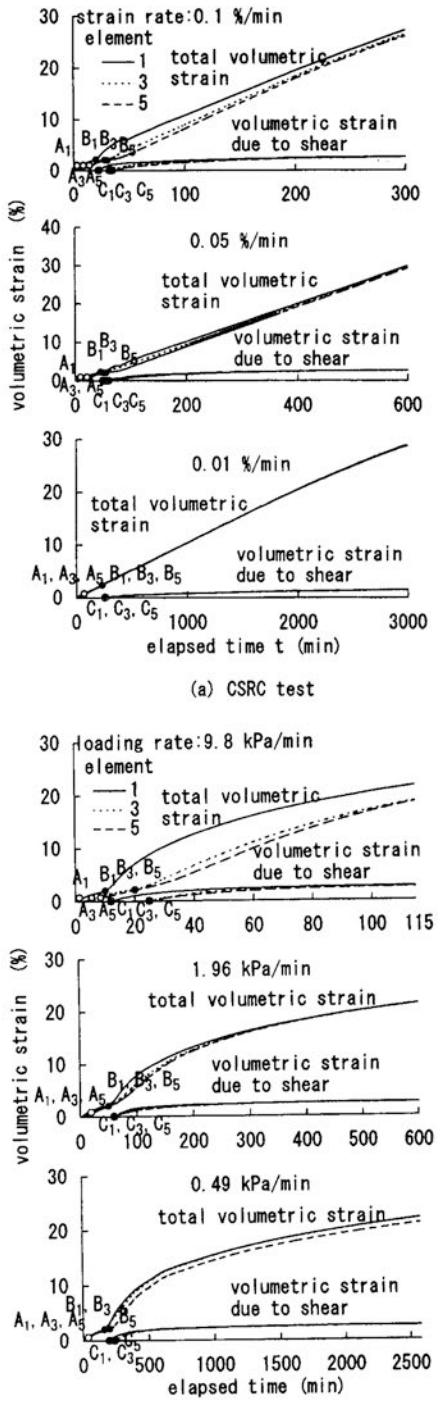


Fig. 18. Components of volumetric strain

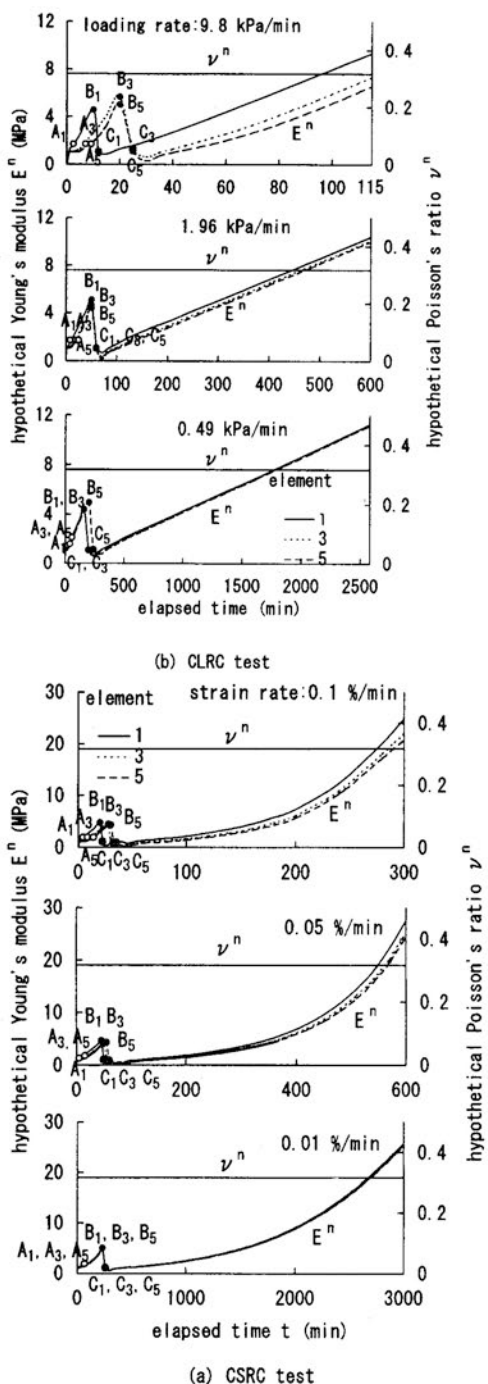


Fig. 19. Hypothetical elastic constants

Since no volume change due to shear is assumed at the over-consolidated state, the apparent consolidation yield stress is not affected by the duration of loading as seen in Fig. 24. As long as assuming no volume change due to shear at the over-consolidated state, the consolidation yield stress has to be determined uniquely in SC test.

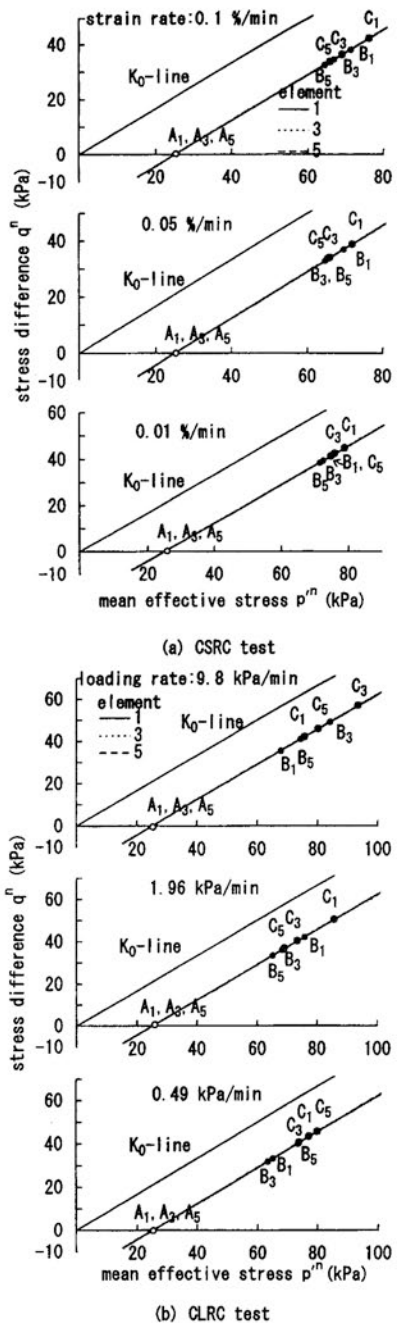


Fig. 20. Stress path

Figure 24 compares the e-log  $\sigma_v$  relationship in SC test with those in CLRC test. All of these relationships are obtained from the numerical results calculated by the proposed procedure.

For CLRC test,  $e$  and  $\sigma_v$  are calculated by Eq. (13) from the numerical results. Only rapid CLRC test gives larger consolidation yield stress. This is because in some finite elements the effective stress state has not attained to the normally consolidated state yet at the apparent consolidation yield stress calculated by Eq. (13), due to extremely non-uniform distribution of pore water pressure in rapid CSRC test (see Fig. 21). There is the possibility that rapid CSRC or CLRC test may give larger consolidation yield stress.

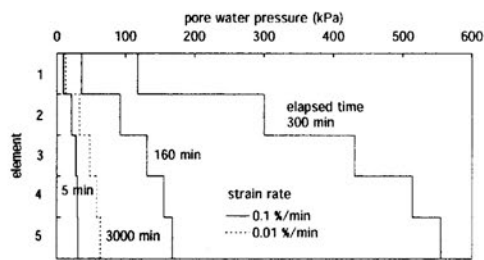
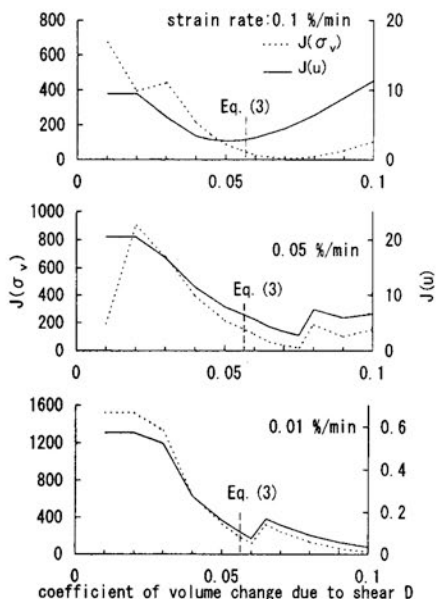


Fig. 21. Distribution of pore water pressure in CSRC test

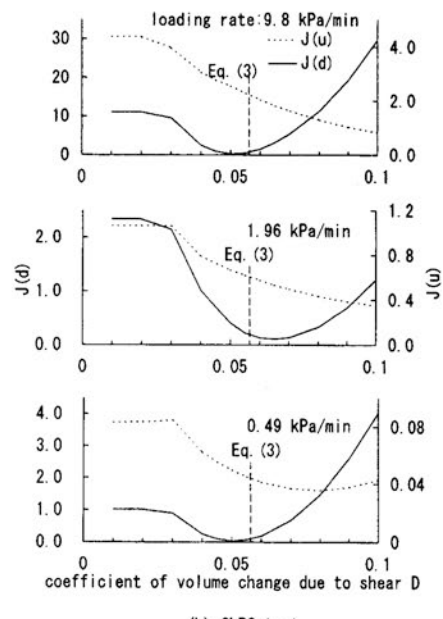
## CONCLUSIONS

Subjected to remolded young clay, this paper has shown that a lot of time dependent behaviour in SC, CSRC and CLRC tests is represented by simple assumption concerning the time dependency of volume change due to shearing.



(a) CSRC test

Fig. 22. Coefficient of volume change due to shear



(b) CLRC test

Fig. 22. Coefficient of volume change due to shear

This paper assumes the time dependency of volume change due to shearing as shown in Fig. 1 and Eqs. (4) and (5). The behavior in SC test is as follows. At the first stage of each loading step the state of specimen is at the quasi-elastic state where little volume change due to shearing takes place. A little time after step loading, volumetric strain due to shearing begins to occur. Because the stress ratio becomes approximately constant at the latter state of each loading step, volume change with shear deformation occurs proportionally with the logarithm of elapsed time, which is observed as the secondary compression.

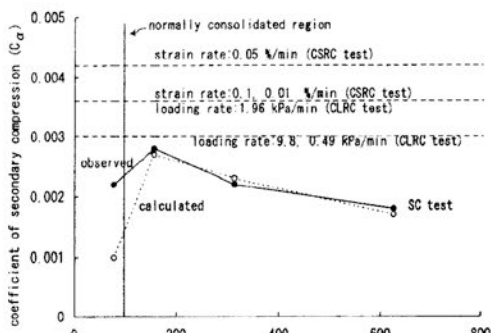


Fig. 23. Coefficient of secondary compression

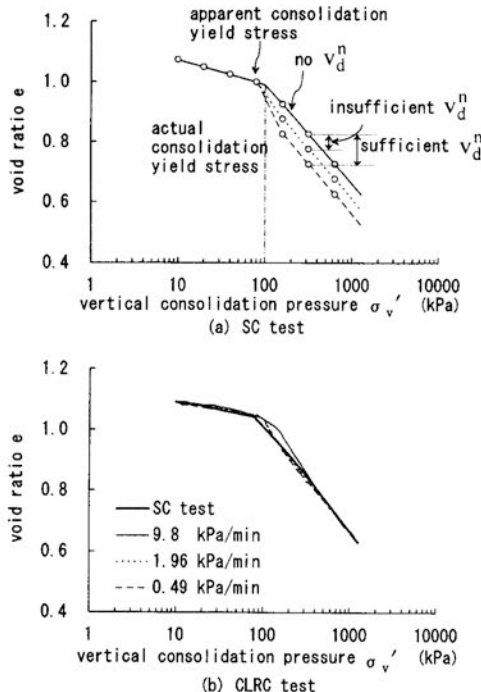


Fig. 24. Consolidation yield stress

The volume change behaviour due to shear in CSRC and CLRC tests is as follows. When the stress state enters the normally consolidated region, the stress state moves to the quasi-elastic state. Since the duration of quasi-elastic state is short in CSRC and CLRC tests, the state does not give a dominant effect to the global behavior of the test specimen. Some time period after the stress state has entered the normally consolidated region, volumetric strain due to shearing tends to occur rapidly with the increase in stress ratio. Since most of volumetric strain due to shearing has taken place at the earlier stage of consolidation, little volumetric strain due to shearing occurs at the latter stage of CSRC or CLRC process. Consideration to such behavior may be effective to correctly interpret the results of CSRC and CLRC tests. Based on these aspects, this paper proposed the procedure for estimating the secondary compression coefficient from CSRC or CLRC test, and discussed the effect of loading rate to the consolidation yield stress observed in SC, CSRC and CLRC tests.

## REFERENCES

- AKAI, K. and TAMURA, T. (1978). Numerical analysis of multi-dimensional consolidation accompanied with elasto-plastic constitutive equation. *Journal of JSCE*, No. 269, pp. 95-104 (in Japanese).
- ARAI, K. (1985). Representation of soft clay behavior based on minimization of dissipated energy. *Proceedings of the 5<sup>th</sup> International Conference on Numerical Methods in Geomechanics*, Nagoya, Japan, Vol. 1, pp. 277-284.
- ARAI, K. (1994). Relationship between time effects in triaxial test and secondary compression. *Soils and Foundations*, Vol. 34, No. 3, pp. 59-69.
- JSSMFE (The Japanese Society of Soil Mechanics and Foundation Engineering) (1994). Designation: JSF T 412-1993 Method for Constant strain rate Consolidation Test on Soils.
- CRAWFORD, C.B. (1964). Interpretation of the consolidation test. *ASCE Journal of Soil Mechanics Foundations Divisions*, Vol. 90, No. SM5, pp. 87-102.
- JANBU, N., TOKHEIM, O. and SENNESET, K. (1981). Consolidation tests with 22 continuous loading. *Proceedings of the 10<sup>th</sup> International Conference on Soil Mechanics and Foundation Engineering*, Stockholm, I, pp. 645-654.
- LEE, K. (1981). Consolidation with constant rate of deformation. *Géotechnique*, Vol. 31, No. 2, pp. 215-229.
- LEROUEIL, S., KABBAJ, M., TAVENAS, F. and BOUCHARD, R. (1985). Stress-strain-strain rate relation for the compressibility of sensitive natural clays, *Géotechnique*, Vol. 35, No. 2, pp. 159-180.
- NAGARAJ, T. S., PANDIAN, N. S. & Narashima Raju, P. S. R. (1994). Stress-state permeability relations for overconsolidated clays, *Géotechnique*, Vol. 44, No. 2, 349-352.
- OHTA, H. (1971). *Analysis of deformations of soils based on the theory of plasticity and its application to settlement of embankments*. Dr. Eng. Thesis, Kyoto University.
- SEKIGUCHI, H and OTHA, H (1977). Induced anisotropic and time dependency in clays, constitutive equations of soils. *Proceedings of the 9<sup>th</sup> International Conference on Soil Mechanics and Foundation Engineering*, Tokyo, pp. 229-238.
- SHIBATA, T. (1963). On the volume change of normally consolidated clays. Annals, Disaster Prevention Research Institute, Kyoto University, No. 6, pp. 128-134 (in Japanese).
- SMITH, R.E. and WAHLS, H.E. (1969). Consolidation under constant rates of strain. *J. Soil Mech. Fdns Div.*, Am. Soc. Civ. Engrs 95, No. SM2, pp. 519-539.
- WISSA, A.E.Z., CHRISTIAN, J.T., DAVIS, E.H. and HEIBERG, S. (1971). Consolidation at constant rate of strain. *ASCE Journal of Soil Mechanics Foundations Divisions*, Vol. 97, No. SM10, pp. 1393-1413.
- YIN, J. H. and GRAHAM, J. (1988). Viscous-elastic-plastic modeling of one-dimensional time dependent behavior of clays, *Canadian Geotechnical Journal*, Vol. 26, pp. 199-209.
- ZNIDARCIC, D., SHIFFMAN, R.L., PANE, V., CROCE, P., KO, H.Y. and OLSEN, H.W. (1986). The theory of one-dimensional consolidation of saturated clays: part V, constant rate of deformation testing and analysis. *Géotechnique*, Vol. 36, No. 2, pp. 227-237.

## NOTATION

$A$	cross-sectional area of the specimen	$T$	time length required to make volume change with shear take place completely
$C_a$	approximation of secondary compression coefficient	$u^n$	excess pore water pressure
$c_v^n$	coefficient of consolidation	$q^n/p^n$	stress ratio
$C_c$	compression index	$\Delta q^n/\Delta p^n$	incremental stress ratio
$C_s$	swelling index	$v^n$	volumetric strain
$C_a$	coefficient of secondary compression	$\Delta v^n$	incremental volumetric strain
$D$	coefficient of volume change with shear	$\Delta v_c^n$	incremental volumetric strain due to consolidation
$e_0$	initial void ratio	$\Delta v_{ce}^n$	incremental elastic component of volumetric strain due to consolidation
$e^n$	void ratio	$\Delta v_{cp}^n$	incremental plastic component of volumetric strain due to consolidation
$E^n$	Young's modulus	$\Delta v_d^n$	incremental plastic component of volumetric strain due to shearing
$G^n$	shear rigidity	$v_d^n$	volumetric strain due to shearing
$H^n$	height of the specimen	$v_d^*$	value of volume change due to shearing determined by Eq. (4) and (5a) at the stress ratio ( $q^n/p^n$ ) <sup>*</sup> using effective stress path in conventional triaxial test as given $v_d^* = 0.004$ (Arai, 1985)
$H^s$	height of solids	$\Delta$	increment of succeeding physical quantity
$k^n$	coefficient of permeability	$\epsilon^n$	shear strain
$K_o$	the at rest earth pressure coefficient	$\Delta\epsilon^n$	incremental shear strain
$K^n$	bulk modulus	$\kappa$	gradient of over consolidation line on e-log $\sigma_v$ diagram as given $\kappa=0.434C_s$
$M$	slope of critical state line	$\lambda$	gradient of normal consolidation line on e-log $\sigma_v$ diagram as given $\lambda=0.434C_c$
$m_v^n$	coefficient of volume compressibility	$\sigma_v^n$	vertical stress
$n$	a discretized time step number	$\sigma_h^n$	horizontal stress
$p^n$	mean effective stress	$\nu^n$	Poisson's ratio
$\Delta p^n$	incremental mean effective stress		
$p^n$	axial loading force		
$q^n$	stress difference		
$\Delta q^n$	incremental stress difference		
$\Delta t^n$	length of discretized time step		
$t_l^n$	elapsed time after stopping the increase in the stress ratio		

## TECHNICAL NOTE

# A SHORT-CUT METHOD FOR PREDICTING STRENGTH OF CEMENT TREATED SOFT BANGLADESH CLAYS AND THE ALTERATION OF OTHER ENGINEERING PARAMETERS

M. M. Rahman<sup>1</sup>, M.A. Taiyab<sup>2</sup>, A. Siddique<sup>3</sup> and M. K.Uddin<sup>4</sup>

**ABSTRACT:** Various regions of Bangladesh with deep deposits of soft clays at high water content cause many problems associated with the engineering construction since they have low strength and high compressibility. Chemical admixture improvement is one of the effective techniques to solve the Problems. This technique can be applied for the deep and shallow foundations. Surplus clay, such as soft clays from construction works, can also be improved by this technique to be an engineered geo-material. Based on the consolidation, triaxial and unconfined compression test results, here it is revealed that the clay-water content/cement ratio,  $w_c/c$  is the dominant parameter, which governs deformation and strength characteristics of the stabilized soft clays. As a result, simple numerical equations related to  $w_c/c$  for short-cut predicting strength and combining the relation among strength, curing time, water content and cement content are presented. Alteration and relation of other engineering parameters are also explained.

**Keywords:** cementation bond, cement stabilized clay, clay-water/cement ratio, high water content, Unconfined compression test.

## INTRODUCTION

Chemical admixture stabilization has been extensively used both in deep and shallow foundations in order to improve inherent properties of soil such as strength and deformation behavior by deep mixing method. Moreover, the soft clays being released from the construction works can be made by mixing with cement. Such soft clay formations in Bangladesh, especially when the in-situ water contents are high, unless they are markedly naturally cemented, have large potential for settlement with low inherent axial strength (Siddique et al., 2002). There are three types of clay in Bangladesh on the basis of plasticity, namely high plastic (HP) clay, medium plastic (MP) clay and low plastic (LP) clay.

It is of interest to understand and be able to predict the strength development of stabilized clays. There are very few researches on this area. Horpibulsuk (2002) and Chew et al. (2004) have examined the behavior of compressibility and permeability of cement stabilized soft clays. Also, the prediction of strength development of cement stabilized clays has been presented by Nagaraj et al. 1996; Horpibulsuk et al., 1999; 2000; and Horpibulsuk and Miura, 2000; 2001. But most the use of this prediction is limited for the clays at their liquid limit stages. To overcome this limitation in the paper, a factor- $w_c/c$  is proposed as the influential parameter for predicting strength and combining the relation among strength, curing time, clay water content and cement content. With this relation, one can short-cut estimate the strength at any curing times and conditions of clay-water content and cement content from only one set of strength data. Also, the relations of yield strength and effective cohesion with unconfined

strength are proposed.

## EXPERIMENTAL INVESTIGATION

### Soil Samples

Soft clays were collected in various districts of Bangladesh such as HP clay from Gazipur, MP clay from Gopalganj and LP clay from Khulna. The samples were collected from depth of 2 to 3 m from existing ground level with disturbed and undisturbed state. Their physical and engineering properties are listed in Tables 1 and 2, respectively. Type I Portland cement was used in this study. Samples were prepared from these clays and cement slurries.

**Table 1 Characteristics values of the physical properties of the untreated base clays**

Properties	Characteristics Values		
Type of Soil	HP clay (LL > 50%)	MP clay (LL =35 - 50%)	LP clay (LL < 35%)
Liquid Limit, LL, (%)	78	47	33
Plastic Limit, PL, (%)	31	25	20
Plasticity Index, PI, (%)	47	22	13
In-Situ Water Content, $w_n$ (%)	43	36	27
Liquidity Index, LI	0.83	1.68	2.54
*Clay (%)	73	63	56
*Silt (%)	23	29	34
*Sand (%)	4	8	10
Bulk Unit Weight, $\gamma_b$ (kN/m <sup>3</sup> )	15.05	14.67	14.45
Dry Unit Weight, $\gamma_d$ (kN/m <sup>3</sup> )	8.85	9.05	9.44
Specific Gravity, $G_s$	2.680	2.673	2.668
Activity of clays, $A_c$	0.64	0.35	0.23
Degree of saturation, $S_r$ (%)	89	84	78
Unified Soil Classification System	CH	CL	CL

<sup>1,2</sup>Assistant Professor, Department of Civil Engineering, Dhaka University of Engineering and Technology, Gazipur, Bangladesh.

<sup>3</sup>Professor, Department of Civil Engineering, Bangladesh University of Engineering and Technology, Dhaka, Bangladesh.

<sup>4</sup>Professor, Institute of Appropriate Technology, Bangladesh University of Engineering and Technology, Dhaka, Bangladesh.

## Methodology Of Testing

The clay paste was passed through a 2-mm sieve for removal of shell pieces and other bigger size particles. The intentional increase in water content is to simulate the water content increase taking place in the wet method of injecting cement admixture in deep mixing without compaction and the significant in jet grouting. The clay with its water content corresponding to the above simulating levels quantity of cement resulting in clay-water/cement ratio,  $w/c$  of 7.5, 10 and 15 was thoroughly mixed so as to ensure uniform dispersion of the cement. The clay water content ( $w_i$ ) would be 120%, 150%, 200% and 250%. Cement contents,  $c$  as low as 8% and as high as 33% were adopted for the clay-cement mixtures of initial clay water content of 120% at  $w/c$  of 15 and initial clay water content of 250% at  $w/c$  7.5 respectively. Also,  $w/c = 2, 2.5, 4$  and 30 was used to mix with 120% water for only unconfined compression test. The mixing time was arbitrarily fixed at 10 minute. Such a uniform paste was transferred to cylindrical moulds of 50 mm diameter ' 100 mm height and 75 mm diameter ' 100 mm height with connecting 50 mm height top collars and bottom ended cap, taking care to prevent any air entrapment. Cylindrical moulds of 50 mm diameter ' 100 mm height were used for unconfined compression and triaxial compression test samples. Cylindrical moulds of 75 mm diameter ' 100 mm height were used for consolidation test samples. After 24 hours the cylindrical samples were dismantled. All the cylindrical samples were wrapped in thick polythene bags and these were stored in a room of approximate constant temperature and humidity room ( $25 \pm 2^\circ\text{C}$ ) until the lapse of different planned curing times.

Unconfined compression tests were carried out after 1, 2, 4, 12, 24, 52 and 104 weeks of curing. Isotropically consolidated undrained (CIU) triaxial compression and consolidation tests were run on samples after 4 and 12 weeks of curing. The effective confining pressures,  $p'_0$  for CIU triaxial test were 50, 100, 200 and 400 kPa. A back pressure of 100 kPa was maintained to insure high levels of degree of saturation at all levels of testing.

## Parameters

Horpibulsuk and Miura (2000) proposed, "..... for given clay-cement mixtures, the strength at any curing time depends on one factor clay-water content/cement ratio,  $w/c$ ". As an analogy the parameter that can be identified by Horpibulsuk et al., (2001) and Miura et al., (2001), is clay-water cement ratio,  $w/c$ , which is the ratio of initial water content of the clay,  $w_i$  (%) to the cement content,  $c$  (%). The cement content,  $c$  is the ratio of cement to clay by weight both reckoned in the dry state. To obtain the same value of  $w/c$ , it is possible to vary the water content of the clay, or the amount of cement, or both as the case might be. In order to examine to what extent the applicability of  $w/c$  is varied, the water content of clay is varied over a wide range in this study.

## Effect of clay water content/cement ratio and clay type on physical properties ( $w, \gamma_d, G_s$ and $S_r$ )

Table 3 shows the physical properties of the cement treated clays from triaxial and unconfined compression tests. Comparing Tables 1 and 3, dry unit weight ( $\gamma_d$ ) and specific gravity ( $G_s$ ) of cement treated clays at high water

content are lower than those of untreated base clays.  $\gamma_d$  are decreased but  $G_s$  are increased with increasing clay water/cement ( $w/c$ ) ratio (decreasing cement content).  $\gamma_d$  are decreased but  $G_s$  are increased with increasing plasticity index of soil. The existing water content ( $w$ ) and degree of saturation ( $S_r$ ) at 4 weeks of cement treated clays are increased with increasing  $w/c$  ratio.  $w$  and  $S_r$  are increased with increasing plasticity index of soil.

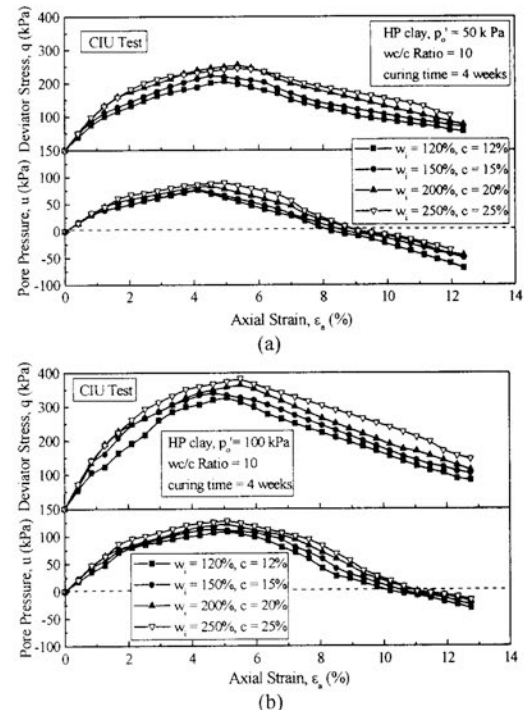


**Fig. 1 Deviator stress and pore pressure versus axial strain response at same  $w/c = 10$  for varying pre-shear effective consolidation pressure,  $p'_0$**   
**(a) 50 kPa and (b) 100 kPa**

## Effect of clay water content/cement ratio and clay type on compressibility( $e, \epsilon_v, C_c, C_s$ and $\sigma_y'$ )

The effects of clay water content/cement ratio and clay type on compressibility characteristics of cement treated clay are presented by the results of consolidation tests. Comparing Tables 2 and 4, void ratio ( $e$ ) and volumetric strain ( $\epsilon_v$ ) of cement treated clays at high water content are higher than those of untreated base clays.  $e$  and  $\epsilon_v$  of cement treated clays are increased with increasing clay water/cement ( $w/c$ ) ratio (decreasing cement content), while they are decreased with increasing curing time and increasing plasticity index of soil. Compression index ( $C_c$ ) are increased and swell index ( $C_s$ ) are decreased of cement treated clays at high water content are higher than those of untreated base clays.  $C_c$  and  $C_s$  of cement treated clays are increased with increasing clay water/cement ratio, while they are decreased with increasing curing time and they are increased with increasing plasticity index of soil (PI) and mixing water content ( $w_i$ ). The yield stress ( $\sigma_y'$ ) of cement treated clays at high water content are higher than those of untreated base clays.  $\sigma_y'$  are decreased with increasing clay water/cement ratio, while they are increased with increasing

curing time.  $s_y$  of HP clay ( $PI = 47\%$ ) are more than that of LP clay ( $PI = 13\%$ ) but  $\sigma_y$  of LP clay are more than that of MP clay ( $PI = 22\%$ ). It can be inferred that physicochemical changes depend on illite and kaolinite mineral in the clay which controls the compressibility. The changing of these clay minerals due to cementation have been confirmed from X-ray diffraction analysis for these three clays studied.

#### Effect of clay water content/cement ratio and clay type on strength parameters ( $c'$ and $\phi'$ )

The effects of clay water content/cement ratio and clay type on strength parameter characteristics of cement treated clays are explained by the results of consolidated undrained triaxial compression tests. In Table 5, effective cohesion ( $c'$ ) and effective friction angle ( $\phi'$ ) of cement treated clays at high water content are higher than those of untreated base clays.  $c'$  and  $\phi'$  of cement treated clays are decreased with increasing clay water/cement (wc/c) ratio (decreasing cement content), while  $c'$  are increased and  $\phi'$  are decreased with increasing curing time.  $c'$  and  $\phi'$  of cement treated clays are decreased with increasing mixing water content.  $c'$  of HP clay are more than that of LP clay but  $c'$  of LP clay are more than that of MP clay.  $\phi'$  of HP clay are more than that of LP clay but  $\phi'$  of LP clay are more than that of MP clay. This may be due to the effect of stiffness and more lubricating effect in cement treated condition that prevents soil slippage and frictional movement.

#### Effect of clay water content/cement ratio and clay type on stress-axial strain and pore pressure-axial strain

The effects of clay water content/cement ratio and clay type on strength characteristics of cement treated clays are

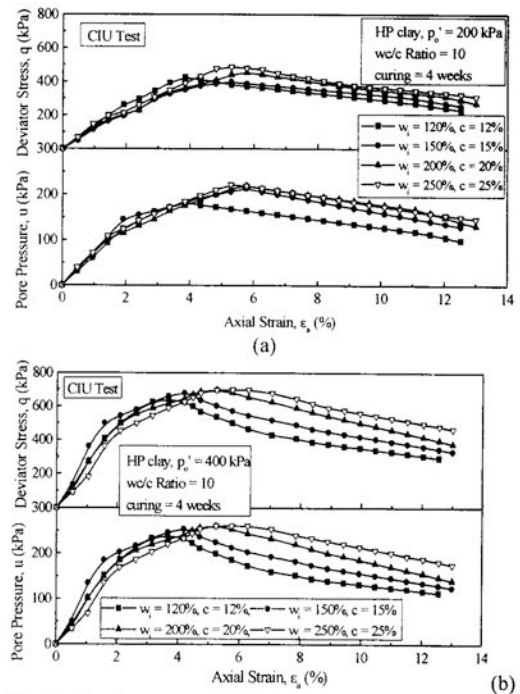


**Fig. 2 Deviator stress and pore pressure versus axial strain response at same  $wc/c = 10$  for varying pre-shear effective consolidation pressure,  $p_o'$**   
**(a) 200 kPa and (b) 400 kPa**

**Table 2 Characteristics values of the engineering properties of the untreated base clays**

Properties	Characteristics Values			
	Type of Soil	HP clay ( $PI = 47\%$ )	MP clay ( $PI = 22\%$ )	LP clay ( $PI = 13\%$ )
Unconfined Strength, $q_u$ (kPa)		50	41	58.5
Strain at Failure, $\epsilon_f$ (%)		3.67	3.65	4.00
Initial Void Ratio, $e$ at $\sigma_v' = 12.5$ kPa		1.81	1.96	2.10
Volumetric Strain, $\epsilon_v$ (%) at $\sigma_v' = 1600$ kPa		3.0	4.0	5.4
Compression Index, $C_c$		0.737	0.781	0.863
Swell Index, $C_s$		0.124	0.127	0.131
Yield Stress, $\sigma_y$ (kPa)		70	61	65
Overconsolidation Ratio (OCR)		1.33	1.18	1.26
Deviator Strength, $q$ (kPa) at $p_o' = 200$ kPa		98	92	89
Axial Strain at Failure, $\epsilon_f$ (%)		11	10.7	10.2
Peak Pore Pressure $u$ (kPa) at $p_o' = 200$ kPa		139	131	126

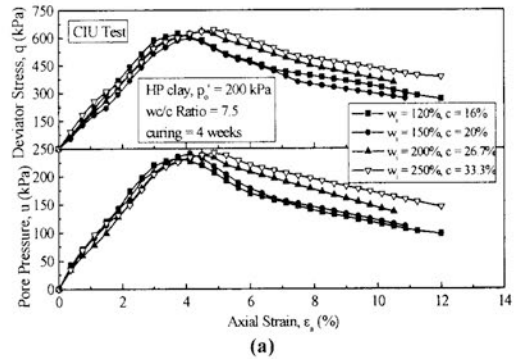
**Table 3 Physical properties of cement treated clays at 4 week curing and  $w_i = 120\%$**

Clays	wc/c ratio	c (%)	w (%)	$\gamma_d$ (kN/m <sup>3</sup> )	G <sub>s</sub>	S <sub>r</sub>
HP clay ( $PI = 47\%$ )	7.5	16	96.7	6.37	2.661	97.8
	10	12	103.4	5.94	2.667	98.1
	15	8	108.9	5.47	2.670	98.6
MP clay ( $PI = 22\%$ )	7.5	16	87.4	6.98	2.634	96.7
	10	12	95.4	6.72	2.653	96.9
	15	8	103.6	6.43	2.660	97.3
LP clay ( $PI = 13\%$ )	7.5	16	74.8	7.52	2.617	95.3
	10	12	79.3	7.31	2.631	95.5
	15	8	92.7	6.83	2.644	96.1

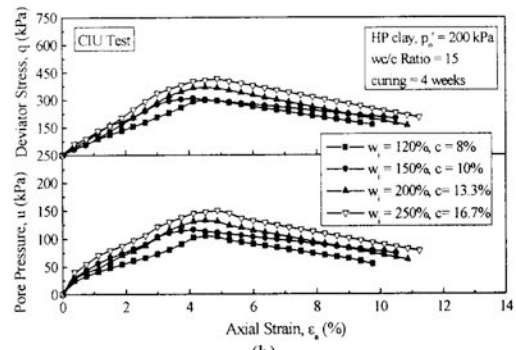
**Table 4. Values of void ratio, volumetric strain, compression index and yield stress for cement treated clays**

Clays type	w/c ratio	w <sub>i</sub> (%)	Curing (weeks)	e at $\sigma'_v = 12.5$ kPa	$\epsilon_v$ (%) at $\sigma'_v = 1600$ kPa	$C_s$	$C_c$	$\sigma'_y$ (kPa)
HP clay (PI = 47%)	15	120	4	2.53	18.8	0.012	0.982	394
		150	4	2.97	27.3	0.015	1.115	397
		200	4	3.63	29.3	0.021	1.228	402
		250	4	4.31	31.6	0.026	1.311	411
	10	120	4	2.41	16.0	0.010	0.916	501
		150	4	2.85	19.8	0.013	1.082	508
		200	4	3.30	22.6	0.019	1.203	517
		250	4	3.98	25.8	0.024	1.261	510
	7.5	120	4	2.32	14.4	0.009	0.882	611
		12	12	1.79	12.2	0.007	0.849	709
		150	4	2.77	17.8	0.011	0.991	617
		200	4	3.10	20.6	0.016	1.154	622
		12	12	2.87	17.8	0.014	1.142	718
		250	4	3.75	23.1	0.021	1.213	620
		12	12	3.35	21.2	0.019	1.181	710
		120	4	2.47	18.0	0.004	0.847	316
MP clay (PI = 22%)	7.5	150	4	2.94	21.2	0.008	0.878	320
		200	4	3.34	23.6	0.010	0.976	331
		250	4	4.07	26.6	0.014	1.131	325
		120	4	2.63	19.5	0.007	0.855	371
LP clay (PI = 13%)	7.5	150	4	3.01	22.3	0.009	0.912	366
		200	4	3.52	26.4	0.014	1.065	365
		250	4	4.33	30.4	0.018	1.108	375

the ( $q$ ,  $\epsilon_a$ ) curves of sample are found that the deviator stress increases to a peak value and afterward strain softens to a lower value of  $q$ . With the incremental values of confining pressure ( $p_o'$ ), the enhancement of more axial clearly manifested by the results of isotropically consolidated undrained (CIU) triaxial and unconfined compression tests and pore pressure characteristics by CIU triaxial tests. Figures 1 to 3 show the deviator stress,  $q$  and axial strain  $\epsilon_a$  relationships of stabilized HP clay samples at w/c values of 7.5, 10 and 15. The characteristic shapes of stress is evident in the Figs. 1 and 2. Moreover, the lower the w/c have larger peak deviator stress and lower failure strain than the higher the w/c (Fig. 3). The excess pore pressure development with axial stain is shown in Figs. 1 to 3 for the samples cured for 4 weeks with w/c value of 7.5, 10 and 15. In contrast, the behavior of samples for cement treated clays is similar to that of over-consolidated clay. The ( $u$ ,  $\epsilon_a$ ) curves show distinct peaks that occur at low values of axial strain and the negative pore pressure is found for the sample subjected to low  $p_o'$  value of 50 kPa and 100 kPa as illustrated in Fig. 1. The role of  $p_o'$  is very clear that the higher value of  $p_o'$ , the greater is the pore pressure generation. It is moreover noted that the cement treatment modifies the pore pressure response behavior by reducing considerably the strain at peak excess pore pressure,  $u_{max}$ . The  $u_{max}$  occurs at very low strain for the sample of low effective cell pressure but at larger strain for the sample of higher effective cell pressure.



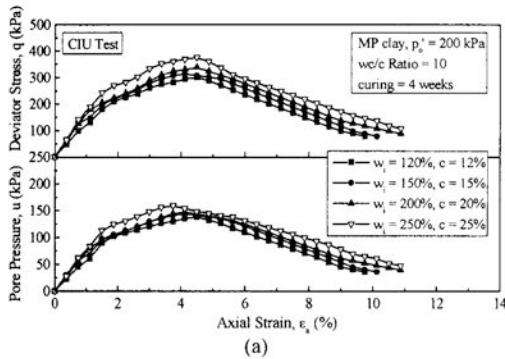
(a)



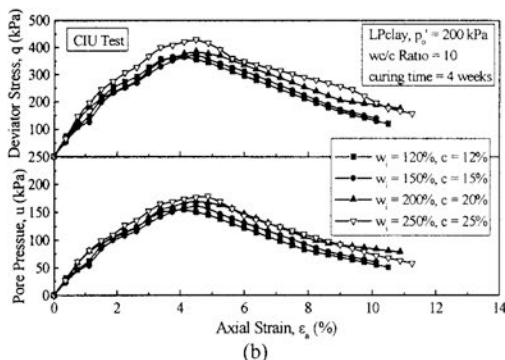
(b)

**Fig. 3 Deviator stress and pore pressure versus axial strain response for HP clay at  $p_o' = 200$  kPa and w/c Ratio of (a) 7.5 and (b) 15**

Figures 4 and 5 show the deviator stress-axial strain and excess pore pressure-axial strain behavior at 4 and 12 weeks respectively for MP and LP clays having the same w/c value of 10 and  $p_o'$  of 200 kPa. Both mixtures show practically the same feature of ( $q$ ,  $\epsilon_a$ ) and ( $\Delta u$ ,  $\epsilon_a$ ) relations. From the above results, it is of interest to conclude that the clay water content/cement ratio is a salient parameter controlling the engineering behavior such as strength and deformation characteristics. As a result, the strength predication can be proposed in terms of w/c. It reveals that the higher curing time, the greater strength. Results for same w/c,  $p_o'$ -values and curing periods, HP clay is gained more deviator strength than LP clay but LP clay is gained more deviator strength than MP clay.



(a)

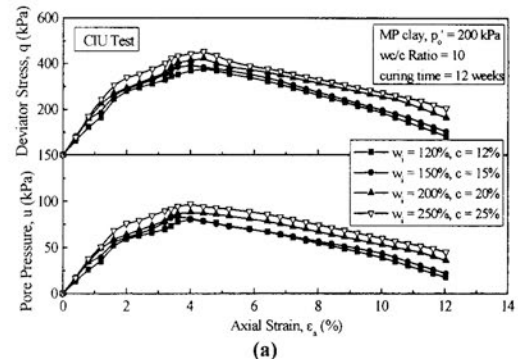


(b)

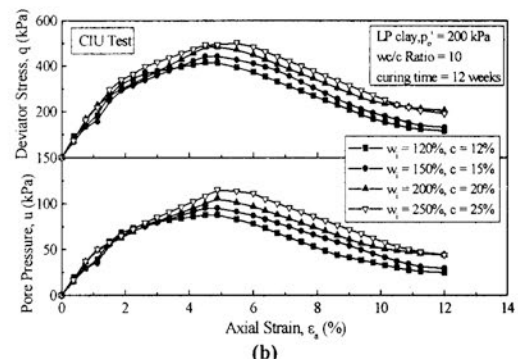
**Fig. 4 Deviator stress and pore pressure versus axial strain response at same w/c = 10 and  $p_o' = 200$  kPa at 4 weeks for (a) MP clay and (b) LP clay**

Figures 6 and 7 show the typical stress-strain relationships in unconfined compression tests of samples with different initial water contents, different types of clay and different levels of cementing agent but at the same w/c ratio, at a curing time of 4 and 12 weeks. The w/c ranges included in these figures are 7.5, 10 and 15. It reveals that the lower the w/c (higher the cement content), the greater the enhancement of the cementation bond strength inducing higher strength. Such results are confirmed from previous study of Horpibulsuk and Miura, (2000); Miura et al., (2001) and Horpibulsuk et al., (2001). The similar stress-strain behaviors are shown for treated samples having the same clay-water/cement ratio. It reveals that the higher the curing time, the higher strength and the lower strain (Fig. 6). For the improvement of soft clay at high water content by cement admixture, it is concluded that high plastic clay undergoes better improvement than low plastic clay but low

plastic clay undergoes better improvement than medium plastic clay. This is because as possibly, the chemical properties response such as pH value, electrical conductivity, exchangeable cations and finally cementitious products for MP clay (PI = 22%) have lowest values than those of HP clay (PI = 47%) and LP clay (PI = 13%), which have been found from the clays studied. Another possible cause, according to the criteria of pH value determination for the base soil, HP clay and LP clay are alkaline in nature and MP clay is acidic in nature, which have exchangeable H<sup>+</sup> ion. Thus, it may be called that MP clays have a large reserve of potential acidity or buffering capacity. As buffering capacity was defined as the capacity of the soil to release exchangeable H<sup>+</sup> ion into the soil solution to restore the equilibrium pH and due to which there is no soil reaction with cement until the reserve H<sup>+</sup> ion is exhausted. And it is also added other causes.



(a)



(b)

**Fig. 5 Deviator stress and pore pressure versus axial strain response at same w/c = 10 and  $p_o' = 200$  kPa at 12 weeks for (a) MP clay and (b) LP clay**

#### Strength prediction based on clay-water/cement ratio's concept

Now, strength prediction of cement treated clays are discussed based on the test results of Bangladesh soft clays (HP, MP and LP clays). Detail properties of these clays are shown in Tables 1 and 2. This strength prediction of cement stabilized clays merits examination for engineering considerations, which was already examined by Horpibulsuk and Miura, 2000; Miura et al., 2001 and Horpibulsuk et al., 2001. For instance, it will be possible to estimate how much cement content is needed for obtaining a required level of strength corresponding to the curing time and clay-water content. The predication referred to the clay water content/cement ratio's concept was proposed by Horpibulsuk and Miura (2000). The observed relationship

between unconfined compressive strength after a certain period of curing can be expressed by a formula having the following equation:

$$q_u = \frac{A}{B^{(w/c)}} \quad (1)$$

where,  $q_u$  is the unconfined compressive strength of cement stabilized clay at a stated age, ( $w/c$ ) is the clay-water content/cement ratio, A and B are constant depending on the characteristic of clay, type of cement and curing time.

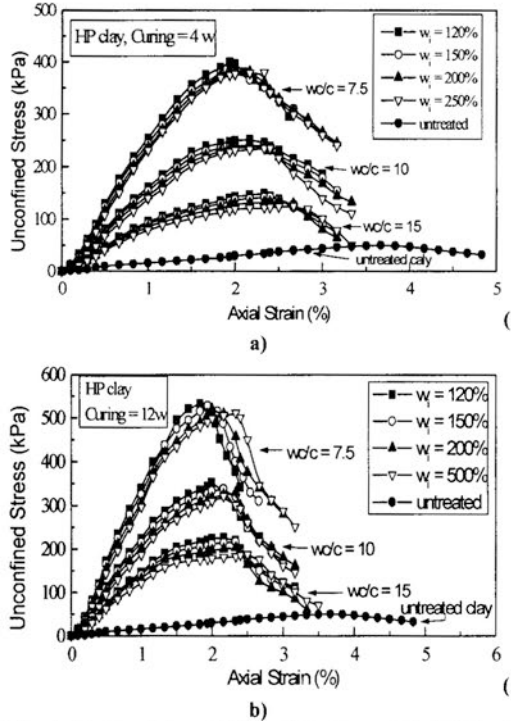


**Fig. 6 Stress-strain relationships of cement-stabilized HP clays in unconfined compression test at different w/c ratio for curing (a) 4 weeks and (b) 12 weeks**

Figure 8(a) shows the strength prediction of cement stabilized high plastic (HP) clay, which agrees well with this proposed method indicated by the coefficients of correlation are higher than 0.97 for all cases. For the clays having their water contents are equal to and higher than liquid limit and  $w/c$  ranging from 2 to 30, the A-values are 1241, 1562, 1771, 2952 kPa for 1, 4, 12, 52 week-curing time, respectively and the B-value is 1.24 for all cases of 1, 4, 12, 52 week curing time which are derived from equation (1). The relationship between  $q_u$  and  $w/c$  of medium plastic (MP) clay is also performed well with high coefficients of correlation (higher than 0.98 for all cases) as shown in Fig. 8(b). The A-values are 943, 1211, 1395 and 2211 kPa for 1, 4, 12, 52 week-curing time, respectively. The B-value is 1.24 for all cases for curing time. Similarly, the strength prediction of cement stabilized low plastic (LP) clay is presented with coefficients of correlation being higher than 0.98 as shown in Fig. 8(c). The A-values are 1054, 1354, 1557, 2492 kPa for 1, 4, 12 and 52 week-curing time, respectively. The B-value is 1.24 for all cases of curing. While, Horpibulsuk and Miura (2000) reviewed

the results for cement treated Bangkok clay and found the A-values, 969, 1130 and 1739 kPa for 7, 14 and 28 day-curing time, respectively and the B-value, 1.24 ( $R^2 = 0.99$ ).

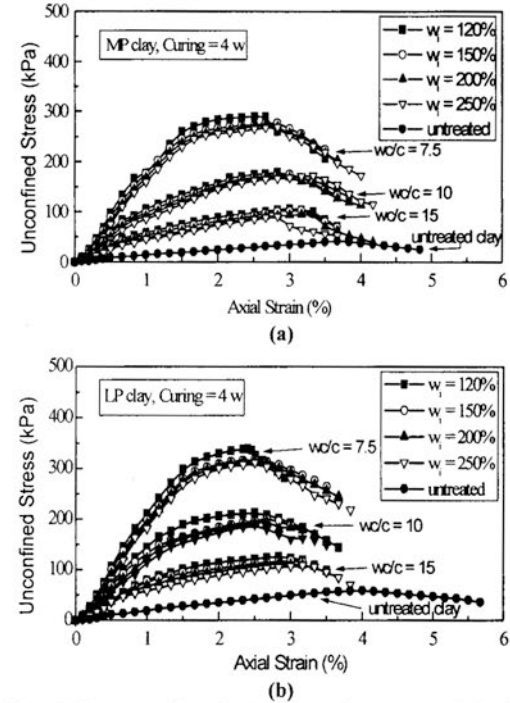


**Fig. 7 Stress-strain relationships of cement-stabilized clays in unconfined compression test at different w/c ratio and curing, 4 weeks for (a) MP clay and (b) LP clay**

From above prediction, the B-value can be taken as 1.24 for the all cases of Bangladesh (HP, LP and MP) clays but the A-values are different. For every curing time, the A-values of stabilized clays for HP clay are highest. Among the clays presented here, such the HP clay provide the highest strength at the same conditions of curing time, clay-water content and cement content. Since B-value is identical for all clays, the same strength ratio equation of cement stabilized clays at a particular curing time can be obtained in terms of clay water content/cement ratio as follows:

$$\left( \frac{q_{(w/c)1}}{q_{(w/c)2}} \right) = 1.24 \left[ \left( \frac{w/c}{w/c} \right)_2 - \left( \frac{w/c}{w/c} \right)_1 \right] \quad (2)$$

where,  $q_{(w/c)1}$  is the strength to be estimated at clay water content/cement ratio of  $(w/c)_1$  and  $q_{(w/c)2}$  is the strength value at clay water content/cement ratio of  $(w/c)_2$ . From this prediction, it reveals that the  $w/c$  does not play any role on the strength development with time. As a result, the strength normalization of stabilized clays as shown in Fig. 9 by the 28 day-strength, (i.e., 4 week-strength) can be performed by the linear regression analysis in terms of curing time only as follows:

$$\frac{q_D}{q_{28}} = a + b \ln D \quad (3)$$

where, SD is the strength after D days of curing, S28 is the 28 day-strength, D is the curing time, a and b are constant depending upon the type of clay. It is found here that  $a = -0.51$  and  $b = 1.07$  for Bangladesh clay. While, the a and b for inland clays have investigated by Nagaraj et al. (1996) as -0.18 and 0.46, respectively.

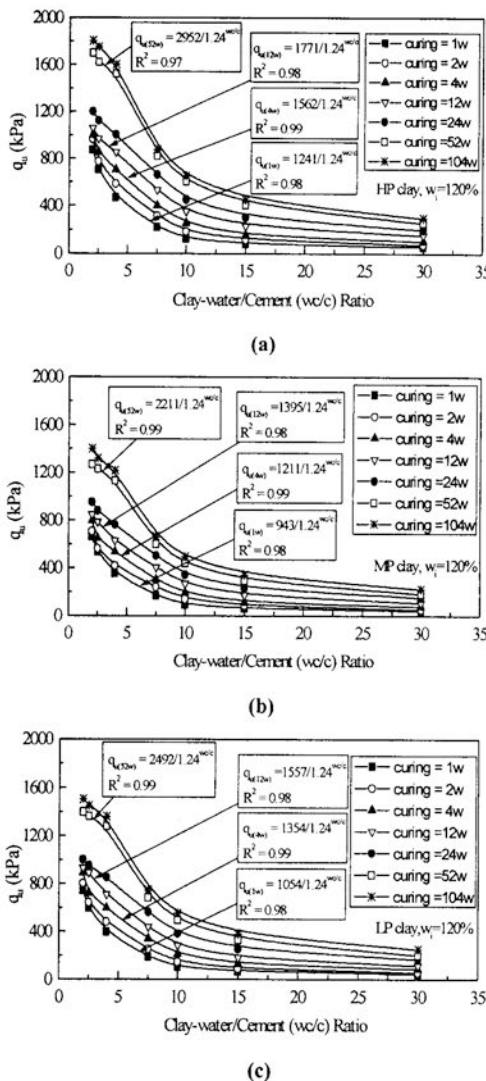


**Fig. 8 Strength prediction based on clay-water/cement ratio's concept of cement stabilized Bangladesh clay ( $w_i = 120\%$ ) [(a) HP clay, (b) MP clay and (c) LP clay]**

The interrelationship among strength, curing time and clay water content/cement ratio, wc/c for predicting strength development of generalized cement stabilized Bangladesh clays is expressed by combination of equations (2) and (3) as follows:

$$\left( \frac{q_{(wc/c)1,D}}{q_{(wc/c)28}} \right) = 1.24 \left\{ (wc/c)28 - (wc/c)_{DI} \right\} (-0.513 + 1.07 \ln D) \quad (4)$$

where,  $q_{(wc/c)1,D}$  is strength of stabilized clay to be estimated at clay water content/cement ratio of  $(wc/c)_1$  at D day-curing time and  $q_{(wc/c)28}$  is strength of stabilized clay at clay water content/cement ratio of  $(wc/c)$  after 28 day-curing time.

#### Relation between yield strength and unconfined strength

The magnitudes of the yield strength,  $\sigma_y$  (found from consolidation test at confined condition) and unconfined compressive strength,  $q_u$  (found from compression test at unconfined condition) depend on the degree of cementation (bond strength), it appears logical to relate these two parameters, it was reported by Horpibulsuk (2002). Depending on this logic, Fig. 10 represents the relationship between  $\sigma_y$  and  $q_u$ , which is generated based on test results of cement admixed clays studied (HP, MP and LP clays). In this figure, the test results are generalized on four way depending on initial mixing water ( $w_i$ ) contents (120%, 150%, 200% and 250%) with mixed tests data for the clays studied at wc/c ratios of 7.5, 10 and 15 and curing time of 4 weeks. The equations for the relationship between  $\sigma_y$  (kPa) and  $q_u$  (kPa) are as follows:

$$\sigma'_y = 2.56 q_u \quad \text{for } wc/c = 7.5 \quad (5a)$$

$$\sigma'_y = 2.07 q_u \quad \text{for } wc/c = 10 \quad (5b)$$

$$\sigma'_y = 1.34 q_u \quad \text{for } wc/c = 15 \quad (5c)$$

with coefficient of correlations of 0.97, 0.99 and 0.94 respectively.

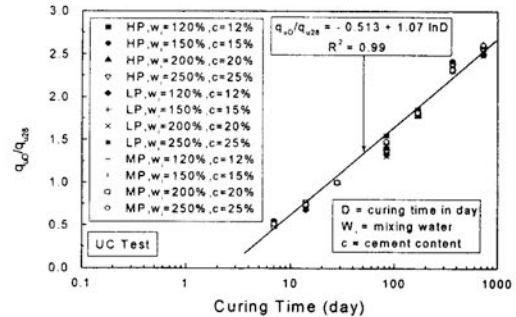


**Fig. 9 Strength development with time and its generalization for Bangladesh clay**

Horpibulsuk (2002) found that the relationship between  $\sigma'_y$  and  $q_u$ , which was  $\sigma'_y = 2.20 q_u$ , for cement admixed clays, while Takahashi and Kitazume (2004) also found that the same relation, which was  $\sigma'_y = (1.27 \text{ to } 2.55) q_u$ .

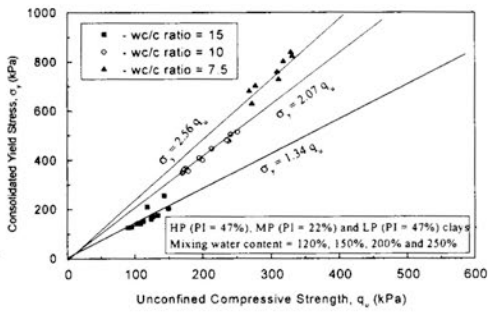


**Fig. 10 Relation between Yield Strength and Unconfined Strength for Bangladesh clay**

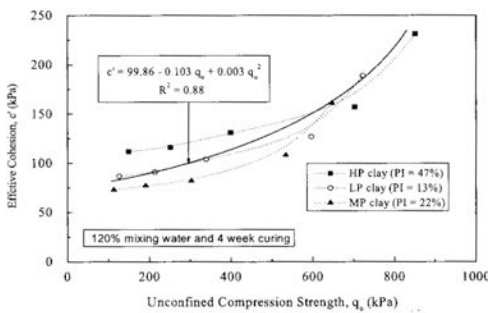


**Fig. 10 Relation between Effective Cohesion and Unconfined Strength for Bangladesh clay**

#### Relation between effective cohesion and unconfined strength

The relation between the effective cohesion and unconfined strength results for HP, MP and LP clays treated with 8% to 30% cement content and 120% mixing water contents, cured for 4 weeks is shown in Fig. 11. Although, there are some data points scattered, the plot demonstrates a general validity. From the regression analysis, the following relations have been obtained:

$$c' = 99.86 - 0.103q_u + 0.003q_u^2, \text{ (}c'\text{ and }q_u\text{ in kPa)} \quad (6a)$$

or

$$c' = 0.103 - 0.113q_u + 2.976q_u^2, \text{ (}c'\text{ and }q_u\text{ in kg/cm}^2\text{)} \quad (6b)$$

Similar relationship was proposed by Porbaha et al. (2000) as  $c' = 0.53 + 0.37q_u - 0.0014q_u^2$ , where,  $c'$  and  $q_u$  in  $\text{kg}/\text{cm}^2$  for all specimens cured up to 4 weeks.

#### CONCLUSIONS

- 1) The specific gravity reduces while unit weight increases with increasing cement content (or decreasing w/c ratio) and curing time for treated clays at high water content. The specific gravity increases while unit weight reduces with increasing mixing water content and plasticity of soil. Existing water content and degree of saturation for cement treated clays are increased with increasing plasticity index of soil.

- 2) The cement-treated clays are gained higher void ratio and volumetric strain than those of cement-treated clays. The significant increase in yield stress and reduction in compression index ( $C_c$ ) and swell index ( $C_s$ ) have been found with increasing cement content (or decreasing w/c ratio) and increasing curing time.  $C_c$  and  $C_s$  increases with the decrease in plasticity index of clays.
- 3) It has been found that the effective cohesion ( $c'$ ) and friction angle ( $\phi'$ ) of samples increased with increasing cement content (or decreasing w/c ratio) but  $c'$  increases and  $\phi'$  decreases with increasing curing time.
- 4) For a given soft clay, the cementation bond strength increases as the clay-water/cement ratio, w/c decreases. The stress-strains behavior and strength characteristics in the unconfined compression test are practically the same as long as the w/c is identical.
- 5) The clay type has a great influence on the stress-strain behavior for samples made up at a low to high w/c and subjected by low to high effective cell pressures. Their states of stress lie on the state boundary surface where the samples exhibit elasto-plastic behavior. It is revealed that samples having the same w/c develop practically about to same peak deviator stress.
- 6) Cement treated samples show negative to very small negative excess pore pressure development at higher strain in consolidated undrained triaxial compression tests during the shearing stage at low in-situ stress range. Hence, the behavior of cement treated Bangladesh clays are found to be similar the over-consolidated clays.
- 7) For the improvement of soft clay at high water content by cement admixture, it is found that high plastic clay undergoes better improvement than low plastic clay but low plastic clay undergoes better improvement than medium plastic clay. The unconfined compressive strength of cement treated Bangladesh clays increases with the increase of cement content (or decrease of w/c ratio) and curing time. The resulting effect of improvement of strength leads to the formation of more structured cemented clay.
- 8) The salient effect of clay water content/cement ratio, w/c on the stabilized (treated) clays is found that the w/c is the influential parameter governing the strength and deformation characteristics. The mixtures having the same w/c develop practically about to same yield and peak strength. Lower the w/c, higher the yield and peak strength.
- 9) Since the behavior of stabilized clays is remarkably governed by w/c, the short-cut strength prediction in terms of w/c as well as the interrelationship involving strength, w/c and curing time are proposed as presented in equations  $\left( \frac{S_{(w/c)_1}}{S_{(w/c)_2}} \right) = 1.24^{\{(w/c)_2 - (w/c)_1\}}$  and  $\left( \frac{S_{(w/c)_1,D}}{S_{(w/c)_2,D}} \right) = 1.24^{\{(w/c)_2 D - (w/c)_1 D\}} (-0.513 + 1.07 \ln D)$

- respectively, the implementation of the presented method is to simplify the task of arriving at the cement content and curing time in the laboratory investigations to realize the target values.
- 10) The correlation between  $\sigma'_y$  (yield strength) and  $q_u$  (unconfined strength) of cement treated clays (where w/c are varied from 15 to 7.5) as  $\sigma'_y = (1.34 \text{ to } 2.56) q_u$  for the clays studied has been proposed.
  - 11) The correlation between  $c'$  (effective cohesion) and  $q_u$  (unconfined strength) of cement treated clay as  $c' = 99.86 - 0.103q_u + 0.003q_u^2$  for the clays studied has been proposed.
  - 12) This paper reveals that the strength of the treated clays strongly depends upon only w/c. Thus to obtain uniform strength of stabilized clays for engineering works such as deep foundation, shallow foundation by improvement of deep mixing methods without compaction at high water content may be controlled. The clay water content/cement content ratio's concept, thus, overcomes not only the engineering requirement but also the economical viewpoint.
- REFERENCES**
- CHEW, S.H., KAMRUZZAMAN, A.H.M. and LEE, F.H. (2004): Physicochemical and engineering of cement treated clays, *ASCE Journal of GEE*, pp. 696-706.
- HORPIBULSUK, S. (2002): Analysis of compressibility of cement admixed clays, *Proceedings of the International Conference on Lowland Technology*, Saga University, Saga, Japan.
- HORPIBULSUK, S. and MIURA, N. (2000): A new method for predicting strength of cement stabilized clays, *Coastal Geotechnical Engineering in practice*, Rotterdam, ISBN 50 5809 1511.
- HORPIBULSUK, S. and MIURA, N. (2001): A new approach for studying behavior of cement stabilized clays, *Proceedings of the 15<sup>th</sup> International Conf. on Soil Mechanics and Geotechnical Engineering*, Turkey, Vol.3: 1759-1762.
- HARPIBULSUK; S., MIURA, N. and NAGARAJ, T.S. (1999): Prediction of strength and consolidation parameters of cement stabilized clays, *Saga University, Japan* Vol. 28, No. 2, pp. 27-38.
- HORPIBULSUK, S., AND MIURA, N. and NISHIDA, K (2000): Factors influencing field strength of soil-cement column, *Proceedings of GEC*, AIT, Bangkok, Thailand, pp. 623-634.
- MIURA, N., HORPIBULSUK, S. and NAGARAJ, T. S. (2001): Engineering behavior of cement stabilized clay at high water content. *JGS Soils and Foundations*, Vol. 41, No. 5, pp.33-45.
- NAGARJ, T.S., YARIGAR, P., MIURA, N., and YAMADERA, A. (1996): Prediction strength development cement admixture based on water content. *The 2<sup>nd</sup> International Conference*, Tokyo.
- PORBAHA, A., SHIBUYA, S. AND KISHIDA, T. (2000): "State of the art in deep mixing technology. Part III: geo-material characterization", Technical Research Institute, Yokohama, Japan, 4 (3), pp. 91-110.
- SIDDIQUE, A., SAFIULLAH A. M. M., and ANSARY M. A., (2002): Characteristic features of soft ground engineering in Bangladesh. *Proceedings of International Symposium*, Japan.

# TECHNICAL NOTE

## FREQUENCY EFFECT ON LIQUEFACTION USING SHAKE TABLE TESTS

J. Kumar<sup>1</sup> and P. Samui<sup>2</sup>

**ABSTRACT:** Liquefaction experiments were conducted on two different sand samples by varying the frequency of the excitation from 1.0 Hz to 4.0 Hz. Vertical settlements at the centre of the sample's free surface and the pore water pressure near the bottom of the sample were monitored. The samples were subjected to harmonic uniaxial horizontal excitation and the amplitude of the horizontal acceleration was always kept equal to 0.1g. On account of the decrease in the displacement amplitude of the horizontal excitation with an increase in the frequency of the excitation, it was clearly observed that the number of cycles to attain (i) the peak magnitude of the pore water pressure, and (ii) the associated maximum settlement, increases with an increase in the frequency of the excitation.

**Keywords:** earthquakes, liquefaction, sands, shake table

### INTRODUCTION

The liquefaction of saturated loose sands during earthquakes becomes the cause of severe damage to various civil engineering structures. Large shear box/shake table tests are often used to assess the liquefaction of a given soil sample subjected to harmonic/earthquake excitation (Finn et al., 1970, 1971; Pyke et al., 1975; De Alba et al., 1976; Seed et al., 1978; Ishihara and Yamazaki, 1980; Ishihara and Nagase, 1988; Hushmand et al., 1988; Van Laak et al., 1994; Sato, 1994; Endo and Komanobe, 1995; Taylor et al., 1995; Mohajeri and Towhata, 2004; Ueng et al., 2004). These shear box/shake table tests provide a better simulation technique for assessing the response of saturated ground to liquefaction than that observed by using cyclic shear tests. In most of the existing research investigations using large shear box/shaking table tests subjected to harmonic excitation, liquefaction studies have been normally carried out at one particular frequency. The effect of frequency on liquefaction response, using large shear box/shaking table tests, seems to be still not very clearly investigated. In the present note, it was intended to carry out a few liquefaction experiments using the large rigid rectangular box, made from Perspex sheets, mounted on a shake table having size of 1.2 m x 1.2 m and subjected to uniaxial harmonic excitation. For all the tests, the amplitude of horizontal acceleration was kept invariably the same (0.1g) and the magnitude of frequency was varied between 1 Hz and 4 Hz. Two different samples of sand were chosen. With an increase in the number of cycles of excitation, vertical settlement at the centre of the free surface of the sample and the pore water near the bottom surface of the tank wall were recorded. It should be mentioned that, unlike liquefaction tests using laminar box, the box used in performing the present experiments had rigid walls; consequently, it was expected that the results obtained using this box will have definitely some boundary effects on account of the reflection of waves from the wall surface perpendicular to the direction of the excitation.

### EXPERIMENTAL PROCEDURE

A rigid box made of transparent Perspex sheets of size

<sup>1</sup>Associate Professor, Civil Engineering Department, Indian Institute of Science, Bangalore-560012, India (Corresponding author: [jkumar@civil.iisc.ernet.in](mailto:jkumar@civil.iisc.ernet.in))

<sup>2</sup>Former Research Scholar

80 cm (length), 40 cm (width) and 70 cm (height) was firmly fixed on the top of the shake table. The soil sample was prepared by spreading the sand-water jet, from a given height of fall, uniformly in a chosen box. By building a very small hydraulic head, the water was allowed to seep very slowly from the bottom of tank towards the free surface of the sample in order to achieve a better saturation (Kuerbis and Vaid, 1988). The supply of the water was stopped until the water starts accumulating at the free surface of the sand. Subsequently, the top surface of the soil sample was carefully levelled and then the initial height of the soil sample was measured. The initial heights of the samples for all the tests were varied between 40.5 cm to 43.8 cm. The sample was then subjected to continuous sinusoidal uniaxial horizontal excitation. The response of the sample was then studied by measuring the increase in the pore water pressure with time by using a piezometer installed at a point P<sub>1</sub> as shown in Fig.1; the point P<sub>1</sub> lies at a vertical distance 2.5 cm above the bottom surface of the tank. The vertical settlements of the free surface of the sand at the point S<sub>1</sub>, as shown in Fig.1, were also simultaneously measured with time. The images of the tank at different times were captured to measure the settlements of the free surface of the sample (soil mass not water); it should be mentioned that the settlements of the free surface of the sample in a direction perpendicular to the direction of the excitation was found to be almost the same. However, in the direction of the excitation, a maximum settlement was noticed at the centre of the free surface and the minimum at the edge (along the wall of the box). In the present study, surface settlements only at the point S<sub>1</sub> were monitored. After attaining the complete surface liquefaction, that is, the stage when the accumulation of water on the free surface of the material was noted and also when the surface settlements of the soil mass no longer increase further with time, the experiments were then terminated.

### DETERMINATION OF INITIAL VOID RATIO

In order to determine the initial void ratio of the prepared soil sample, a large metal container was buried in the sample. After preparing the sample of a given height, the container was taken out from tank and the excess soil mass in the container was trimmed off; the soil mass in the place of container was then refilled in the tank almost in the same state as before starting the experiment. Dry and wet unit weights of the soil sample in the container were then determined. The void ratio was then determined by

knowing the bulk unit weight ( $\gamma_b$ ), water content (w) and the specific gravity (G) of soil solids. The relationship  $\gamma_b = \frac{G\gamma_w(1+w)}{(1+e)}$  was then used to determine the void ratio of the soil mass.

#### MATERIAL PROPERTIES

The characteristics of two different chosen sands, sand-A and sand-B, are given in Table 1. In this table,  $D_{60}$  and  $D_{30}$  are the sizes corresponding to which 60% and 30% of the soil mass by mass are finer than that size;  $C_u$  and  $C_c$  are the uniformity coefficient and the coefficient of curvature, respectively; and  $e_{max}$  and  $e_{min}$  define the maximum and minimum void ratios of the chosen material. It should be mentioned that both the chosen sands have hardly any clay fractions and the difference between the grain size parameters for sands A and B is very marginal.

**Table 1. Gradation characteristics of the chosen sand**

Soil Sample	$D_{60}$ (mm)	$D_{30}$ (mm)	$C_u$	$C_c$	$e_{max}$	$e_{min}$
Sand-A	0.480	0.275	3.43	1.125	1.120	0.612
Sand-B	0.460	0.270	3.03	1.068	1.214	0.623

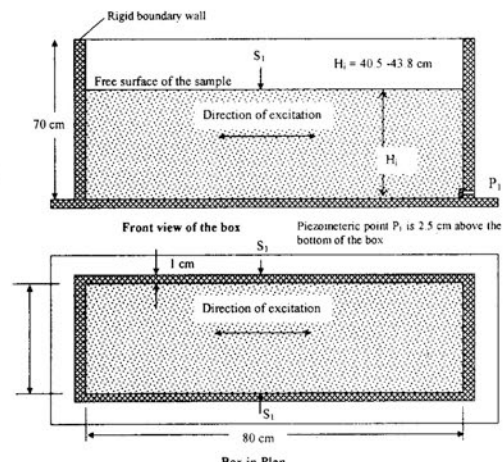


**Fig. 1 Dimensions of the box chosen in the present study**

#### RESULTS AND OBSERVATIONS

Experiments were conducted at three different frequencies, namely, 1.0, 2.0 and 4.0 Hz. With an increase in the number of cycles of excitation, the magnitudes of the pore water pressure at the point  $P_1$  and the vertical surface settlements at the point  $S_1$  were continuously monitored. All the experimental results were plotted in a non-dimensional form, that is, (i) the percentage settlement with respect to initial height of the sample versus number of cycles, and (ii) the pore water pressure ratio versus number of cycles; where

$$\text{Pore water pressure ratio} = \frac{\text{total pore water pressure at a given depth}}{\text{total vertical overburden pressure at the same depth}}$$

$$\text{Percentage settlement} = \frac{\text{vertical settlement of the sample surface at its centre}}{\text{initial height of the sample}} \times 100$$

For the magnitude of the pore water pressure ratio  $\geq 1.0$ , the liquefaction of the material at  $P_1$  will assume to take place. The results are presented in Figs. 2 and 3. The values of the peak pore water pressure, ultimate settlement and the number of cycles to achieve either the peak pore water pressure or the final settlement are also shown exclusively in Table 2. Following observations were made:

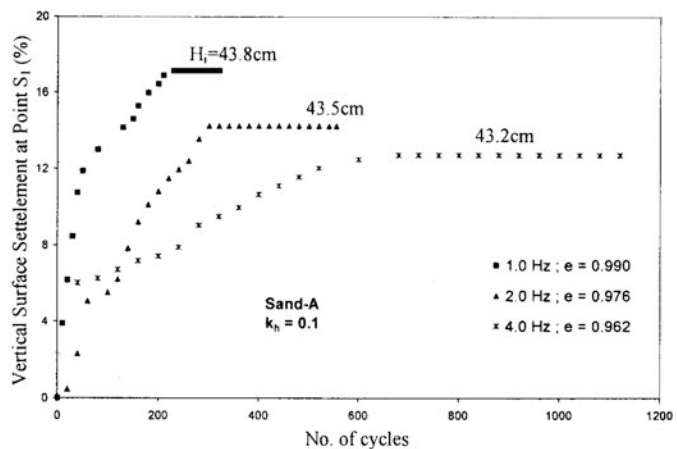
1. The settlement at the free surface of the sample at point  $S_1$  increases invariably with an increase in the number of cycles up to a certain extent and thereafter, it becomes almost constant. The number of cycles required to achieve the final settlement increases extensively with an increase in the frequency of the excitation. For both the sands, the magnitude of the final settlement increases with a decrease in the magnitude of frequency; it should be mentioned that the initial void ratio was, however, very marginally higher for tests with lower frequency.
2. The pore water pressure at  $P_1$  increases with an increase in the number of cycles up to a certain peak and, subsequently, its magnitude reduces continuously with a further increase in number of cycles until the magnitude of pore water pressure becomes almost equal to that of the initial hydrostatic water pressure. The number of cycles required to reach the peak pore water pressure increases with an increase in the frequency of the excitation. It should be noted that the magnitude of the pore water pressure ratio for all the tests at point  $P_1$  remains a little smaller than 1.0. This is due to the fact that the liquefaction of the material was observed at the free surface whereas the pore water pressure was recorded at bottom of the sample.

#### DISCUSSIONS

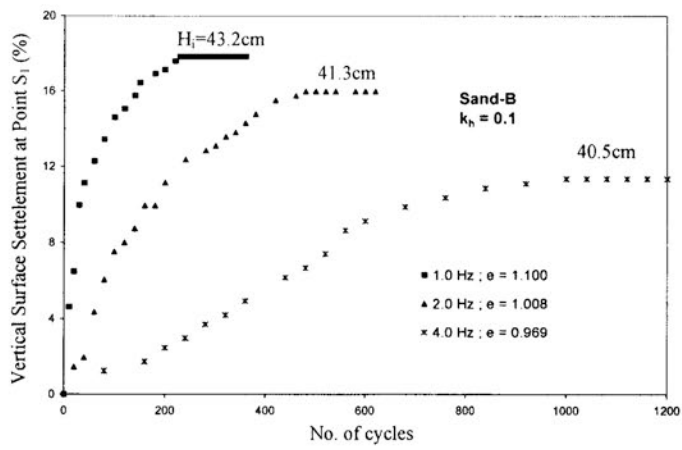
An increase in the number of cycles with an increase in the frequency of the excitation, to reach either the peak pore water pressure or the final settlement, is due to the fact that the amplitude of the horizontal displacement (stroke length of the shake table) decreases continuously with an increase in the frequency of the excitation for a given amplitude of horizontal acceleration. The magnitudes of the stroke lengths were 2.484 cm, 0.621 cm and 0.155 cm corresponding to the magnitude of frequency equal to 1 Hz, 2 Hz and 4 Hz, respectively. A decrease in the amplitude of the horizontal displacement indicates a decrease in the level of shearing strain and, therefore, a large number of cycles were required to achieve liquefaction at greater frequencies even though the magnitude of the peak acceleration was kept equal to 0.1g for all the cases.

**Table 2 Peak pore water pressure, ultimate settlement and corresponding number of cycles for all the tests**

Soil	$e_i$	Frequency (Hz)	No of cycles required to reach peak pore water pressure at $P_1$	Peak pore water pressure ratio ( $u/\gamma_{sat}Z$ ) at $P_1$	No of cycles required to reach ultimate settlement	Ultimate vertical settlement at $S_1$ ( $s_f/H_i$ ) (%)
Sand-A	0.990	1.0	20	0.969	230	17.12
	0.976	2.0	40	0.920	300	14.25
	0.962	4.0	80	0.876	680	12.73
Sand-B	1.100	1.0	10	0.992	230	17.82
	1.008	2.0	20	0.933	480	15.98
	0.969	4.0	40	0.908	1000	11.36



(a)



(b)

**Fig. 2 Vertical settlement at the centre ( $S_1$ ) of the sample free surface for (a) sand -A and (b) sand-B**

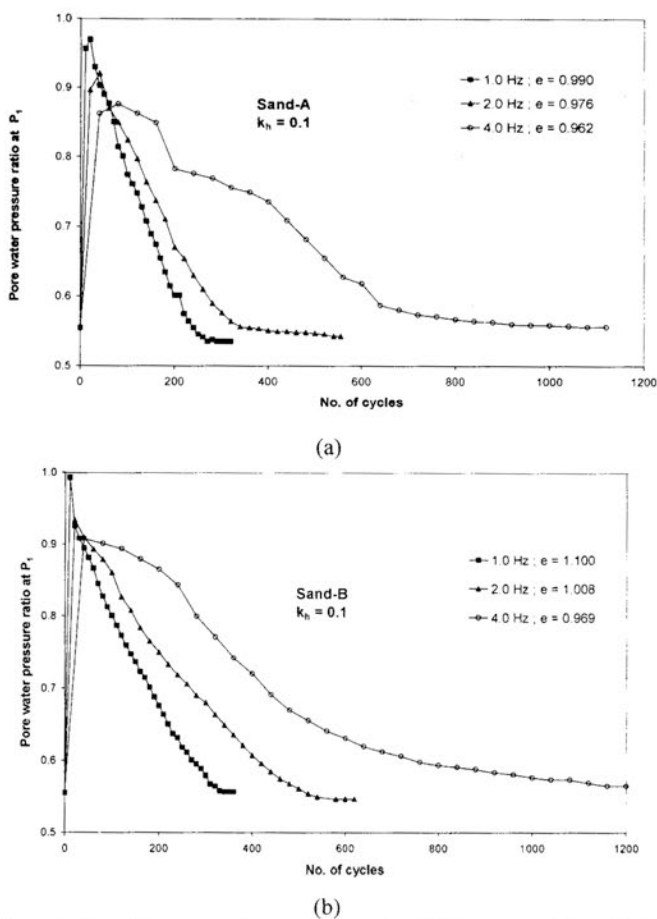


Fig. 3 The variation of the pore water pressure ratio at  $P_1$  for (a) sand -A and (b) sand-B

## CONCLUSIONS

Shake table liquefaction studies, involving continuous uniaxial sinusoidal horizontal vibrations, were reported in this note. During the period of continuous excitation, the magnitude of the pore water pressures increases up to a certain peak value and, thereafter, its magnitude decreases continuously until it again becomes the hydrostatic pressure before the excitation of the material. The settlement at the free surface of the sample increases continuously with the time up to a certain peak value and, thereafter, its magnitude becomes almost constant. The number of cycles to reach either the peak pore water pressure or the final settlement increases significantly with an increase in the frequency of the excitation even though the amplitude of the acceleration was kept equal to 0.1g.

## ACKNOWLEDGEMENTS

This work forms the part of the work carried out under the DST project: "Liquefaction Studies for the recent Bhuj Earthquake". The authors would like to gratefully acknowledge the financial support provided by the DST in doing this work. The authors would also like to thank Mr. C. O. Reddy for his help during shake table testing at Indian Institute of Science.

## REFERENCES

- De ALBA, P., SEED, H.B. and CHAN, C.K. (1976). Sand liquefaction in large scale simple shear tests. *ASCE Journal of the Geotechnical Engineering Division*, Vol.102, No. 9, pp. 909-927.
- ENDO, O. and KOMANOBE, K. (1995). Single and multi-directional shaking table tests of sand liquefaction. *Proceeding of the 1<sup>st</sup> International Conference on Earthquake Geotechnical Engineering*, Tokyo, Japan, pp. 675-680.
- FINN, W.D.L., EMERY, J.J. and GUPTA, Y.P. (1970). A shaking table study of the liquefaction of saturated sands during earthquakes. *Proceedings of the 3<sup>rd</sup> European Symposium on Earthquake Engineering*, Sofia, Bulgaria.
- FINN, W.D. L., EMERY, J.J. and GUPTA, Y.P. (1971). Liquefaction of Large Samples of Saturated Sand Excited on a Shaking Table. *Proceedings of the 1<sup>st</sup> Canadian Conference of Earthquake Engineering*, Vancouver, Canada.

- HUSHMAND, B., SCOTT, R.F. and CROUSE, C.B. (1988). Centrifuge Liquefaction Tests in a Laminar Box. *Geotechnique*, Vol. 38, No. 2, pp. 253-262.
- ISHIHARA, K. and YAMAZAKI, F. (1980). Cyclic Simple Shear Tests on Saturated Sand in Multi-Directional Loading. *Soils and Foundations*, Vol. 20, No. 1, pp. 45-59.
- ISHIHARA, K. and NAGASE (1988). Multi-Directional Irregular Loading Tests on Sand. *Soil dynamics and Earthquake engineering*, Vol. 7, No. 4, pp. 201-212.
- KUERBIS, R. and VAID, Y.P. (1988). Sand sample preparation- the slurry deposition method. *Soils and Foundations*, Vol. 28, No. 4, pp. 107-118.
- MOHAJERI, M. and TOWHATA, I. (2003). Shake table tests on residual deformation of sandy slopes due to cyclic loading. *Soils and Foundations*, Vol. 43, No. 6, pp. 91-107.
- PYKE, R.M., SEED, H.B. and CHAN, C.K. (1975). Settlement of sands under multidirectional loading. *ASCE Journal of Geotechnical Engineering Division*, Vol. 101, No. 4, pp. 379-398.
- SATO, M. (1994). A new dynamic geotechnical centrifuge and performance of shaking table tests. *Proceedings of the Centrifuge 94*, C.E. Leung, F.H. Lee and T.S. Tans, Eds., Balkema, Rotterdam, pp. 157-162.
- SEED, H.B., PYKE, R.M. and MARTIN, G.R. (1978). Effect of multidirectional shaking on pore pressure development in sands. *ASCE Journal of Geotechnical Engineering Division*, Vol. 104, No. 1, pp. 27-44.
- TAYLOR, C.A., DAR, A.R. and CREWE, A.J. (1995). Shaking table modeling of seismic geotechnical problems". *Proceeding of the 10<sup>th</sup> European Conference on Earthquake Engineering*. Vienna, Austria, pp. 441-446.
- UENG, T.S., CHEN, C.H. and CHEN, H.W. (2004). Pore water pressure changes in saturated sand during one and two dimensional shaking table tests. *Proceedings of the 3<sup>rd</sup> International Conference on Earthquake Geotechnical Engineering*, Berkeley, California, U.S.A., pp. 682-687.
- VAN LAAK, P.A., TABOADA, V.M., DOBRY, R. and ELGAMAL, A.W. (1994). Earthquake centrifuge modeling using a laminar box. *Dynamic Geotechnical Testing II*, ASTM STP 1213, ASTM International, West Conshohocken, PA, U.S.A.